

A SIMPLIFIED MODEL FOR LIGHTNING EXPOSURE OF WIND TURBINES

by

Pape Momar Lo

Electrical and Computer Engineering Department
McGill University, Montreal



December 2008

**A thesis submitted to McGill University in partial fulfillment of the
requirements of the degree of Master in Engineering.**

© Pape Momar Lo, 2008

ACKNOWLEDGMENTS

I am deeply indebted to my supervisor, Dr. Farouk A. M. Rizk, for his constant guidance and support.

Without his help, this work would have never been possible. His invaluable advices and patience are mostly appreciated. And most importantly, he greatly enriched my knowledge with his exceptional insights in science.

I would also like to thank Prof. Banakar and Prof. F. Vidal for their precious tutoring on the Femlab software.

In addition, I would like to thank my dear friend Lamine Diallo for his support and presence during those very late nights at the library at the end of my work.

Lastly, I would like to thank my family for their support. I am greatly indebted to my brother and sisters Ousmane, Aissatou and Marie-Therese who have given me tremendous encouragements during my difficult times.

Above all, I cannot express my never-ending gratitude to my beloved parents who made all this possible with their financial and moral support during my entire academic path.

**I dedicate this thesis to my parents, with a special address to my mother
who will always be my inspiration.**

ABSTRACT

Reliability requirements of wind turbines become more important as the share of wind energy in the global energy balance continues to grow. Lightning protection of wind turbines has therefore become an issue of great importance considering the location and size of modern wind turbines.

Analysis of lightning performance of wind turbines includes both lightning exposure and lightning response once a turbine is actually struck.

In Chapter 1, lightning exposure and protection of wind turbines is introduced from a technical and field point of view, and common methods of analysis are mentioned.

In Chapter 2, basic lightning attachment theories with special reference to wind turbine exposure and methods of analysis are presented. Models used in previous work to determine lightning incidence to structures are described in details.

In Chapter 3, a simplified model for lightning exposure of wind turbines is presented. Based on electric field and space potential calculations, it has been shown that a wind turbine with a down conductor can be treated as a slender structure.

Due to the enormous difference between the speed of downward stepped leader and the blade speed, it has been shown that from a lightning exposure point of view, a wind turbine blade could be treated as static.

The findings of the thesis allow significant simplification of the analysis of lightning exposure of the wind turbines.

RESUME

Les exigences de fiabilité des éoliennes deviennent de plus en plus importantes vu que la place qu'occupe l'énergie éolienne dans le bilan énergétique global ne cesse de croître. Prenant en compte l'emplacement et de la taille des éoliennes aujourd'hui, leur protection contre la foudre est devenu une question de grande envergure.

L'analyse de l'effet de la foudre sur les éoliennes réside sur l'analyse de leur exposition à celle-ci et sur les impacts après foudroiement.

Dans le chapitre 1, les concepts d'exposition et de protection des éoliennes contre la foudre d'un point de vue technique et pratique sont mis en avant. Des méthodes d'analyse sont aussi mentionnées.

Dans le chapitre 2, nous présentons des théories fondamentales sur la foudre avec une attention particulière sur l'exposition des éoliennes à celle-ci et sur des méthodes d'analyse. Les modèles utilisés lors de recherches antérieures afin de déterminer l'incidence de la foudre sur les structures sont décrits en détails.

Dans le chapitre 3, un modèle simplifié de l'exposition des éoliennes à la foudre est présenté. En se basant sur des calculs de champ électrique et de potentiel, nous avons démontré qu'une éolienne et son câble de protection peuvent être représentés par une tige cylindrique.

En raison de l'énorme différence entre la vitesse de descente des éclairs et la vitesse des pales des éoliennes, nous avons démontré que les pales peuvent être considérées stagnantes lors de nos analyses.

Cette thèse met en avant une simplification de l'analyse de l'exposition des éoliennes à la foudre.

TABLE OF CONTENTS

ACKNOWLEDGMENTS	I
ABSTRACT.....	III
RESUME	V
TABLE OF CONTENTS	VII
LIST OF FIGURES.....	IX
LIST OF TABLES	XIII
CHAPTER 1 : INTRODUCTION.....	1
CHAPTER 2 LITERATURE REVIEW	7
2.1. LIGHTNING	7
2.1.1. Lightning Mechanism.....	7
2.1.2. Risks of Lightning strikes.....	12
2.2. LIGHTNING INTERACTION WITH WIND TURBINES	14
2.2.1. Damage Mechanism	14
2.2.1.1. Current and Voltage path on the turbine.....	14
2.2.1.2. Damage on blades and bearing.....	23
2.2.1.3. Comments	30
2.3. METHOD OF ANALYSIS AND COMPUTATIONAL MODELS	32
2.3.1. Lightning incidence modeling	32
2.3.1.1. Concept of Attractive Radius	35
2.3.1.2. Comparison with analytical model.....	35
2.3.1.3. Comparison with power line observations.....	38
2.3.2. Recent lightning exposure modeling.....	40
2.3.2.1. Description of the model.....	40
2.3.2.2. Simulation of the downward leader.....	41
2.3.2.3. Simulation of the upward leader	42
2.3.2.4. Modeling of the clouds	44
2.3.2.5. Results of the Model.....	45
2.3.2.6. Check of the Model	47
2.3.3. Lightning incidence to tall structure modeling	49
2.3.3.1. Downward Negative Flash.....	49
2.3.3.2. Upward Flash	53
2.3.3.3. Lightning incidence	54
2.3.3.4. Check of the model.....	55

2.3.4.	Lightning leader inception modeling	58
2.3.4.1.	Stable leader inception physical model	58
2.3.4.2.	Corona Charge calculation.....	61
2.3.4.3.	Implementation of the model	63
2.3.4.4.	Simplified procedure	65
2.3.5.	Numerical model to determine lightning attachment points on wind turbine	68
2.3.5.1.	Electrical discharges related to a wind turbine blade	68
2.3.5.2.	Modeling	71
2.4.	Comments.....	76
CHAPTER 3	MODELING APPROACH.....	79
3.1.	Modeling Wind Turbine for Electric field distribution.....	79
3.1.1.	Finite Element Modeling (Femlab).....	79
3.1.2.	Charge Simulation Modeling.....	89
3.2.	Comparison between Rizk model and IEC standard	93
3.2.1.	Attractive Radius.....	93
3.2.2.	Number of direct lightning flashes.....	97
3.3.	Modeling Wind Turbine for Proportion of upward and downward flashes....	105
3.3.1.	Blade Position vs Time.....	105
3.3.2.	Proportion of upward and downward flashes	113
CHAPTER 4	DISCUSSION	119
4.1.	Electric field and Potential Evaluation.....	119
4.1.1.	Discussion.....	119
4.2.	Lightning Exposure.....	121
4.2.1.	Discussion.....	121
4.2.2.	Recommendations	125
CHAPTER 5	: CONCLUSION	127
CHAPTER 6	: REFERENCES.....	129
APPENDIX	133

LIST OF FIGURES

Figure 1 - Lightning Discharge Phenomena.....	9
Figure 2 - Formation of downward flash – Progressive steps	10
Figure 3 - Profile of a negative upward flash (not to scale)	11
Figure 4 - Reduced size model of a wind turbine generation system	15
Figure 5 - Configuration of the experimental setup	16
Figure 6 - Measured results for case 1-A and 1-B	18
Figure 7 - Generated over voltage between down-conductor and lead-in cable.....	22
Figure 8 - Stitch pattern in a blade surface	24
Figure 9 - Lightning discharge on wind turbine blade	25
Figure 10 - Pitch bearing test arrangement.....	27
Figure 11 - Close-up of bearing damage caused by a high-current test	30
Figure 12 - Observed incidence of strikes to structures of various heights.....	34
Figure 13 - Representation of a downward leader element approaching a structure of height, H	36
Figure 14 – Comparative downward leader striking distance analyses-as determined through analytical modeling.....	37
Figure 15 - Attractive radii in relation to tower height and peak current.....	38
Figure 16 - Equivalent attractive radius for lines – derived from the observed strike incidence on practical power lines	39
Figure 17 - Sketch of the step-by-step progression of the lightning as simulated in the calculation	41
Figure 18 - U_1 and U_{50} versus R_{eq}	43
Figure 19 - Example of the application of the model to a free-standing structure 220 m height	45
Figure 20 - Example of the computed leader paths of a 420 KV line in different orographic conditions	46
Figure 21 – (a) Computed lateral distance as function of lightning current of a structure of different height (b) Shielding failure width as function of lightning current of a 420 KV line with a shielding angle of 20 degrees	47
Figure 22 - Number of flashes on thin structures in various orographic conditions.....	48
Figure 23 - Schematic diagram of free-standing mast of height: h on flat ground and over a mountain simulated as semi-ellipsoid (prolate spheroid) with semiminor axis (base radius): a , and semimajor axis (height): b	50
Figure 24 – Variation of the attractive radius Ra , with mast height for flat terrain and	

different.....	52
Figure 25 - Variation of negative downward lightning strikes with mast height for flat and mountain terrains and comparison with empirical results	56
Figure 26 - Variation of total strike frequency N_s and comparison with empirical results	56
Figure 27 - Probability of upward flash on mast height over flat ground and comparison with empirical results.....	57
Figure 28 - Potential distribution before and after corona formation in a front of a rod. .	59
Figure 29 - Schematic example of the leader advancement simulation	60
Figure 30 - CSM modeling of the corona zone in a rod electrode (a) Distribution of the ring charges in the corona zone and a plane around the discharge axis (b) Detail of the location of the potential points on a plane.....	62
Figure 31 - Leader Stabilization fields for a 10^{-2} m tip radius rod.....	64
Figure 32 - Leader Stabilization fields for a 60 x 80 m rectangular building	65
Figure 33 - Comparison of the leader stabilization fields computed with the CSM and with the simplified geometrical approach for the different values of K_Q (a) for the lightning rod (b) for the rectangular building	67
Figure 34 - Common blade design, discrete receptors connected to an internal down conductor.....	69
Figure 35 - Discharges on new and clean blade, mainly from metallic components.....	70
Figure 36 - FEM model of a single wind turbine to determine the normalized stabilization field at different locations.	72
Figure 37 – Relative probability of a strike for a wind turbine with one blade in horizontal position.....	73
Figure 38 – Relative probability of a strike for a wind turbine with one blade in vertical position.....	74
Figure 39 – Model Approach.....	80
Figure 40 – Solution by finite element (a) at the tip of the down conductor (b) the full model	83
Figure 41 - Electric field distribution at the tip of the wire conductor.....	84
Figure 42 – Electric field distribution from 160 m to 162 m height	85
Figure 43 – Space potential distribution from 160 m to 162 m height	85
Figure 44 - Model defined in Femlab - wire conductor only	87
Figure 45 – (a) Electric field distribution from 160 m to 162 m height (b) Potential distribution from 160 m to 162 m height	88
Figure 46 - Equivalent collection area of the wind turbine	93

Figure 47 – Comparison Attractive Radius Rizk and IEC Model	96
Figure 48 - Attractive radius Ratio between Rizk and IEC Model.....	96
Figure 49 - Number of flashes and ratio for different heights for a value $N_g = 1$ flash/km ² /year computed with Rizk and IEC methods.....	99
Figure 50 - Number of flashes and ratio for different heights for a value $N_g = 2$ flash/km ² /year computed with Rizk and IEC methods.....	100
Figure 51 – Number of flashes and ratio for different heights for a value $N_g = 10$ flash/km ² /year computed with Rizk and IEC methods.....	101
Figure 52 - Number of flashes and ratio for different heights for a value $N_g = 25$ flash/km ² /year computed with Rizk and IEC methods.....	103
Figure 53 - Number of flashes and ratio for different heights for a value $N_g = 25$ flash/km ² /year computed with Rizk and IEC methods.....	104
Figure 54 – (a) Highest Configuration of the wind turbine (b) Y and Lowest configuration of the wind turbine.....	108
Figure 55 – Vertical length of the Wind turbine vs Time	109
Figure 56 – Position of heights of the Wind turbine Blades vs Time	110
Figure 57 - Position of each blades of the wind turbine vs Time	111
Figure 58 - Heights of the wind turbine rotating at different time t for one cycle of 2π .	113
Figure 59 - Attractive radius of the wind turbine at different height at a time t.....	114
Figure 60 - Number of Flashes and Proportion of upward and downward flashes for different blade tip heights at a time t for $N_g = 2$ fl./km ² /yr.....	117
Figure 61 - Number of Flashes and Proportion of upward and downward flashes for different blade tip heights at a time t for $N_g = 10$ fl./km ² /yr.....	117
Figure 62 - Number of Flashes and Proportion of upward and downward flashes for different blade tip heights at a time t for $N_g = 25$ fl./km ² /yr.....	118
Figure 63 - Number of Flashes and Proportion of upward and downward flashes for different blade tip heights at a time t for $N_g = 65$ fl./km ² /yr.....	118

LIST OF TABLES

Table 1- Lightning protection system levels.....	13
Table 2 – Electric Field and Potential @ 160 m and 162 m (FEMLAB).....	86
Table 3 – Electric Field and Potential @ 160 m and 162 m (FEMLAB).....	89
Table 3a – Electric Field and Potential @ 160 m and 162 m (Charge Simulation).....	91
Table 3b – Electric Field and Potential @ 160 m and 162 m (Charge Simulation)	91
Table 4 – Comparison Attractive Radius Rizk and IEC Model	95
Table 5 – Attractive radius Ratio between Rizk and IEC Model.....	96
Table 6 – Total number of flashes for different heights for a value $N_g = 1$ flash/km ² /year computed with Rizk and IEC methods	98
Table 7 – Total number of flashes for different heights for a value $N_g = 2$ flash/km ² /year computed with Rizk and IEC methods	99
Table 8 – Total number of flashes for different heights for a value $N_g = 10$ flash/km ² /year computed with Rizk and IEC methods	101
Table 9 – Total number of flashes for different heights for a value $N_g = 25$ flash/km ² /year computed with Rizk and IEC methods	102
Table 10 – Total number of flashes for different heights for a value $N_g = 65$ flash/km ² /year computed with Rizk and IEC methods.....	103
Table 11 – Heights of the wind turbine rotating at different time t	112
Table 12 – Attractive radius of the wind turbine at different height at a time t	114
Table 13 – Number of Flashes and Proportion of upward and downward flashes for different blade tip heights at a time t and for different values of N_g	116

CHAPTER 1 : INTRODUCTION

In the last years, renewable energies are taking an important role in our society. Wind turbines are rapidly becoming important generators of electric energy. Their utilization is considerably increasing in electric power supply and it will increase further with the new rules restricting the CO₂ emissions.

The increasing number and height of installed turbines have resulted in an increase of lightning damages with repair costs beyond acceptable levels [1].

Lightning stroke can be regarded as a major current source. Maximum recorded value of lightning current produced by a “single stroke” is in the region of 200 – 300 kA. Other parameters of interest are charge transfer and specific energy. The maximum values occur in only a small percentage of flashes worldwide [2]. The median value of peak lightning current is approximately 30 kA. Actually, the electrical characteristics of a stroke vary with the type of lightning flash and the geographical location.

The first research relating to the protection of wind turbines against lightning damage was conducted in the late 1970s and early 1980s in the USA [3]. The first reports focused on the lightning protection of a vertical axis wind turbine, a substantially different design from the horizontal axis machine now in widespread use. In later years, further studies were carried out dealing with machines more similar to modern designs. Until 1994 a number of papers stated that no records of lightning striking a wind turbine existed and as such the scale of the problem was not known [3].

More recently, there has been considerable work that has examined the application of wind turbines protection to a lightning stroke [48]. An IEC technical report has recently been written that summarizes those experiences [4].

Cotton and N. Jenkins stated that damages on wind power plants due to lightning strikes concern with about 25% the wind turbine power system and with about 50% the associated electronic system resulting mostly in power interruption of the plants [3].

It can be stated that wind turbines are vulnerable to lightning damage. An important factor in how much power a wind turbine will produce is the height of the tower. Since wind speed increases with height, increases to the tower height will increase in the amount of electricity generated by a wind turbine. The area of the blade disc covered by the rotor, (and wind speeds, of course), determines how much energy a wind turbine can harvest in a year [5]. For instance, to raise a 10 kW generator from a 60 foot tower height to a 100 foot tower could produce 25% more power. This is the reason why wind structures are often placed in high elevation locations where they are, unfortunately more vulnerable to lightning activities.

As a consequence, it is important that wind turbines are treated as other power system components and meets the standards for reliability, protection and safety used in the electric industry in order to reach an acceptable level of operational reliability.

Even if blades are made of polymers, they are the most common attachment point of lightning, and therefore must be adequately protected. In fact, when they are wet by the rain, they become conducting. In addition, the passage of lightning current through wind turbine bearings introduces a risk of lightning damage to the electrical and electronic system.

As explained earlier; unlike other electrical installations, such as transmission lines, substations and power plants; wind turbines are often placed in high elevation in order to increase their power production, thus, their lightning protection system has to be fully integrated into the different parts of structure to ensure that all parts likely to be lightning attachment points are able to withstand the impact of the lightning.

That lightning current should be conducted safely from the attachment points to the ground without unacceptable damage or disturbances to the systems.

Therefore, it is necessary to identify the lightning currents to tall structures as primary source of interference with respect to electromagnetic compatibility (EMC).

Information about lightning current parameters either comes from direct measurements, using, for example tall instrumented towers [9], or is based on quantification of lightning electromagnetic fields from which lightning currents are inferred adopting some empirical [6], [7] or theoretical [8] relations.

Experimental observations and theoretical investigations have shown that the presence of an elevated strike object, such as a tall tower, could affect substantially lightning currents and their radiated electromagnetic fields. Accurate knowledge of lightning electromagnetic fields is essential for achieving an efficient insulation design of electric-power networks and for determining electromagnetic compatibility requirements of telecommunication systems, as many lightning-caused disturbances are due to lightning electromagnetic fields [10].

It is interesting to know that there are few numerical methods to analyze the electro-magnetic impact of a lightning strike on a certain component within a complex mechanical structure.

The results of the modeling are in fact the surface transient current, voltage distribution and electromagnetic distribution inside or outside the wind turbine after a lightning strike. Those results can be used to specify the field influence inside the hub on personnel and materials (generator, control system, mechanical system, etc...) which will allow to identify more exposed areas in order to minimize hardware damage to a tolerable level in wind turbine installations.

On the next chapter of this thesis, we will review the studies made by most research organizations about lightning process. We will first focus on the characteristics, then we will discuss about lightning interaction with wind turbines and we will review past modeling investigations and results of lightning exposure to tall structures.

On the 3rd chapter, we present the modeling approach based on a 1.8 MW turbine which is engineered to be used in most exposed sites [11]. We have chosen this turbine because more than 2,000 of this type of turbines have already been installed around the world, and have proved themselves to be the most used in the market because of their seasoned performers in both onshore and offshore environments [11]. In fact, a cylindrical representation of the conducting wire attached to the blades is modeled to determinate the electric field at the tip of the wind turbine. The effect of the tower will also be investigated in order to verify whether a slender rod model will be applicable.

Subsequently, the resulting model will be used to compare different concepts of attractive radius equations, number of flashes and to analyze the proportion of upward and downward flashes related to the motion of the blades.

Chapter 4 gives a discussion and recommendations of our work and chapter 5 gives the main conclusion of the thesis.

CHAPTER 2 LITERATURE REVIEW

The literature review of this chapter primarily concerns three subjects: (2.1) Lightning mechanism and statistics; (2.2) Lightning interaction with wind turbines and (2.3) Method of analysis and computational models.

2.1. LIGHTNING

2.1.1. Lightning Mechanism

Lightning, the thunderbolt from mythology, has long been feared as an atmospheric flash of supernatural origins: the great weapon of the gods. The Greeks both marveled and feared lightning as it was hurled by Zeus. For the Vikings, lightning was produced by Thor as his hammer struck an anvil while riding his chariot across the clouds. In the East, early statues of Buddha show him carrying a thunderbolt with arrows at each end of it. Indian tribes in North America believed that lightning was due to the flashing feathers of a mystical bird whose flapping wings produced the sound of thunder [12].

Today, scientific rather than mystical techniques are used to explain lightning with experimental procedures replacing intuitive concepts. Yet, we remain in awe of lightning which still shines with its mystery, and rightly so. Each year, lightning is responsible for the deaths of a hundred or so people, injuries to several hundred more, and hundreds of millions of dollars in property damage.

The Lightning process is detailed in numerous papers and books by researchers such as UMAN in 1986; GOLDE in 1977 and RAKOV in 2003 [13]

From those researches and many others, one can summarize the lightning stroke mechanism. As the ice particles within a cloud (called hydrometeors) grow and interact, they collide, fracture and break apart.

It is thought that the smaller particles tend to acquire positive charge, while the larger particles acquire more negative charge. These particles tend to separate under the influences of updrafts and gravity until the upper portion of the cloud acquires a net positive charge and the lower portion of the cloud becomes negatively charged. This separation of charge produces electrical potential both within the cloud and between the cloud and ground. This can amount to millions of volts, and eventually air breakdown and a flash begins [13]. Lightning, then, is an electrical discharge between positive and negative regions of a thunderstorm.

A lightning flash is the ionized path that may last more than 1 s and its individual components are called **strokes**. It is composed of a series of strokes with an average of about four. The length and duration of each lightning stroke vary, but typically average about 30 microseconds. (The average peak power per stroke is about 10^{12} watts) [12].

Lightning discharges are one of two basic types, downward or upward initiated. A downward initiated discharge starts at the thundercloud and heads towards the earth. In contrast an upward initiated discharge starts at an exposed tall grounded structure.

Occasionally, lightning discharges can be intra-cloud, where the discharge occurs between regions of opposite charge. Without the benefit of conducting earth, intra-cloud lightning does not produce a return-stroke-like feature. Rather, it is characterized by slower propagating "recoil streamers" and "K" changes (millisecond-scale electric field changes that occur in cloud discharges). Nevertheless, tremendous energy, bright light, and thunder are still produced by intra-cloud lightning. Figure 1 shows the lightning discharge formation [16].

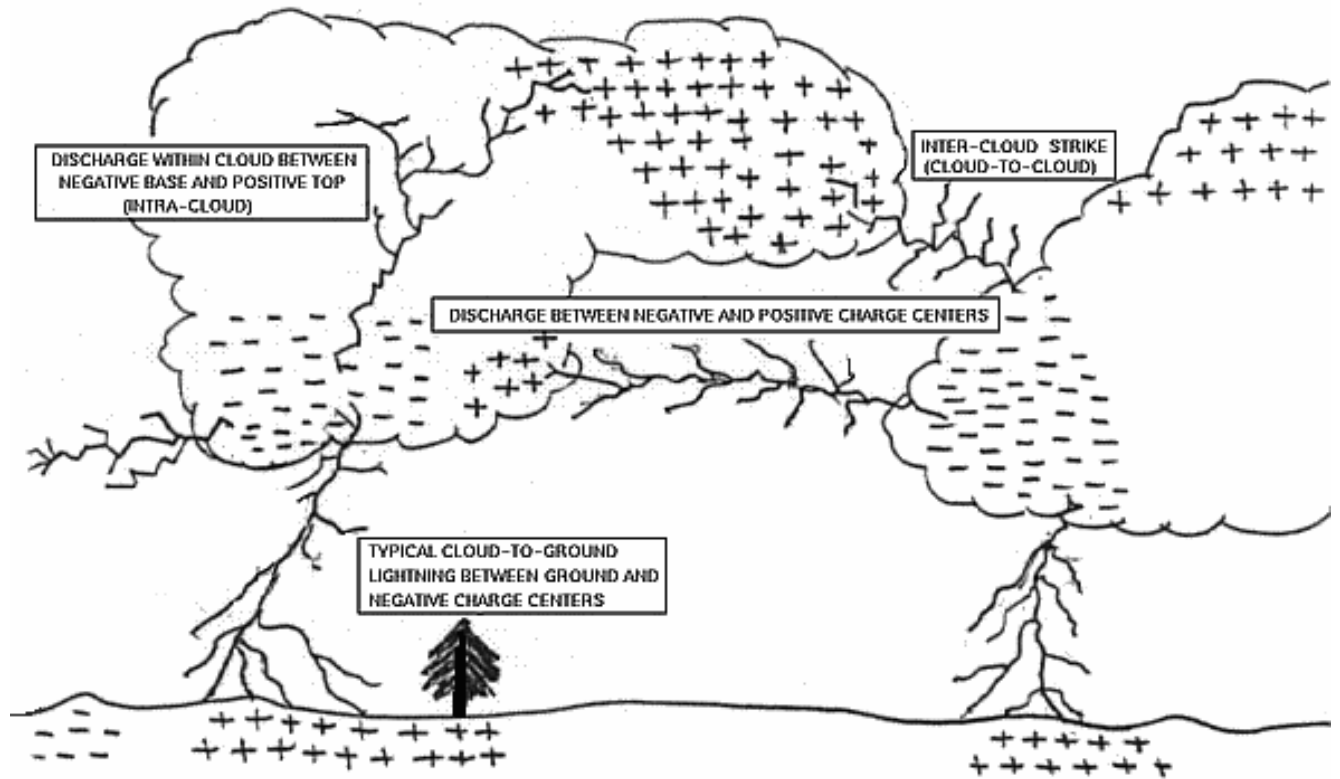


Figure 1- Lightning Discharge Phenomena

- **Downward initiated discharge**

With a preliminary breakdown of the air in a region of strong electric fields, a leader begins to propagate downward toward the Earth. It moves in discrete steps of about 50 meters each and is called a stepped leader (impulse currents of more than 1 kA). [1]

As the leader tip approaches the earth this high potential raises the electric field strength at the surface of the earth and leaders are emitted from the earth or from structures on the ground. These upward moving leaders are commonly termed upward connecting leaders.

When the descending stepped leader meets the upward moving connecting leader a continuous path from cloud to ground is established. This process is termed the first return stroke (peak value up to 100 kA). The process of downward propagating lightning attachment is illustrated in figure 2.

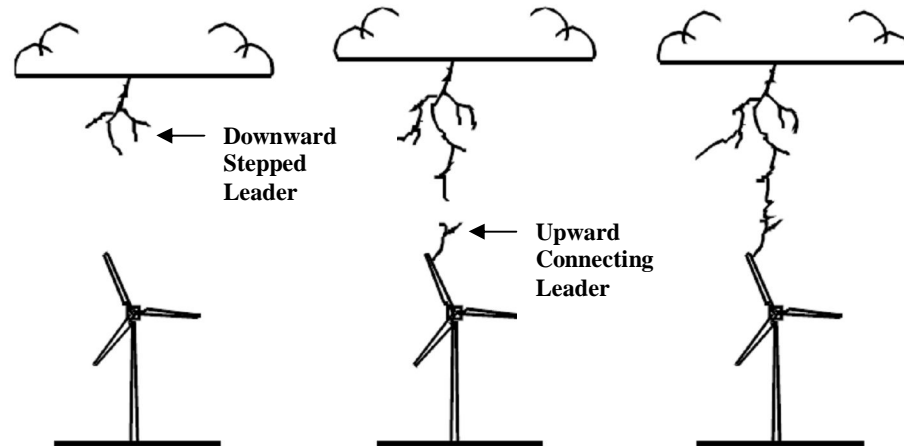


Figure 2 - Formation of downward flash – Progressive steps

After a certain time interval, further subsequent return strokes may follow the path taken by the first return stroke.

- **Upward initiated flashes**

The charge in the thundercloud causes an elevation of the electric field on the surface of the earth and the electric field may be significantly enhanced at mountains or at tall structures like wind turbines. At such locations the electric field strength becomes large enough to initiate an upward moving leader from ground towards the thundercloud [1].

An upward initiated flash starts with a continuing current phase. On the continuing current impulse currents can be superimposed (figure 3). The continuing current phase may be followed by subsequent return stroke(s) along the same channel [1].

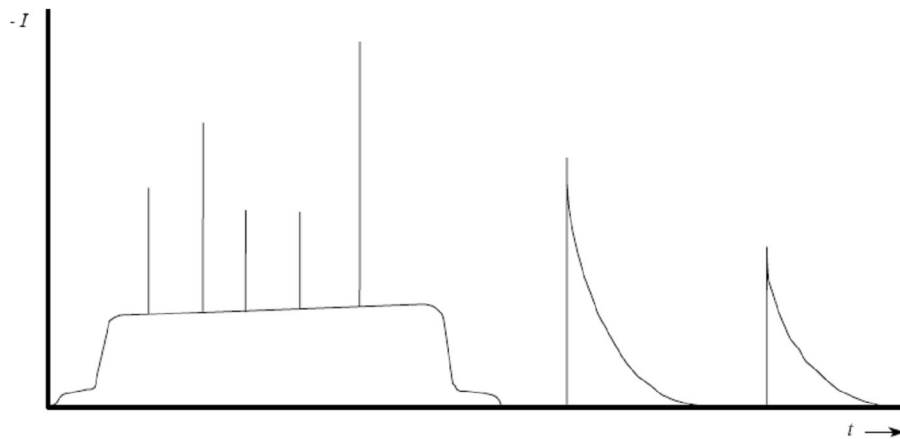


Figure 3 - Profile of a negative upward flash (not to scale)

Measurements of upward initiated discharge parameters are made on tall objects that are prone to this type of stroke. Research led by JANISCHEWSKYJ, W., HUSSEIN, AM., SHOSTAK, V., RUSAN, I., Li, JX., and CHANG,JS between 1975 and 1995 stated that the CN tower in Toronto, Canada receives at least 50 such flashes per year [14].

The location where an upward lightning stroke attaches to a structure is simply the same point where the upward leader is formed. Although the current peak values of about 10 kA are relatively low, the charge transfer associated with the initial continuing current can be as high as 300 C [1].

Upward initiated discharges, too, may be composed of various combinations of the different current components mentioned above.

2.1.2. Risks of Lightning strikes

As wind turbines are preferentially placed at high and windy locations in order to achieve high productivity, they are also subjected to a relatively high risk of lightning strikes.

An important initial step in a risk analysis is the estimation of the frequency of direct strikes to the wind turbine. This frequency is mainly a function of the lightning activity at the installation site, the local geographical topology, and the dimensions of the turbine.

The estimation of the frequency of direct lightning flashes to the wind turbine is a first step of a risk analysis.

The next step is an investigation as to whether the lightning protection system being installed is adequate. The considerations for this step of the risk analysis are based on the fact that not every lightning flash to the turbine causes damage, depending on the efficiency of the lightning protection system.

A failure of the lightning protection system is called a “critical event”. IEC 61024-1-1 [1] states that the number of permitted annual critical events N_c may be expressed by:

$$N_c \geq N_d \times (1 - E) \quad (1)$$

where E is the lightning protection system efficiency;

N_d is the number of annual average number of direct lightning strikes to the structure;

N_c is the permitted annual number of critical events.

The minimum lightning protection system efficiency can be defined following the concept taken up in IEC 61024-1[1]:

$$E \geq 1 - \frac{N_c}{N_d} \quad (2)$$

Thus, four lightning protection system levels can be defined (level I through level IV). These Protection levels are shown below in table 1.

Protection levels	Interception efficiency E_i	Sizing efficiency E_s	Efficiency $E = E_i \times E_s$
I	0,99	0,99	0,98
II	0,97	0,98	0,95
III	0,91	0,97	0,90
IV	0,84	0,97	0,80

Table 1- Lightning protection system levels

The lightning protection system efficiency is a product of two individual efficiencies, the interception efficiency (ability to intercept a flash) and the sizing efficiency (ability to safely conduct the flash current).

A level I lightning protection system must be able to carry higher peak current value without damage.

According to IEC61024-1 [1], these data are the basis for analytical calculations, tests, and simulations of the lightning protection system of the wind turbine being considered. More detailed risk analyses must be carried out for the various selected areas of the system. In order to calculate the risk of damage for these areas it is necessary to determine the electro-magnetic field distribution. This field distribution depends on the lightning current path from the point of impact to the ground.

2.2. LIGHTNING INTERACTION WITH WIND TURBINES

As mentioned above, wind turbines are placed at high and windy locations in order to achieve high productivity; they are then subjected to a relatively high risk of lightning strikes.

Several research efforts have been undertaken in the past to determine the responses of distribution systems to direct or nearby lightning strikes.

2.2.1. Damage Mechanism

2.2.1.1. Current and Voltage path on the turbine

In 2007, a work supported in part by the grant-in-aid for scientific research in Japan was presented at the International Conference on Power Systems Transients (IPST'07) in Lyon, France by K. Yamamoto, T. Noda, S. Yokoyama and A. Ametani. The project consisted on studying lightning overvoltages in Wind Turbine Generation Systems [15].

- **Modeling**

A reduced-size model, as shown in Fig. 4, was used by the researchers in the experiments. It was a 3/100-scale model of an actual wind turbine generation system that has blades with a length of 25 m and a tower that is 50 m high. The material of the blades was vinyl chloride, and an insulated copper wire with a cross sectional area of 2 mm² is traced on each blade to represent a lightning conductor. The tower of the scale model was of the tubular-type with an outer diameter of 10 cm and a thickness of 3 mm. The nacelle was a metal cube with a side length of 15 cm [15].

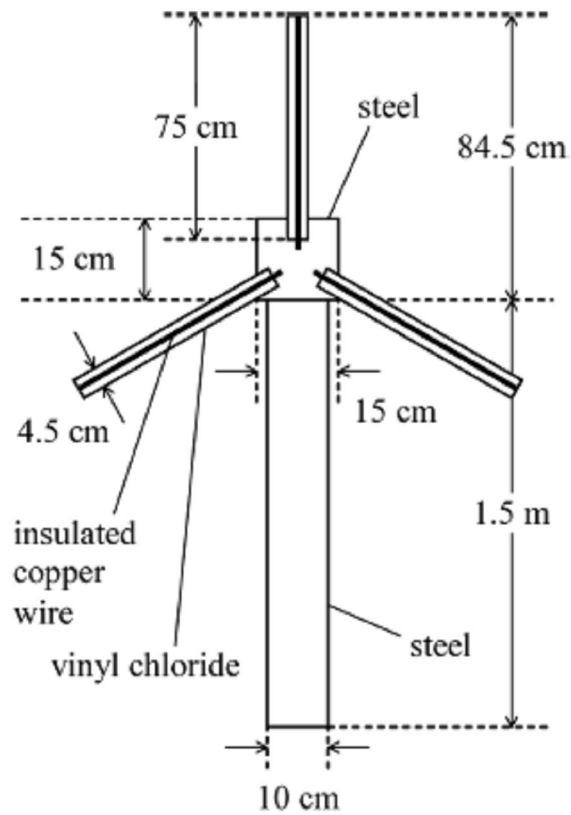


Figure 4 - Reduced size model of a wind turbine generation system

The time axis of the measured voltages and currents was compressed 3/100 times according to the scale of the reduced-size model. The scale didn't have any effect on the impedances and voltage rises obtained from the measurements.

The pulse generator was set up above an assumed point of lightning strokes; this point is the tip of one of the blades or the rear portion of the nacelle, as shown in Fig. 5.

A fast front current was generated by a 63-V battery pulse generator and was discharged via a mercury relay. A resistance of 9.4Ω , which represents the grounding resistance, was radially inserted between the tower foot and the copper plate.

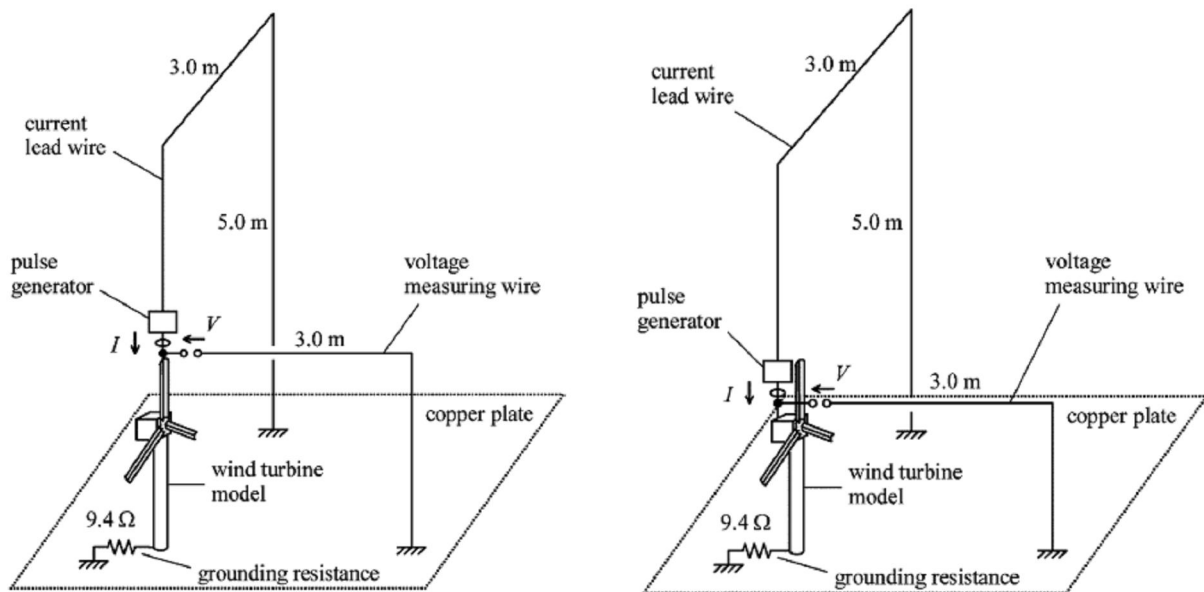


Figure 5 - Configuration of the experimental setup

- **Experimental cases**

Three experimental cases were investigated where the injected currents I and voltages V at the points of strikes are measured - A: point of strike is the tip of the blade and B: represents point of strike in the nacelle

- Cases 1-A and 1-B: V_1 represented the voltage difference between the tower footing and an incoming conductor which was an insulated copper wire traced on a copper plate from a distant point and grounded at the remote end. The large earth capacitance of the traced conductor is comparable to that of the coaxial cables in actual cases of wind turbine generation systems.

- In Cases 2-A and 2-B: a down conductor is set up inside the tower at a distance of 1 cm from the inner surface. The top end of the down conductor is short-circuited to the tower, and the bottom end is open-circuited to measure the voltage V_2 with respect to the incoming conductor. The down conductor represents a power line between the generators in the nacelle and a power converter on the ground level installed inside the tower.
 - Cases 3-A and 3-B: experimented to understand the induced voltage in the loop circuit that exists in power, telecommunication, and control equipment. A loop conductor was placed inside the tower at a height of 1 cm from the copper plate and at a distance of 1 cm from the inner surface of the tower. The voltage V_3 induced in the loop conductor is measured.
- **Experimental results**

In Fig. 6 shows the injected currents and the voltages measured at the stroke points for Cases 1-A and 1-B.

A few differences exist between the injected currents in Cases 1-A and 1-B; however, the current rise time in both cases was approximately 10 ns, and the waveform can be considered a ramp wave. The voltage response rise time was approximately 5 ns in case 1-A and 10 ns in case 1-B.

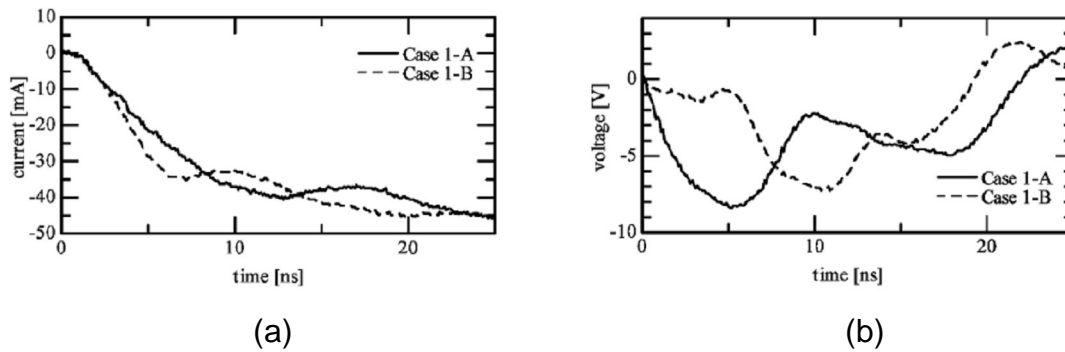


Figure 6 - Measured results for case 1-A and 1-B

The waveform was explained by the researchers as follows: when current was injected at the tip of the blade equipped with a parallel lightning conductor, the current propagated along the lightning conductor. During that process, electric and magnetic fields generated around the lightning conductor increased, resulting in an increase in the voltage at the tip of the blade. After the traveling wave reached the nacelle, the surge impedance of the nacelle was smaller than that of the lightning conductor; therefore, a negative reflection was caused at the nacelle, and the negative traveling wave returned to the tip of the blade. The electric and magnetic fields around the blade started to decrease; further, the voltage at the tip attained the peak value when the negative reflected wave reached the tip.

As the return propagation time of the blade was 5 ns, the peak of the voltage appeared after approximately 5 ns. The second peak of the voltage at approximately 20 ns was mainly influenced by the surge impedance of the tower, and the traveling waves on the lightning conductors that have an open end were superimposed on the voltage.

As soon as current was injected into the rear portion of the nacelle, the traveling wave dispersed to the three blades and the tower. Because these surge impedances were connected in parallel, the voltage rise was small at first.

Subsequently, the positive traveling waves returned to the nacelle from the open-end tips of the blades, and the voltage at the rear portion of the nacelle started to increase because of the current flow through the tower.

The voltage rise exhibited a peak when the negative traveling wave at the tower foot reached the nacelle. The traveling waves on the lightning conductors that have an open end were superimposed on the voltage.

Based on the theories of traveling waves, if the return propagation time between the injected points of the current and the tower foot is greater than the rise time of the injected current, the maximum voltage rise at the stroke points depends on the peak of the current and not on the rise time.

From the results, they stated that the voltage rise at the tower foot in those measurements depended only on the peak of the injected current.

They calculated the voltage rise per unit current as follows:

$$R_{\max} = \frac{V_r}{I_{\text{peak}}} \quad (3)$$

In Case 1-A, they obtained a voltage rise per unit current of 48 V/A. In Case 1-B, the voltage rise per unit current is calculated as 46 V/A

In Cases 2-A and 2-B, the down conductor does not have a significant effect on the current waveforms; the current waveforms are similar to the result of Cases 1-A and 1-B. Since the top of the down conductor was short-circuited to the tower and enclosed in the tower; the voltages of the down conductor and the tower foot were almost identical electrostatically. Therefore, the voltage at the bottom of the conductor as well as that at the tower foot rises. However, since the bottom of the down conductor and the tower foot were not short-circuited, some differences exist between these voltage rises. In Case 2-A, the voltage rise per unit current was calculated as 30 V/A. In Case 2-B, the voltage rise per unit current is calculated as 46 V/A.

At last in Cases 3-A and 3-B, the injected current was almost the same as that in Cases 1-A, 1-B, 2-A, and 2-B; therefore, the loop conductor placed inside the tower does not influence the injected current. If the electromagnetic field caused by the traveling wave flowing through the tower body expands as a plane wave such as a TEM (transverse electromagnetic) wave and the current density in all sections of the tower was uniform, the loop magnetic field in the tower didn't exist theoretically.

Nevertheless, the induced voltage in the loop conductor could be measured; it is believed that the electromagnetic field didn't expand as a plane wave or the current density was not uniform. The results showed the researchers that values of the maximum induced voltages depended on both the wave front of the injected current and its peak value. Therefore, it was difficult to normalize the induced voltage. However, it was confirmed that the induced voltages were significantly larger than the electromagnetic noise.

According to these results, one can say that when lightning currents flow through a wind turbine large magnetic fields are produced. If these changing magnetic fields pass through a loop they will induce voltages within that loop. The magnitude of the voltage is proportional to the rate of change of the magnetic field and the area of the loop in question.

A summary of the damage mechanism can be done now:

- *Overvoltages due to voltage rise at the tower footing*

When lightning strikes a wind turbine, a voltage difference is caused between the tower footing and the incoming conductor from the top of the structure.

That voltage difference is caused by the voltage increase at the tower footing. Further, a voltage difference between the bottom of the down conductor installed inside the tower and the incoming conductor is rather significant. The lightning current flowing through the tower body induces voltage in the main and control circuits that form loops, and the induced voltages are sufficiently larger than the electromagnetic noise.

In most of the cases, that voltage difference becomes an overvoltage between the power line and the power converter or transformer on the ground level installed inside the tower or that between a communication line and a telecommunication device. The average value of the peak lightning current is 24 kA. When lightning corresponding to this average value of the peak current strikes a wind turbine generation system, the maximum overvoltages produced are in the range of 700 kV to 1100 kV

- *Overvoltages in the loop circuit*

The induced voltage goes into the loop conductor in the tower; this indicates that the electromagnetic field caused by the traveling wave flowing through the tower does not expand as a plane wave or the current density of all sections of the tower is not uniform. Over voltages and malfunctions are then induced in the loop circuit in the main and control circuits in the tower.

- *Traveling-wave phenomena*

As mentioned, earlier, when current is injected at the tip of the blade equipped with a parallel lightning conductor, the current propagates along the lightning conductor. After the traveling wave reaches the nacelle, a negative reflection is caused at the nacelle, and the negative traveling wave returns to the tip of the blade. The voltage at the tip reaches the peak value when the negative reflected wave reaches the tip again.

When current is injected in the rear portion of the nacelle, the injected current disperses to the three blades and the positive traveling wave returns to the nacelle from the tip of the blades. The voltage at the rear portion of the nacelle rises because of the current flowing to the tower. The voltage rise exhibits a peak when the negative traveling wave at the tower foot reaches the nacelle.

Figure 7 shows example of generated overvoltage in the loop circuit due to voltage rise at the tower base.

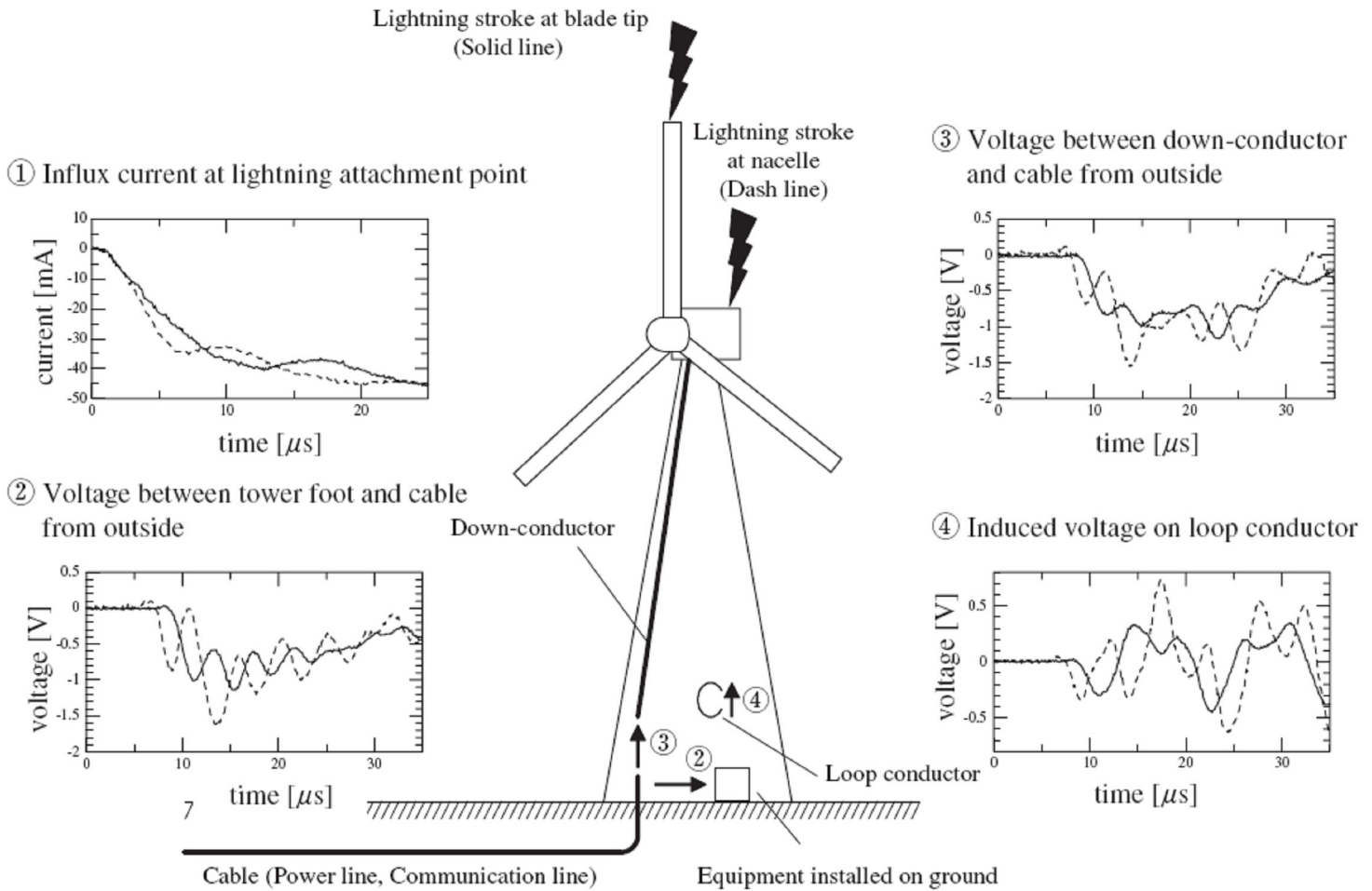


Figure 7 - Generated over voltage between down-conductor and lead-in cable

2.2.1.2. Damage on blades and bearing

Damage mechanism on blades and inside the generation system can also be looked at in more detail.

The researcher Cotton in the high voltage group at UMIST in Manchester, England, has written a very useful document for the wind turbine designer. They have been extensively researching blade protection, bearing damage simulation since the mid 1990s with European Commission and UK Department of Trade funding [3].

They have been working with turbine manufacturers and operators, other high-voltage labs, and the National University of Athens. Their wind turbine application-specific research is unique.

- **Blade damage mechanism**

They have shown that the blade serves as a preferential path for the lightning current in comparison to the air. A simple experiment within a high-voltage laboratory showed that was to be expected, since surfaces have lower electrical breakdown strength than the air around them [3].

They outlined that most severe damage to wind turbine blades was caused when lightning forms arcs inside the blade. The arcs may form in the air filled cavities inside the blade or along the internal surfaces.

In their report [3], Cotton et al showed that when lightning attached to an unprotected wind turbine blade that contained no metallic parts, it could travel in one of three locations. It could travel on the outside surface, the inside surface or within the blade laminations.

Lightning attaching to an unprotected blade usually took more than one of these paths, creating a type of damage that could be described as stitching. This occurred when a lightning discharge made a hole in the blade, progressed a certain distance inside the blade and then jumped back out. This might happen repeatedly, leading to a stitching pattern such as the one shown in Figure 8



Figure 8 - Stitch pattern in a blade surface

Cotton et al stated also that lightning discharge could cause a temperature rise of approximately 30,000 K and produce a high-pressure shock wave that can exert a large force. This shock wave would be heard as thunder if it was propagating through air. The length of the arc and the blade construction were two of the factors that would determine the level of observed lightning damage following the lightning strike [3].

Another type of damage was reported when the lightning current or part of it was conducted in or between layers of composite materials, presumably because such layers held some moisture. The pressure shock wave caused by such internal arcs may literally explode the blade, ripping the blade surface skins apart along the edges and from the internal carrying spar.

The mechanism of damage started when internal arcs form between the lightning attachment point at the tip of the blade and some conducting component internal to the blade.

It was stated that with modern blade with a steel wire, the damage was often limited to the tip section, whereas the main blade remains unharmed. Damage to those blades has been found when an arc has formed inside the main blade. With blades using a flap in the outer of the leading edge, the main blade was destroyed.

According to their research, the phenomenon responsible for the severe structural damage to wind turbine blades was therefore the formation of a pressure shock wave around an arc of lightning inside the blade. Figure 9 shows an example of Lightning discharge on wind turbine blade model.



Figure 9 - Lightning discharge on wind turbine blade

Minor damage might occur when a lightning arc is formed on the outside surface or when the lightning current is conducted by metallic components with insufficient cross-section.

- **Bearing damage mechanism**

Cotton et al in their document [3] reported a UMIST's bearing damage simulation.

- *High-current Testing of Wind Turbine Pitch Bearings*

Simulated lightning current was conducted across stationary blade pitch bearings. The test samples were two bearing races approximately 0.6 m in diameter. One sample was a production bearing without preload and could be turned easily. The second had an effective preload applied by installing slightly oversized ball bearings, and had a running torque of around 60 N m.

In the test arrangement they could be lubricated with grease as would be the case in production bearings.

As shown in Figure 10, the current was conducted to the centre race of the bearing via a top plate which had several fixing bolts all round the circumference of the bearing. The current then left the bearing outer race via a lower plate which was similarly bolted around its circumference, and returned to the capacitor bank. The intention of this design was to allow current to flow through the bearing as uniformly as possible around its circumference.

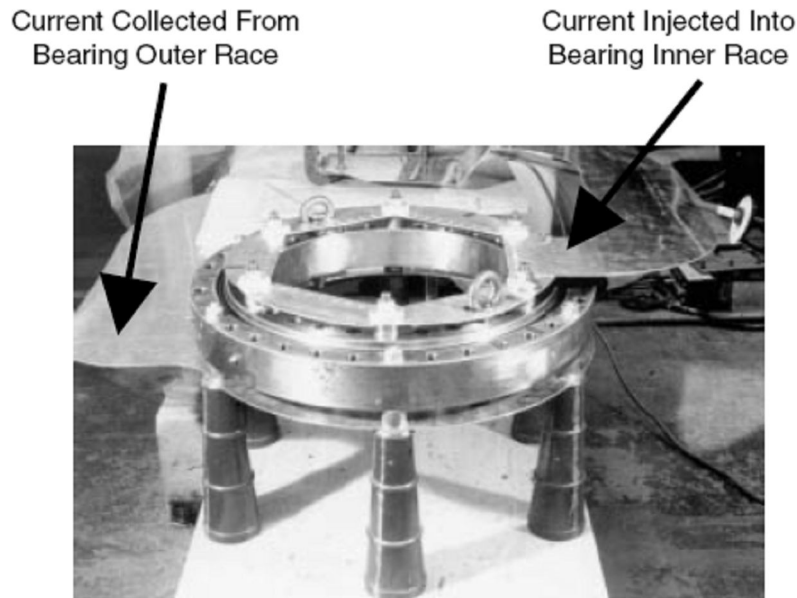


Figure 10 - Pitch bearing test arrangement

Tests were carried out with the pitch bearings in their production state and by applying both the high energy (component A) and the long-duration (component C) currents to simulate a severe lightning stroke.

Surface effects on only a few balls occurred and the damage was so slight as to be barely visible. The surface simply appeared slightly abraded over an area of up to 4 mm d 1 mm. For both the unloaded and preloaded bearings the damage was therefore deemed by the bearing manufacturer to be insignificant. The addition of large quantities of grease to the bearing made no noticeable difference to the levels of damage for the loaded bearings.

The conclusion from this test was that when lightning current is conducted from blade to a stationary pitch bearings, it will pass through it with no big damage because of its conductive surface–surface metallic contact . Surface effects generally occur on only few balls and the damage is so slight as to be barely visible.

It was stated that stationary bearings can withstand the effects of lightning current with no significant damage.

However, bearings within a wind turbine normally rotate and an insulation oil film is normally present between the bearing elements.

The second set of tests was then designed to investigate the effect that this may have on the probability of lightning damage.

- *High current Testing of Rotating Bearings*

In a rotating bearing there will be a hydrodynamic lubricant layer between the roller/ball and the raceways, an intentional feature of bearing operation. Such a film would require a certain voltage to break down before an arc could form. Conduction of currents across an insulating barrier of this type (via a small arc) would be expected to generate relatively severe damage, similar to that produced by an arc welder. A test program to investigate the severity of this damage was carried out.

Two similarly sized sets of roller bearings of 150 and 170 mm internal diameter were used in the test program. They had been removed from a gearbox and therefore had some signs of wear, although there was no evident damage. These bearings tested were somewhat smaller than wind turbine main bearings.

However, as long as the hydrodynamic effects noted below are in operation for both types of bearing, testing a smaller bearing would give, if anything, worse damage.

It was important for these tests that the bearings were operating in a hydrodynamic regime. Advice on how to select such an operating regime for hydrodynamic lubrication was provided by a bearing manufacturer, whose data indicated that for 220 viscosity oil and a bearing diameter of 185 mm (at the rolling surface) the rotational speed should be at least 25 rpm.

For the tests described, a rotational speed of 65 rpm was selected. This was well within the hydrodynamic regime, the hydrodynamic lubricant layer being of the order of 10^{-6} m thick. The effect of loading on the bearing is to reduce further the film thickness, so efforts were made to keep any bearing loads to a minimum [3].

The two bearings were installed in a test rig back-to-back, in such a way that currents could be conducted through one or the other. For these series of tests, one bearing was tested while the rig was rotating at 65 rpm and the second was tested immediately afterwards while the rig was stationary. The same currents were applied for both tests. This provides a direct assessment of the effects of rotation on bearing damage.

The rotating bearing was fed continuously with lubricant during each test. No damage was visible on the stationary bearing during these tests at levels up to a maximum test of 70 kA ($0.25 \text{ MJ } \Omega^{-1}$). Visible damage occurred to the rotating bearing at a relatively low level of 41 kA ($0.04 \text{ MJ } \Omega^{-1}$).

Much more severe damage occurred at 67 kA ($0.24 \text{ MJ } \Omega^{-1}$) and consisted of several pits fairly evenly spaced around the race. The continued rotation of the bearing caused further numerous tiny indentation marks on the race, presumably because of the pitting damage on the rollers 'printing' its impression on the race. Figure 11 shows an example of the type of damage from the final 200 kA ($2 \text{ MJ } \Omega^{-1}$) test.

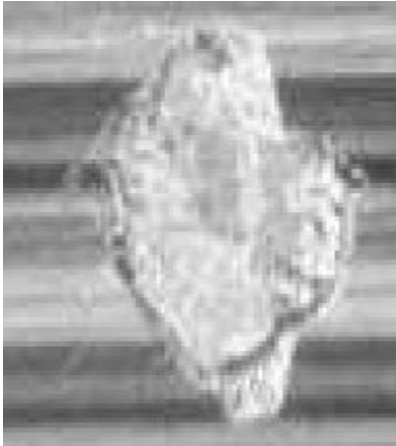


Figure 11 - Close-up of bearing damage caused by a high-current test

The conclusion from this test was that in a rotating bearing with a hydrodynamic lubricant layer between the roller/ball and the raceways (intentional feature of bearing operation), such a film would require a certain voltage to break down before an arc could form. Conduction of currents across an insulating barrier of this type (via a small arc) is expected to generate relatively severe damage, similar to that produced by an arc welder.

2.2.1.3. Comments

From these research works, we can make our own summary and conclusion about damage mechanism:

When lightning strikes a wind turbine blade, the lightning current will inevitably be conducted through the hub with one of the coupling mechanism to one or more electrical and mechanical components, damage and leakage could be caused.

If the nacelle is metallic it may even so have few electrical bonding points, usually only the hinges and latches.

In the event of a lightning strike to the blade the current flow is then not confined to the external nacelle skin (which would be ideal) but is partially along the floor of the nacelle, through the bearing, gearbox and generators and so on.

Wiring will also be exposed to induced voltage transients where it transfers from gearbox or generator to the bed plate. The problem here is the few paths (or constricted paths) for the current flow so that current densities are high, especially if there are anti-vibration mounts with bonding straps across; or electronic connections in the path of the current, which will then be exposed to high magnetic fields and induced transients.

Although protected from direct lightning attachment, the wiring running down the mast is exposed, and will have voltages induced between the wiring and the structure which may be of sufficient to cause flashover and directly inject current into the wiring.

Many sensors in the hub have circuitry which is isolated from its case. Where lightning induces voltages in this circuit, the voltage will stress the highest impedance in the loop, which is the insulation between the case and the circuit.

There is no solid evidence available about damage to gears due to lightning. There have been cases where gears and shaft bearings have been damaged in connection with lightning striking the wind turbine blades. However, so far, it has not been established if such damage is a secondary effect of main bearing lightning damage

2.3. METHOD OF ANALYSIS AND COMPUTATIONAL MODELS

2.3.1. Lightning incidence modeling

A J Eriksson published a paper [24] where he addresses the lightning attractive radius concept and procedures for estimating the number of lightning flashes with particular reference to power lines.

According to the author, in general, excluding local topographic effects, two main factors influence the incidence of direct lightning strikes to practical transmission and distribution lines:

- The regional incidence of lightning in the Area: the annual average ground flash density, N_g (flashes/km²/yr) or, the regional keraunic level T_d (thunderstorm days per year).
- The "attractiveness" of the line and its supporting structures (i.e. the distance over which the line attracts lightning strokes).

The purpose of his paper was to summarize the available data in respect of the observed incidence of lightning to practical structures – including power lines - and thereby to derive expressions for the actual "attractiveness" or attractive area presented by these structures.

He showed that in 1978 [20], researchers assumed a linear relationship with ground flash density ($N_g = 0,1 \times T_d$) – in accordance with the then available literature relating N_g to T_d [21].

But Subsequent to earlier analysis, a wide scale deployment of some 400 lightning ground flash counters throughout Southern Africa [22] provided a unique opportunity to examine the correlation between regional observations of N_g and T_d across a wide range of variations in keraunic level and resulted in the relationship:

$$N_g = 0.04 \times T_d^{1.25} \quad (4)$$

N_g = annual ground flash density ($\text{km}^{-2} \text{yr}^{-1}$)

T_d = thunderstorm days per year

The resultant normalized annual incidence of strikes - for structures having heights varying between 20 m and 500 m assuming a power law trend was then obtained by:

$$N_s = 2.4 \times 10^{-5} H^{2.05} \quad (5)$$

where N_s = average number of strikes per year for $N_g = 1 \text{ km}^{-2} \text{yr}^{-1}$.

H = structure height in meters

However (i.e. around 1944), McCann amongst others, [23] observed during lightning studies on a variety of structures that an increasing proportion of flashes on taller structures (i.e. having heights in excess of about 100 m), were initiated by upward progressing leaders - in contrast to flashes observed on shorter structures, which invariably involved downward leaders.

In the course of the original study of lightning strike incidence [20], the available data on the relative incidence of upward flashes as a function of structure height were also analyzed and they yield the formula:

$$P_u = 52.8 \times \ln H - 230 \quad (6.a)$$

with H in meters

where P_u (in %) is the proportion of upward flashes to a structure, as a function of structure height which is valid in the range of: $78 \leq H \leq 500$

However, upward flashes may still be possible on shorter structures, and an expression was developed: $pu = 1.26 \times 10^{-4} H^{1.48}$ (6.b)

Where pu is in per unit and H in meters

Equation 5 which represents the incidence of flashes of both types combined was then combined with equation 6.b above, to yield a relation for the derived incidence of downward flashes alone - N_d - as a function of structure height: $N_d = N_s(1 - pu)$ leading to:

$$N_d = 2.4 \times 10^{-5} H^{2.05} - 3.0 \times 10^{-9} H^{3.53} \quad (7)$$

The trend of this expression is shown in Figure 24 and, as may be expected, indicates that the contribution of upward flashes to total flash incidence only becomes significant at structure heights well in excess of 100 m.

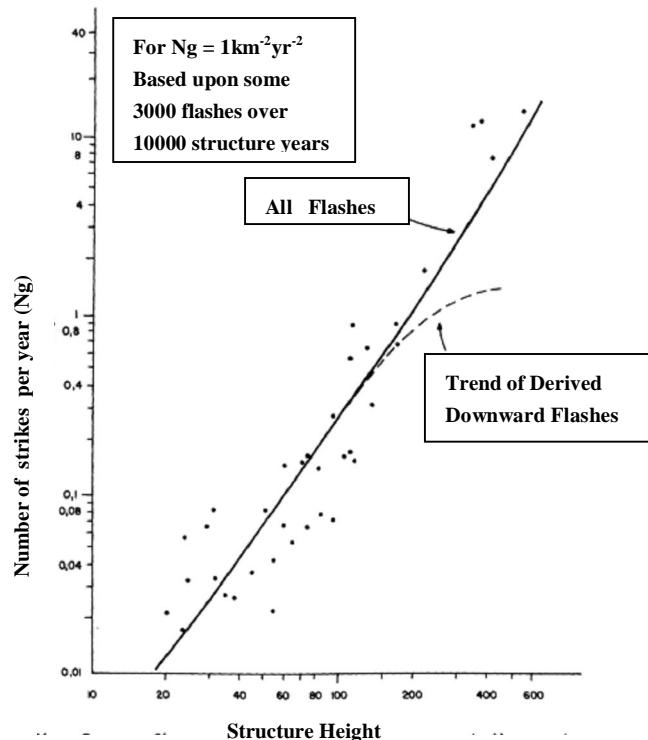


Figure 12 - Observed incidence of strikes to structures of various heights [24]

2.3.1.1. Concept of Attractive Radius

Eriksson took into account the knowledge of regional ground flash density N_g . Given that, the average annual incidence of downward flashes to the structure, N_d , could be represented in terms of an equivalent attractive area, A :

$$N_d = N_g \times A \quad (8)$$

where A is in $\text{km}^2 = \pi r^2 10^{-6}$ for a particular structure,

Taking into account a power curve estimation [24], the attractive radius R_a could be estimated from the observed strike incidence to the structure, using the expression:

$$R_a = 16,6 \times H^{0,55} \quad (9)$$

This equation expressed the average attractive radius presented by structures of various heights - up to at least 100 m.

2.3.1.2. Comparison with analytical model

Previously Golde [25], developed a simple model for estimation of the lightning striking distance on the assumption that a leader charge of 1 C was approximately equivalent to the average stroke current amplitude of 20 kA, he suggested that structure "protective" radii (i.e. attractive radii) could, on average, be expressed by:

$$R_a = 2H \quad (10)$$

In an extension of earlier modeling concepts, Eriksson applied the modern knowledge of lightning parameters and the improved understanding of the mechanisms of leader development during the breakdown of large air gaps, to a study of the simple analytical model depicted in Figure 13.

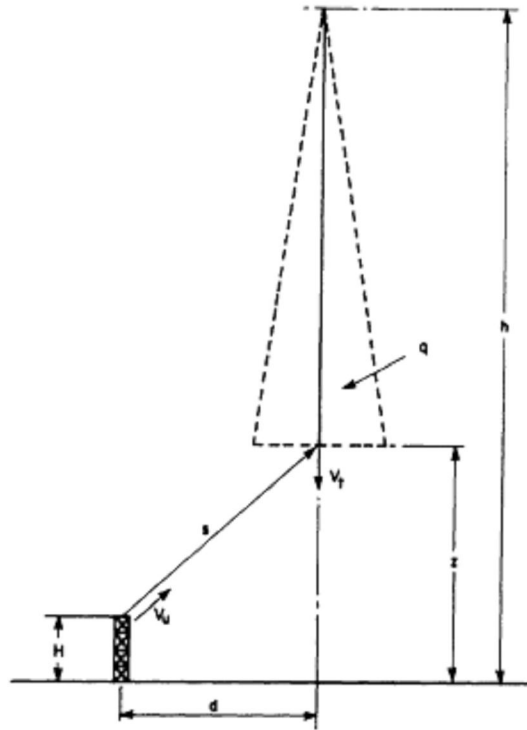


Figure 13 - Representation of a downward leader element approaching a structure of height, H. [24]

The modeling embodied the following aspects:

- The structures were regarded as free-standing and capable of approximate representation by cylindrical geometry
- A major branch of a nearby approaching downward lightning leader was represented by a vertically descending linearly charged leader element.
- The prospective stroke peak current available from that leader element, was related to the integrated leader charge.
- The electric field enhancement at the structure top caused through its protrusion above ground level was expressed in terms of a field enhancement factor - which in turn was derived from the structure dimensional ratio.
- Standard atmospheric conditions were assumed, and the criterion for the initiation of an upward leader is taken at a critical field intensity of 3×10^6 V/m.

Iterative routines were developed for carrying out calculations over a comparatively wide range of the parameters involved (i.e. structure height, leader charge, etc.) and illustrative results for two structure heights are depicted in Figure 14.

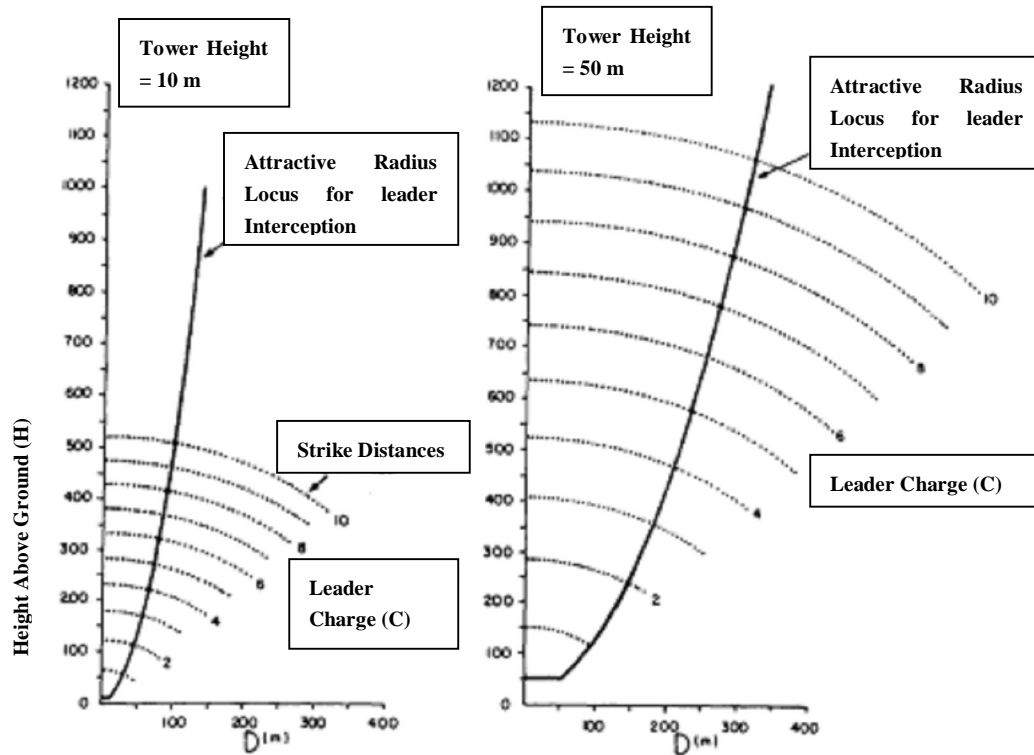


Figure 14 – Comparative downward leader striking distance analyses-as determined through analytical modeling [24]

In terms of this model, the structure attractive radius - for a specific value of leader charge - is defined by the sectional radius of this collection volume - at the particular striking distance.

By repeating the calculations over a broad range of structure heights and lightning parameters, it was possible to derive generalized relationships between attractive radius and structure height - as a function of prospective stroke current as illustrated in Figure 15.

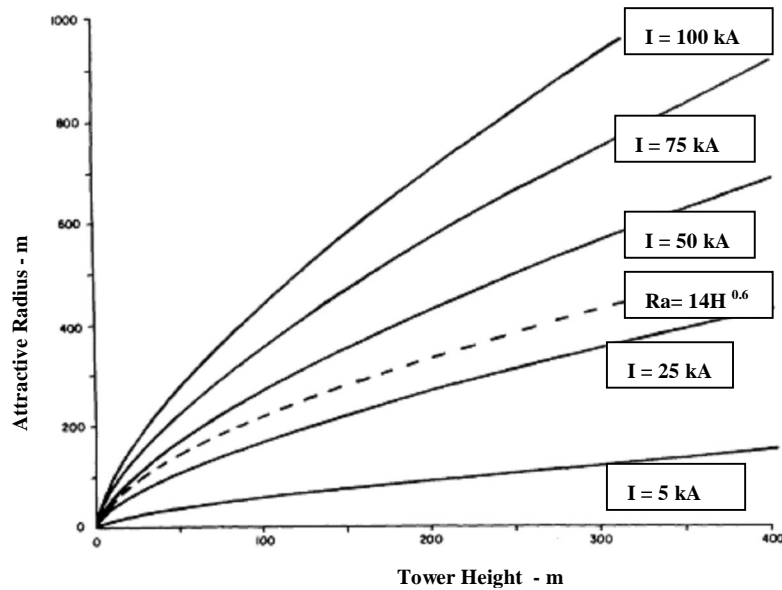


Figure 15 - Attractive radii in relation to tower height and peak current [24]

Estimates of structure attractive radius yields the expression [33]:

$$R_a = 14 H^{0.6} \quad (11)$$

Taken into account a range of power line structure heights of (say 10 - 100 m), a median current amplitude $I_g = 35$ kA, and that both analytical and empirically derived expressions of the broad dispersion should be combined into a simplified expression [24].

But in practice, it was evident that the individual attractive radii presented by structures will vary on a stroke by stroke basis, depending upon the relative stroke intensities.

2.3.1.3. Comparison with power line observations

A J Eriksson examined to what extent trends and concepts of attractive radius were also applicable to power line geometries. He adopted the concept of a shadow width, or attractive swath of horizontal dimensions R_a on each side of the line - in accordance with common practice.

He assumed an annual strike incidence to a line expression to be [24]:

$$N = Ng(b + 2Ra) \times 10^{-1} \text{ per 100 km per year} \quad (12)$$

Equation 12 was applied to an analysis of the observed lightning strike incidence data to lines, to derive the equivalent attractive radii presented by the lines.

The resultant estimates [24] is shown in Figure 16 – together with the trend of the suggested simplified estimating expression ($R_a = 14 H^{0.6}$).

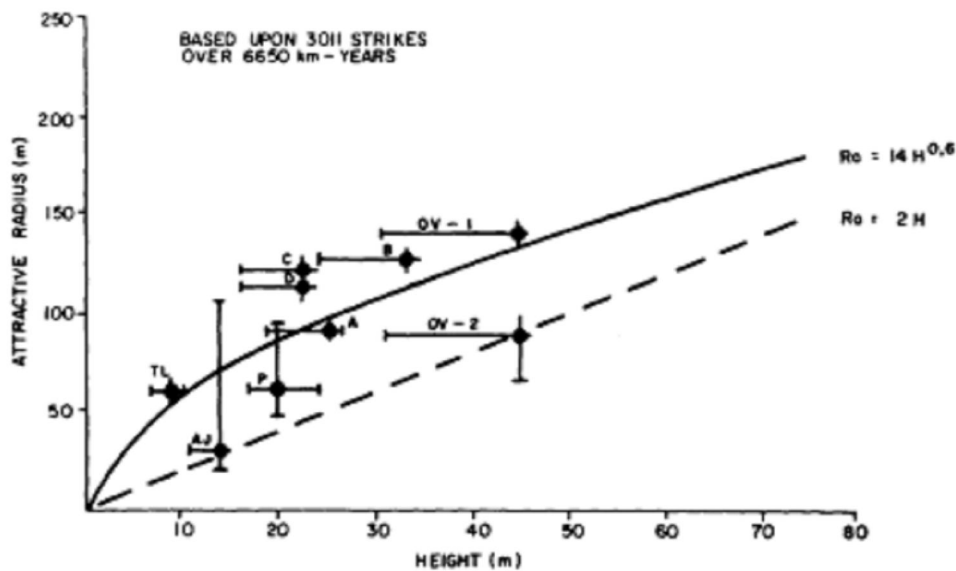


Figure 16 - Equivalent attractive radius for lines – derived from the observed strike incidence on practical power lines [24]

One can see that these estimates of power line attractive distance (as derived from the observed strike incidence to these lines) cluster comparatively closely to the trend of the simplified expression for average attractive radius. But, the trend of the traditional assumption that $R_a = 2H$, displays considerable deviation from the observed data, and in relation also to the attractive radius expression.

This deviation is particularly large in the lower range of structure heights (i.e. below about 30 m).

An important aspect here, is that perhaps the most rigorous source of line performance data in this height range (the 11 kV test-line data), agrees well with the average attractive radius estimation, but deviates considerably from the $R_a = 2H$ trend.

At the end of his paper, A J Eriksson concluded that there was sufficient consistency in the trends of the empirical data on observations of strike incidence to structures and lines together with that of the analytically derived relationship, to suggest that the modified form of estimating expression should yield more realistic estimates of the expected strike incidence to power lines - especially in relation to the earlier 2H-based relations [24].

2.3.2. Recent lightning exposure modeling

Up to the 90's, designs of the lightning protection of structures have been faced using the empirical approach based on the "striking distance" concept. E.Garbagnati and L.Dellera published a paper [39] in 1989 where they presented a model of lightning channel progression towards the earth based on the knowledge on physics of discharge on long air gaps.

Their approach is based on the idea that a substantial similarity exists between lightning phenomena and discharges in large air gaps [40].

2.3.2.1. Description of the model

The simulation of the development of lightning channels is schematically shown in Fig. 17.

The mathematical description of the phenomena requires an evaluation of the electric field strength, repeated at different times, in order to simulate the actual charge displacement into leader channels related with the progression of the leaders.

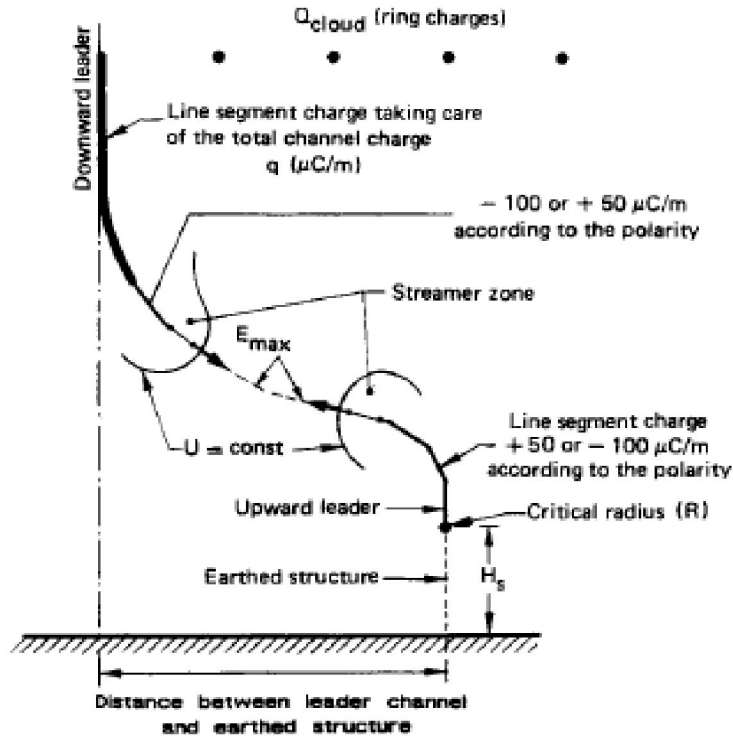


Figure 17 - Sketch of the step-by-step progression of the lightning as simulated in the calculation [39]

The calculation of the field was done by means of the well-known charge simulation method. The three basic kinds of flashes (upward flash, downward flash to earth and downward flash to the structure) which can occur in nature were simulated in the computer program.

2.3.2.2. Simulation of the downward leader

The following considerations and assumptions were applied to the various leader characteristics:

- Leader charge

To assure leader propagation in large air gaps (order of 10-30 meters), the charges per unit leader length observed in laboratory were approximately:

- 50 $\mu\text{C}/\text{m}$ for positive leaders
- 100 $\mu\text{C}/\text{m}$ for negative leaders

- Leader velocity

The mean velocity of advancement of negative leaders was found to be of the order of 5 to 10 $\text{cm}/\mu\text{s}$ for sparks up to 14 m length, with a tendency to increase with the gap length [40].

The mean velocity of advancement of positive leaders, measured in laboratory discharges, was much lower than that of negative (say 1.5 $\text{cm}/\mu\text{s}$) [40].

- Streamer length

Was essentially based on extrapolation of laboratory data [39] assuming that streamers could attain zones characterized by field strength of about 3 kV/cm .

- Leader propagation

As the lightning model, for the time being, did not take into account the tortuosity, the direction of propagation of the leader was directly related to the electric field and was determined as the direction of maximum gradient, at a distance from the leader tip equal to the streamer extension.

2.3.2.3. Simulation of the upward leader

- Leader inception

Tests were performed in a sphere-plane configuration with a constant clearance of 7 m, varying the radius of the earthed sphere and taking some time solved pictures of the discharge.

The progression of the discharge indicated that the discharge consists of a positive leader, originating from the earthed sphere, without any corona phenomenon at the negative energized electrode.

Figure 18 reports the 50 percent breakdown voltage (U_{50}) and the leader inception voltage (U_1) as function of the equivalent radius of the sphere (R_{eq}).

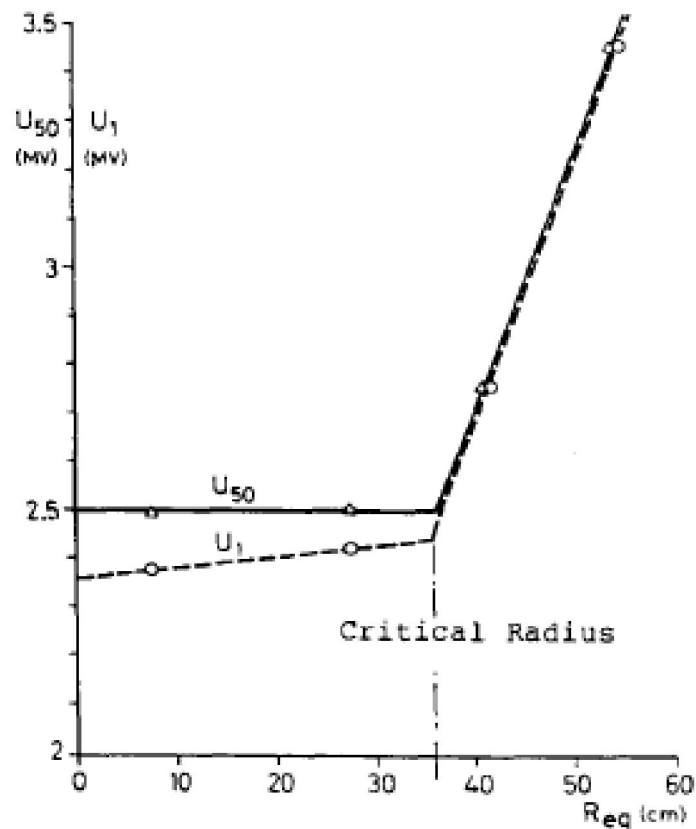


Figure 18 - U_1 and U_{50} versus R_{eq} [39]

The results confirmed that the breakdown voltage and the leader inception voltage were fairly independent of the radius of the earthed electrode up to the critical value of 35 cm

- Leader charge

On the basis of laboratory experience [40] average charges of $50 \mu\text{C}/\text{m}$ and $100 \mu\text{C}/\text{m}$ were taken for positive and negative upward leader respectively.

- Leader velocity

For negative flashes (negative downward and positive upward leaders) a negative leader to positive leader speed ratio of **4/1** has been taken at the inception of the upward leader as typical of both laboratory and field data. Moreover it was assumed that this ratio changes during the development of the upward leader, reaching the **1/1** value just before the connection of the two leaders.

For positive flashes, positive downward and negative upward leaders, due to the limited data available, for the time being, only tentative calculations were made with **1/1** constant ratio.

- Streamer extension

The positive streamer extension was evaluated as the length between the leader tip and the point defined by the intersection of the actual potential distribution curve with a straight line of slope 500 kV/m both computed following the maximum field strength line.

- Leader propagation

The direction of propagation of the positive leaders has been determined in the same way as for the downward negative leader.

2.3.2.4. Modeling of the clouds

In view of adopting a simplified simulation of cloud charges, an estimate of the unipolar equivalent charge which was necessary to cause the inception of upward leaders from earthed structures was made looking at the values of the charge necessary to cause the corona inception from the critical earthed electrode in the following two conditions: [39]

- A bipolar charge having a 10 km extension, uniformly distributed, with the heights of the negative and positive charges of 3 and 4 km, respectively;

- A unipolar negative charge (simplified condition) with an extension of again 10 km, uniformly distributed, at a height of 2 km.

2.3.2.5. Results of the Model

The application of the model to an earthed structure with a selected horizontal distance between the downward channel and the considered structure allowed to define the point of impact.

To evaluate the exposure of a structure to lightning, the maximum horizontal distance at which the downward channel still strikes the structure shall be defined, and was referred as "lateral distance-LD" .[39]

An example of application of the model to a free-standing structure is shown in fig. 19, for a current of 21 kA.

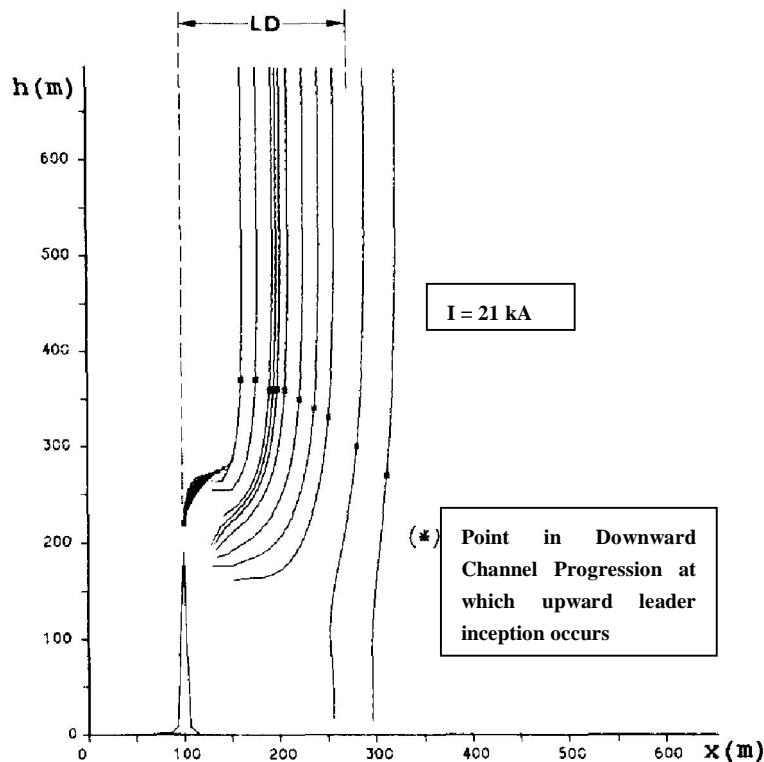


Figure 19 - Example of the application of the model to a free-standing structure 220 m height [39]

In the same way the sky zone from which the lightning can reach an object avoiding protective device could be derived and was referred as "shielding failure width-SFW".

Fig. 20 shows, as an example, the picture of the computed leader paths in the vicinity of a 420 kV transmission line placed in different orographic conditions,

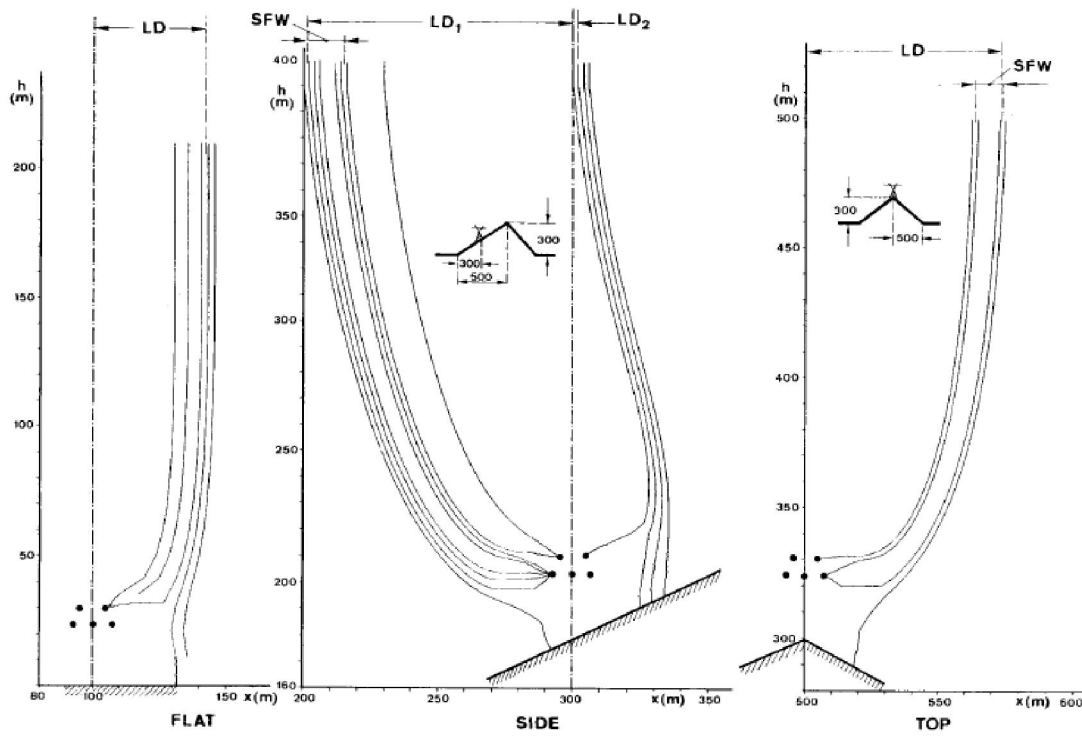


Figure 20 - Example of the computed leader paths of a 420 KV line in different orographic conditions [39]

By many computations, it was possible to derive the lateral distance and the shielding failure width for earthed structures characterized by different heights and Fig. 21 (a) reports the curves of the computed lateral distance as function of lightning current amplitude.

The shielding failure width as function of lightning current amplitude is reported in fig. 21 (b) for a shielding angle of 20 degrees.

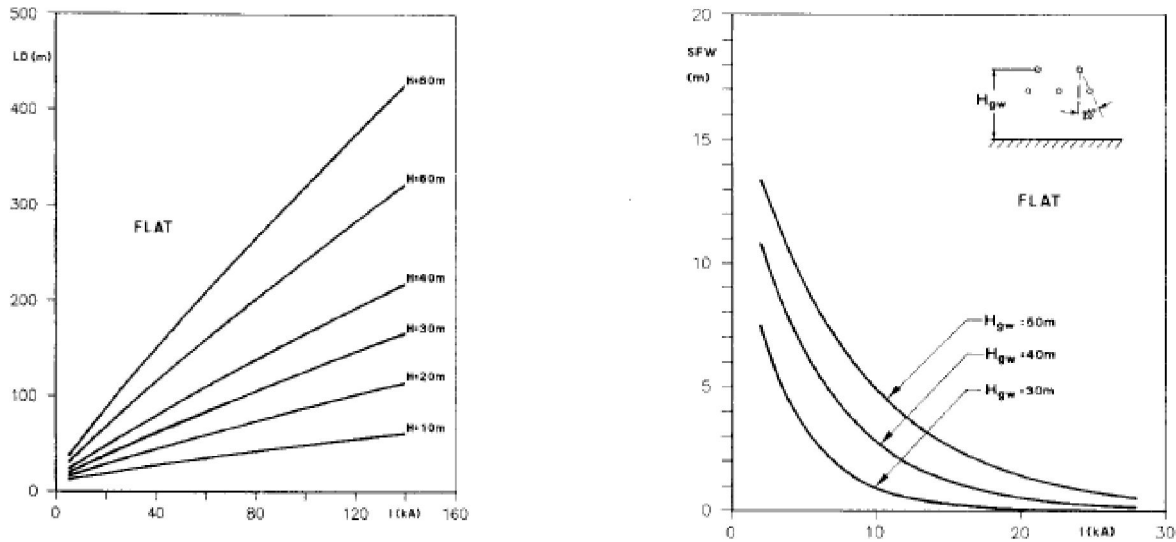


Figure 21 – (a) Computed lateral distance as function of lightning current of a structure of different height (b) Shielding failure width as function of lightning current of a 420 KV line with a shielding angle of 20 degrees [39]

The evaluation of the number of lightning flashes to a structure (N_s) could be then carried out considering the ground flash density (N_g) and the equivalent exposure area (A_{eq}) by using:

$$N_s = N_g \times A_{eq} \quad (13)$$

where $N_g = K.(TD)^\alpha$ and the values of the constants currently being used are $K=0.04$ and $\alpha = 1.25$

2.3.2.6. Check of the Model

In order to check the validity of the model as a whole, a comparison of the computed exposure with field records was carried out.

Field records obtained by different researchers on free-standing structures [41-46] are reported in fig. 22 which shows the number of lightning flashes on each structure per year (N_s) as function of the height of the structure itself (h).

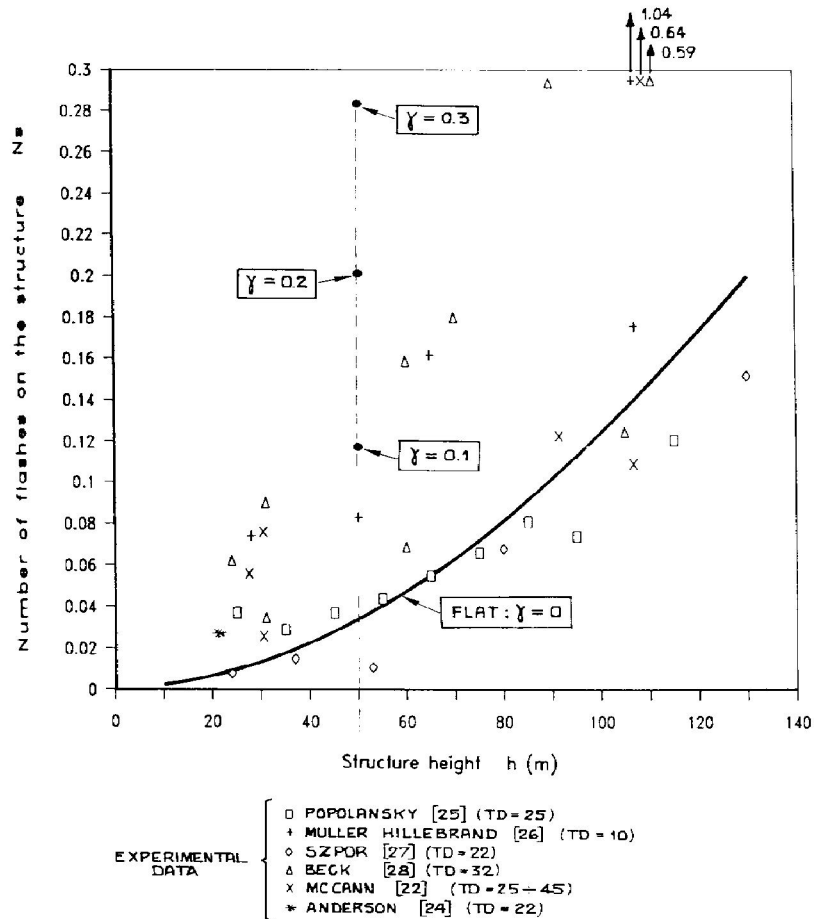


Figure 22 - Number of flashes on thin structures in various orographic conditions [39]

In order to allow a correct comparison between computed values and field data, the presence of upward phenomena was taken into account by increasing the computed values with the relevant percentage of upward flashes.

The comparison showed that the computed curve can be considered a good interpolation of the lowest range at the experimental data.

In their paper, the authors presented an evaluation of the exposure of structures located in flat territory and in different orographic conditions.

Comparison between computed values and experimental data showed that their model fits the lowest measured values while higher values of exposure may be explained taking into consideration the orographic conditions of installations.

2.3.3. Lightning incidence to tall structure modeling

In January 1994, Farouk A.M Rizk published two papers [18] where he presented a recent physical approach to assess both downward negative lightning incidences to tall masts on flat ground and hilly regions as well as upward flash from tall masts under negative cloud.

In fact, Rizk's objectives were to take into account the effects of hilly terrain on negative downward direct stroke incidence to tall freestanding structures, to formulate criteria for the occurrence of an upward flash caused by negative cloud without significant downward negative leader activity, both on flat and hilly terrains; and finally to develop a rigorous mathematical approach to assess the effect of structure height on downward negative stroke current.

2.3.3.1. Downward Negative Flash

Rizk used a basic approach he formulated in one of his previous papers [54] to determine incidence due to a downward negative lightning, to structures and conductors of moderate heights. Figure 23 shows a schematic diagram of freestanding structures on flat ground and on a mountain top.

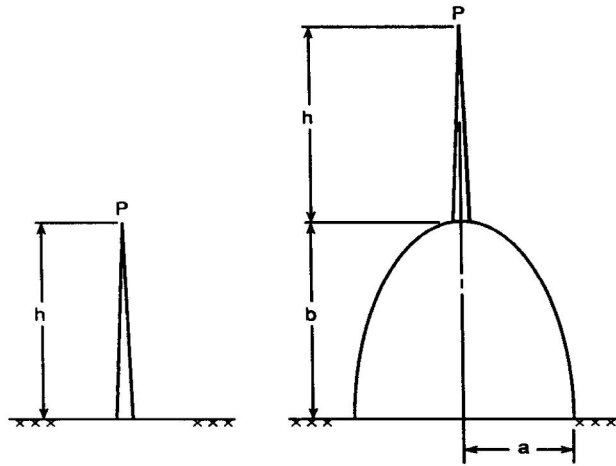


Figure 23 - Schematic diagram of free-standing mast of height: h on flat ground and over a mountain simulated as semi-ellipsoid (prolate spheroid) with semiminor axis (base radius): a , and semimajor axis (height): b .

It was assumed that the total charge of the negative descending leader was only a function of the return stroke current.

Calculation of the negative-leader-induced potential U_{il} at the structure tip position on mountain top could then be made using charge simulation.

In the modeling, the effect of ambient ground field E_g due to cloud charges was neglected for structures of moderate height on flat terrain.

However, for tall structures and mountains regions, the effect of potential induced due to cloud charges and other distant space charges was added to that induced due to the negative descending leader.

An equation for computing the total induced potential U_i for a structure on flat ground was presented as:

$$U_i = E_g \cdot h + U_{il} \quad (14)$$

The critical value U_{ic} necessary for continuous positive leader inception and propagation could be obtained by calculating, using charge simulation technique, the function R needed for the expression:

$$U_{lc} = \frac{1556}{1 + \frac{7.78}{R}} \quad (15)$$

In mountains, the effect of reduced relative air density δ can be introduced in (15) leading to:

$$U_{lc} = \frac{1556}{1 + \frac{7.78}{\delta R}} \quad (16)$$

It was stated that for a slender structure on flat ground the ratio $\frac{R}{h}$ could be approximated to 2.

For the case of a hemispherical shaped mountain of radius and structure of height h at the top, an analytical expression of the function R was presented as:

$$R = 2(h + a) / \left[1 + \frac{2a(h + a)}{(h + a)^2 - a^2} - \frac{2a(h + a)}{(h + a)^2 + a^2} \right] \quad (17)$$

After analysis and simplification of the leader voltage drop, Rizk's leader voltage drop ΔU expression was expressed as:

$$\Delta U_l = lE_\infty + x_0 E_\infty \ln \frac{E_i}{E_\infty} \quad (18)$$

E_∞ is the final quasi-stationary leader gradient, l is the leader length.

$x_0 = v \cdot \Theta$ (v is the ascending positive leader speed and Θ is the arc (leader) time constant)

In the part II of the paper [18] an extensive computer application of the theories advanced in a previous paper [54] was made.

The dependence of the attractive radius of a vertical mast on flat ground on the mast height (in the range of 10-200 m) was determined for different values of return stroke current (in the range of 5-100 kA).

The configuration used was the following:

- Ambient ground field $E_g = 0$, cloud height $H_{cl} = 2500$ m, final positive leader gradient $E_\infty = 3$ kV /m.

The results are shown in figure 24:

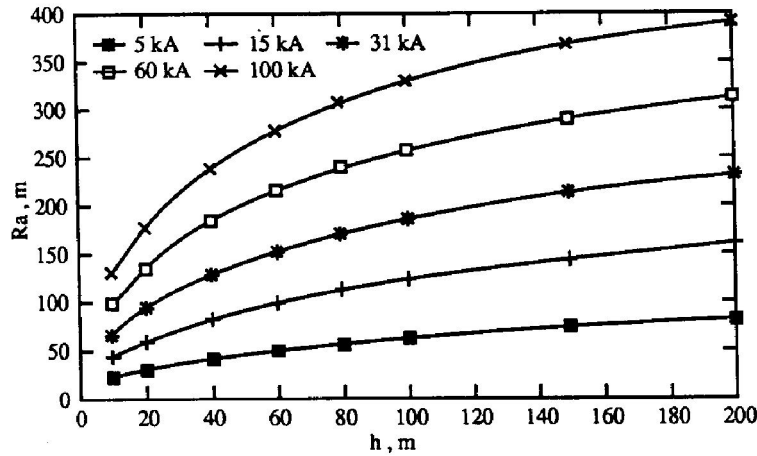


Figure 24 – Variation of the attractive radius R_a , with mast height for flat terrain and different Values of the return stroke current.

For lower structure height the results are practically the same as those presented on his previous work [54].

It was stated that for a median return stroke current $I_g = 31$ kA, with a ground field of 3 kV/m, regression analysis of model results yielded the following expression for the dependence of the overall attractive radius R_{ao} on mast height in the range 10-200 m:

$$R_{ao} = 25.9 \times h^{0.48} \quad (19)$$

h in meters

For a return stroke current of 39 kA, the attractive radius was expressed by:

$$R_a = 26.0 \times h^{0.47} \quad (20)$$

h in meters

Further data analysis made in his paper, showed that the attractive radius for a negative downward flash is rather insensitive to mountain height.

2.3.3.2. Upward Flash

The situation the author analyzed was for free- standing tall mast in flat or mountain region under a negatively charged cloud.

The basic difference between the situation of upward flash and conventional downward negative lightning was that the induced potential at the position of structure top would be essentially determined by the ground field:

$$U_i = \int_0^h E_g(z) dz \quad (21)$$

For positive leader inception U_i must be $\geq U_{lc}$ where U_{lc} was given by expression (14).

The induced voltage (magnitude) at any point z would be then designated using (21) and the critical inception voltage $U_{lc}(z)$ by using (14).

Assuming for simplicity that the positive leader is ascending vertically, at a length l_z , the leader voltage drop would then be derived from (18):

$$\Delta U_l(z) = l_z E_\infty + x_0 E_\infty \ln \frac{E_i}{E_\infty}$$

This would lead to a general criterion: $U_i(z) \geq U_{lc}(z) + \Delta U_l(z)$

For the general case of mountainous region, the corresponding criteria for occurrence of the upward flash were expressed as:

$$\int_0^h E_g(z) dz \geq \frac{1556}{1 + \frac{7.78}{\delta R}} + x_0 E_\infty \ln \frac{E_i}{E_\infty} \quad (22 a)$$

$$\text{and } \frac{1}{l_z} \int_0^{l_z} E(l) dl \geq E_\infty \quad (22 \text{ b})$$

For a mountain represented as a hemisphere of radius a , the induced potential simplified to:

$$U_i = \int_0^h E_g(z) dz = E_g \cdot (h+a) \left[1 - \frac{1-a^3}{(h+a)^3} \right] \quad (23)$$

2.3.3.3. Lightning incidence

Rizk model described the number of negative downward flash per year N_d as related to the ground flash density N_g and the overall attractive radius R_{ao} by:

$$N_d = \pi R_{ao}^2 N_g \quad (24)$$

The number of upward flashes per year on the other hand was determined by the number of times at the location of the structure, the criteria for upward flash were satisfied (when the critical ground field E_{gc} was exceeded) [18].

The number of upward flashes per year N_u could then be expressed as the product of the number of storms per year T_d and the cumulative probability, that once a storm did occur, the critical ground field E_{gc} was exceeded:

$$N_u = T_d \cdot P(E_g \geq E_{gc}) \quad (25)$$

An expression of the cumulative probability function $P(E_g \geq E_{gc})$ was approximated by an exponential function:

$$P(E_g \geq E_{gc}) = e^{-\frac{(E_{gc}-E_{g0})}{E_{g1}}} \quad (26)$$

where E_{g0} is a threshold field, once a storm did occur and E_{g1} is a shape parameter.

A Distribution 1 condition was defined as when it has often been reported that the ground field rarely exceeds 10 kV/m under lightning storm conditions giving values of: $E_{g0} = 2$ kV/m and $E_{g1} = 2$ kV/m.

Distribution 2 condition was also defined for higher fields and corresponds to more severe ground field conditions (specially in mountains) giving the values: $E_{g0} = 3$ kV/m and $E_{g1} = 6$ kV/m.

The critical ground field was quite sensitive to structure height for all terrain configurations investigated. With flat ground and within the limits of the heights investigated an expression was given as:

$$E_{gc}.h \approx 1600 \quad (27)$$

2.3.3.4. Check of the model

The number of times per year a mast is hit by lightning N_s is obviously the sum of the downward flash frequency N_d and the upward flash frequency N_u .

In the final part of his paper, Rizk made some computation in order to verify and compare his theories with field observations. Some of them are mentioned below.

First, his equation for the number of negative downward lightning flashes (24) with mast height for flat and mountains ($I_g = 31$ kA, $N_g = 1$ fl/km².yr and $a = 600$ m) was computed and compared to empirical results [24]. Figure 25 illustrates the results.

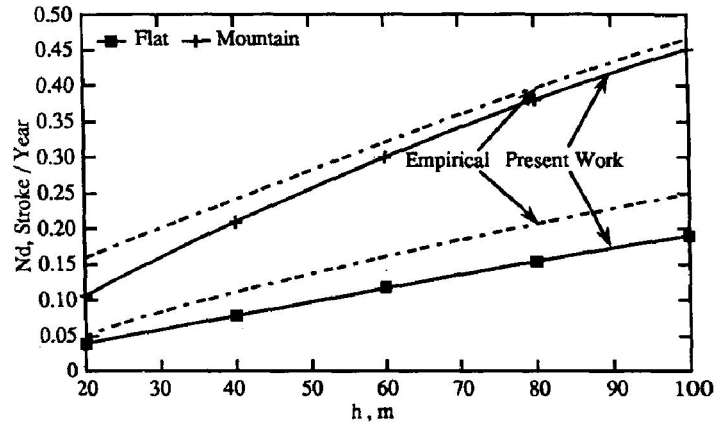


Figure 25 - Variation of negative downward lightning strikes with mast height for flat and mountain terrains and comparison with empirical results

One can see that the agreement between the curves based on field observation and the model results was quite satisfactory,

Rizk's expression for the dependence of the total number of flashes (including downward and upward) on a slender mast height for flat ground with ground field distribution 1 and ground flash density $N_g = 1/(\text{km}^2 \cdot \text{year})$ was evaluated and compared to values obtained from an empirical formula given by Eriksson [24] based on worldwide observations of 3000 flashes involving 10 000 structure.years with heights in the range 20 m - 500 m. Figure 26 illustrates the results.

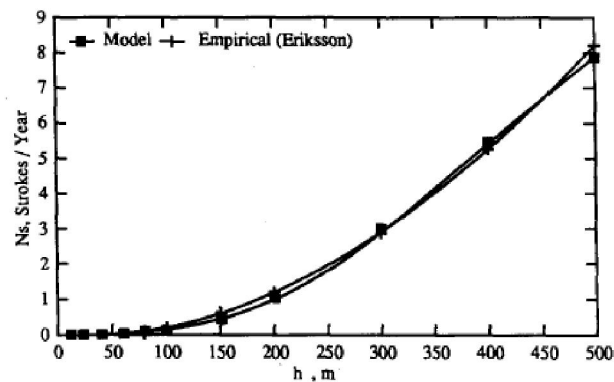


Figure 26 - Variation of total strike frequency N_s and comparison with empirical results

Once again, the agreement between theory and field observation was very satisfactory.

Fig 27 illustrates Rizk's equation for the probability of upward flash (25) for a mast on flat ground, with a ground field distribution 1 computed and compared to the formula given by Eriksson [24].

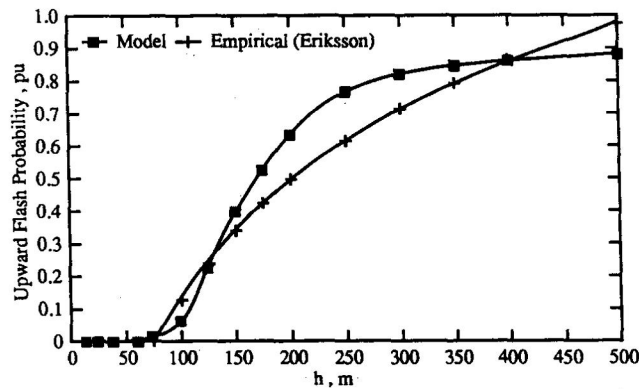


Figure 27 - Probability of upward flash on mast height over flat ground and comparison with empirical results

Here again, the agreement was quite satisfactory but it was mentioned that a constraint must be put on the empirical formula, for which the probability would otherwise exceed 1 above a height of approximately 500 m.

We can then, clearly state that Rizk's model for evaluation lighting incidence on tall structure are in good agreement with empirical formula based on extensive field observations.

This proves that his work and equations can be used for any future estimation of lightning incidence for tall slender structures.

2.3.4. Lightning leader inception modeling

In April 2006, M. Becerra and V. Cooray published a paper [28] where they presented a simplified model to determine the lightning upward connecting leader inception.

Regarding that matter, the main leader inception criteria that have been used up to when they wrote their paper were the critical radius concept, the generalized leader inception criterion, the critical range of field intensification concept, and the Lalande's equation.

Their approach was based in the fact that even though those models could be really useful to analyze the leader inception in complex structures and could also consider the effect of space charge, several problems and complexities arise when practical cases are analyzed following the procedure presented in Goellian et al work [29].

In order to overcome these limitations, they proposed a generalized leader inception model based on an iterative geometrical analysis of the background potential distribution of an earthed structure to simulate the first meters of propagation of an upward connecting leader.

The model followed a similar approach to the Goellian et al work [29], however, a different and simplified way to compute the space charge, the stable leader inception field, the striking distance and the leader potential gradient was used taking into account the effect of the sharp rods, buildings corners, or edges.

2.3.4.1. Stable leader inception physical model

First, the authors explained that as the stepped leader approaches to ground when a lightning flash is initiated, the electric field at sharp points of structures starts increasing. Stable upward leaders emerge from elevated objects

In fact, the discharge process was initiated with the formation of the first corona. Once a streamer was incepted, it started propagating from the sharp electrode and, next, the streamer split into many branches within a conical volume [30]. Thus, filamentary branched channels (streamers) were developed from a common root (stem).

In order to compute the stable leader condition, the first corona inception was initially computed by using the same streamer criterion used in [31].

Basically, the major assumption of that approach was that the corona zone is characterized by an almost constant electric field E_{str} . In that way, the corona space charge produces a distortion on the geometrical background potential distribution, as shown in Fig. 28.

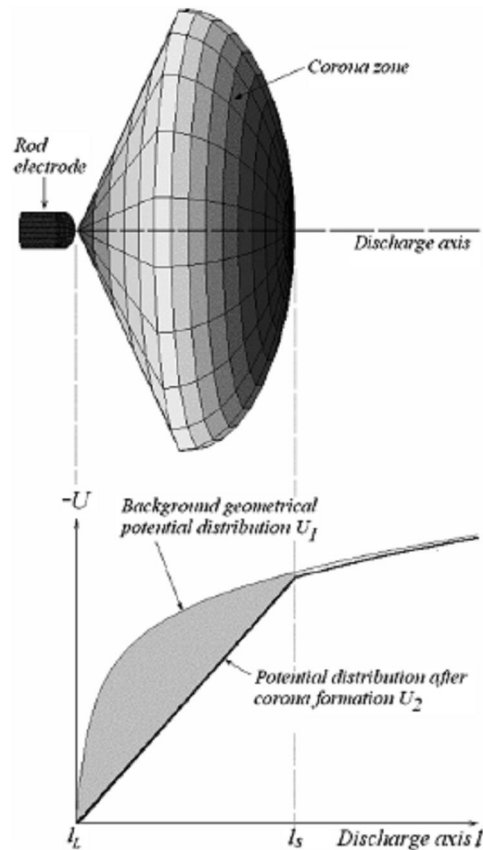


Figure 28 - Potential distribution before and after corona formation in a front of a rod.

Thus, the optimized charge simulation method (CSM) [32] was used for the calculation of the charge in the corona zone. Once the first corona inception has been reached, the total charge in the corona zone was calculated.

A step-by-step computation of the leader length, the leader voltage drop, the potential distribution, and the total charge in front of the leader's head was performed. A schematic example of this calculation is shown in Fig. 29.

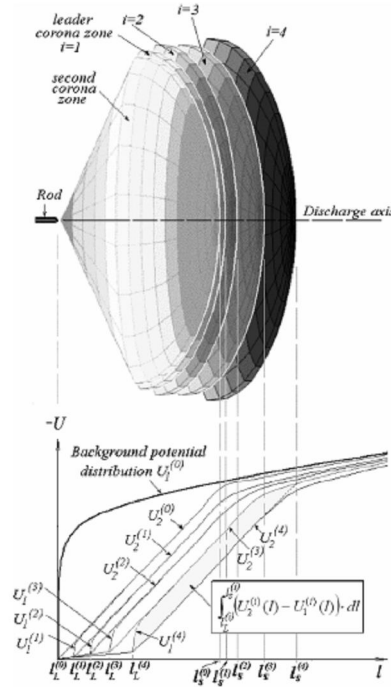


Figure 29 - Schematic example of the leader advancement simulation

The calculation begins at $i=1$, assuming the leader channel as a cylindrical ionized plasma with constant radius r_L and initial length l_L . Next, the potential at the leader's tip is computed by using the following derived by Rizk [33]

$$U_{tip}^{(i)} = l_L^{(i)} \cdot E_\infty + x_0 \cdot E_\infty \cdot \ln \left[\frac{E_{str}}{E_\infty} - \frac{E_{str} - E_\infty}{E_\infty} \cdot e^{-l_L^{(i)}/x_0} \right] \quad (28)$$

where l_L is the leader length at the current simulation step, E_{str} is the positive streamer gradient, E_∞ is the final quasi-stationary leader gradient, x_0 is a constant given by the product $\mathbf{v} \cdot \boldsymbol{\theta}$, where \mathbf{v} is the ascending positive leader

speed and θ is the leader time constant.

Then, the potential distribution $U_1^{(i)}$ is calculated and the total corona charge ΔQ in front of the leader's head is computed and the leader advancement distance is calculated by using the relation :

$$\Delta l_L^{(i)} = \frac{\Delta Q^{(i)}}{q_L} \quad (29)$$

where q_L is a constant that represents the charge per-unit length necessary to achieve the thermal transition from the diffuse glow to the leader channel.

And finally the current leader length is updated as:

$$l_L^{(i+1)} = l_L^{(i)} + \Delta l_L^{(i)} \quad (30)$$

and the advancing process is repeated $i = i+1$.

The simulation would stop either if the leader propagation stops (leader advancement distance Δl_L decreases after some simulation) or if the stable leader condition is fulfilled (leader length reaches a maximum value L_{max} of 2 m) [28].

2.3.4.2. Corona Charge calculation

The CSM was the most suitable method to compute the total charge in the corona zone due to its simplicity in replacing the space charge by fictitious discrete charges [28].

To simulate the analyzed electrode configuration, point charges, finite line charges, and uniform ring charges were used. A point charge at the tip and finite lines with increasing length were used to simulate the stem/leader channel.

Thus, a ring charge was divided in n equal segments according to the degree of asymmetry of the potential distribution with respect to the discharge

axis. Those ring charges were centered on the discharge axis (Fig. 30.a) and placed, forming radial paths from the tip of the stem/leader, as shown in Fig. 30.b

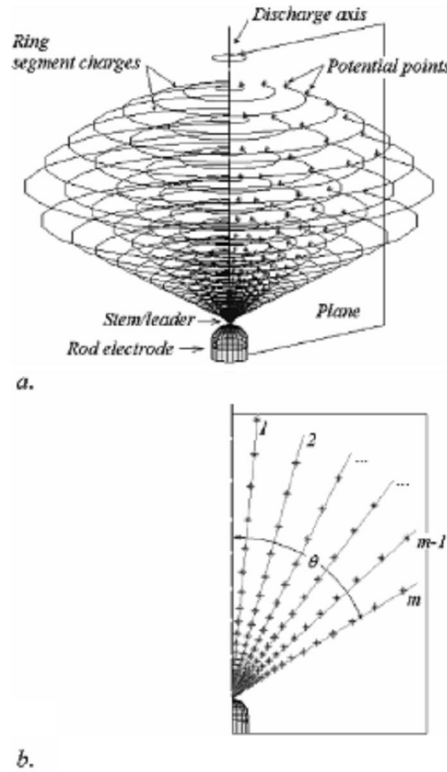


Figure 30 - CSM modeling of the corona zone in a rod electrode (a) Distribution of the ring charges in the corona zone and a plane around the discharge axis (b) Detail of the location of the potential points on a plane

For each segment ring, a potential point was placed close to it at the middle of its angular spread. The potential at each potential point ($j=1$ to N_{rc}) was defined [34] as:

$$U_j^{(i)} = U_{tip}^{(i)} + E_{str} \bullet r_j^i - U_{sc}^{(i-1)} \quad (31)$$

where U_{tip} is the potential at the tip of the stem/leader, E_{str} is the streamer potential gradient, r_j is the distance between the potential point location and the stem/leader tip's position, and U_{sc} is the voltage at the potential point position produced by the ring charges obtained during the previous simulation steps.

Then, the total charge in the corona zone is calculated as

$$\Delta Q^{(i)} = \sum_{j=1}^{N_{sc}^{(i)}} Q_{sc_j}^{(i)} \quad (32)$$

where Q_{sc_j} is the calculated charge of the j th ring segment in the corona zone during the current simulation step .

2.3.4.3. Implementation of the model

The concept of the stabilization field [35] was adopted to define the condition at which a stable leader was incepted. Thus, the lightning rod was placed in a background electric field E_{back} that was supposed to be constant [35]. Hence, the bisection method [36] was used to find the background electric field E_{back} at which the stable upward leader was incepted for each case. The field that fulfilled that condition was called the leader stabilization field.

The Becerra-Cooray model was used to evaluate whether a given background electric field E_{back} was high enough for the stable leader inception or not assuming that the first corona inception condition was fulfilled. Fig. 31 shows the obtained stabilization fields E_{stab} for hemispherically capped rods with different heights.

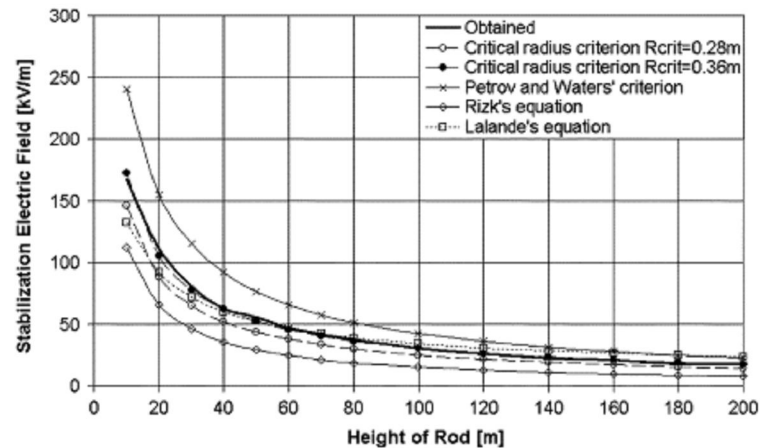


Figure 31 - Leader Stabilization fields for a 10^{-2} m tip radius rod

For comparison, the stabilization fields were also computed according to the critical radius concept ($R_{crit} = 0.28$ m [30] and 0.36 m [6]), the Rizk's equation [18], Petrov and Waters' criterion [37] and the inception equation given by Lalande [38].

There is an agreement with the results computed with the present model and the critical radius concept assuming $R_{crit} = 0.36$ m

After that, the stabilization fields for a corner of a 60 x 80 m rectangular building were computed as a function of height. In this case, a full three-dimensional (3-D) calculation was performed assuming two different conditions for the discharge axis. The obtained results were also compared with the critical radius concept ($R_{crit} = 0.36$ m) and with the Petrov and Waters' criterion [43], as is shown in Fig.32

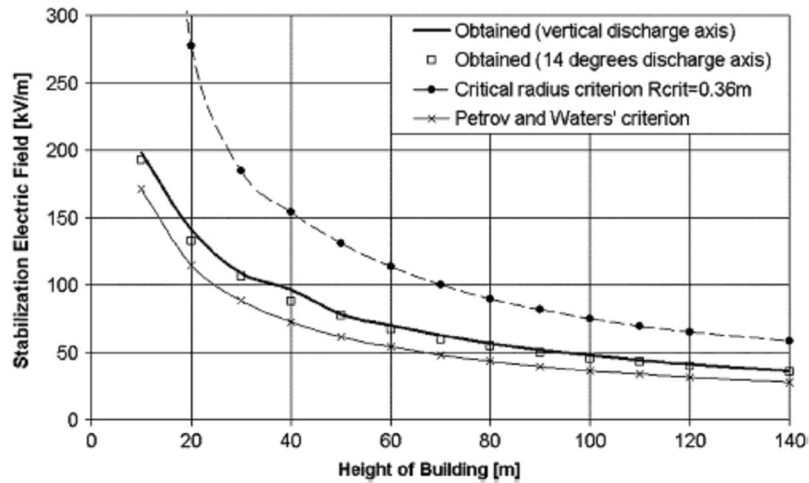


Figure 32 - Leader Stabilization fields for a 60 x 80 m rectangular building

In this case, the difference between the results obtained with the proposed model and the critical radius concept was quite large for short buildings (larger than 50%) and decreases slightly with height.

They observed as well that the stabilization fields depended upon the geometry of the analyzed structure. Thus, the stabilization fields for the used building were larger (from 15% to 60%) than for the lightning rods.

The author suggested that the leader inception criteria derived for the rods (critical radius concept, Petrov and Waters criterion, Lalande and Rizk equation) should not be used to analyze the inception condition of any other different kinds of structures.

2.3.4.4. Simplified procedure

The simplified procedure advanced in the paper was based on the assumption that the total corona charge ΔQ could be determined from the difference between the geometrical potential distribution U_1 and the potential

distribution after the corona formation U_2 as:

$$\Delta Q = K_Q \bullet \int_{l_L}^{l_s} (U_1(l) - U_2(l)) dl \quad (33)$$

where K_Q is a geometrical factor that takes into account the effect of all of the streamers on the total charge.

In order to use (33), it is necessary to determine the value of K_Q for different kind of structures, leader lengths, and potential distributions. Therefore, the CSM calculation was used to compute the factor K_Q .

Once the factor K_Q is defined, the integral term in (32) is evaluated. Therefore, all the other potential distribution and corona charge are computed.

The stabilization fields computed following the simplified procedure with different values of the factor K_Q are shown in Fig. 33. For the sake of comparison, the results obtained for both cases (lightning rod and building) with the full calculation using CSM were also shown.

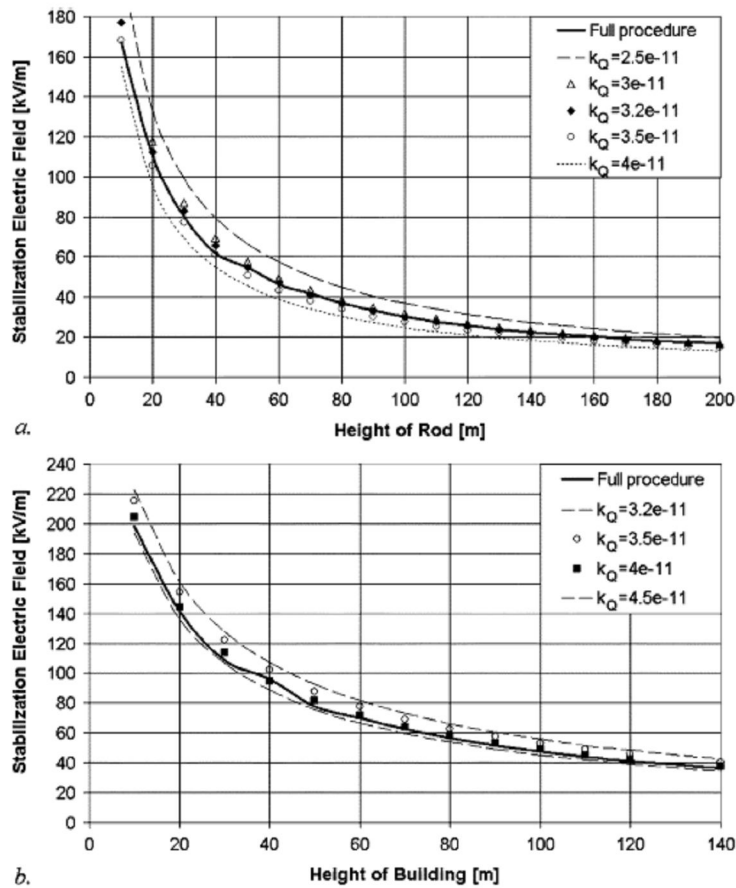


Figure 33 - Comparison of the leader stabilization fields computed with the CSM and with the simplified geometrical approach for the different values of K_Q (a) for the lightning rod (b) for the rectangular building

One could then observe that there was a good agreement between the stabilization fields computed with the full calculation and with the simplified geometrical procedure. Hence, the generalized value of K_Q ($3.5 \cdot 10^{-11}$ C/V.m) gave a good estimate of the results obtained with the full charge calculation.

However, in order to get even better results, the factor K_Q equal to $3.2 \cdot 10^{-11}$ C/V.m might be used for thin structures with axial-symmetry (masts, towers) and K_Q equal to $4 \cdot 10^{-11}$ C/V.m for other kinds of wide structures without symmetry (buildings, complex structures, etc).

M. Becerra and V. Cooray, at the end of their paper stated summarized the main contributions of their model as follows: [28]

- Their model allowed the calculation of the leader inception conditions even when the dynamic analysis of the upward leader development during the approach of the downward leader channel is analyzed.
- Their model drastically reduced the calculation errors compared with the leader inception models based on the electric field.
- Since the proposed method used the potential distribution (mainly far away from the sharp point/corner), the obtained results were much less influenced by curvature chosen for the calculations.
- The simplified version of their model was a straight forward way to calculate the leader inception conditions through the analysis of the leader propagation. It allowed visualizing whether the background potential was high enough to maintain the propagation of the leader or not.

2.3.5. Numerical model to determine lightning attachment points on wind turbine

In 2006, from the technical university of Denmark, S.R. Madsen wrote a Phd. Thesis based on the interaction between electrical discharges and materials for wind turbine blades – particularly related to lightning protection [48]

2.3.5.1. Electrical discharges related to a wind turbine blade

In one part of the thesis, he made an analysis of electrical discharges related to a wind turbine blade knowing that some of the materials used are neither totally conductive, nor fully insulating, and some of the electrical characteristics tend to change with time.

As described on IEC TR 61400-24 [1], discrete air terminations are installed on wind turbines to protect the blade from lightning discharges.

On his paper, a scenario with a 40m common blade design hit by lightning is treated in order to understand the mechanisms that govern the interaction between lightning discharges and composite blades [48]

In the model used in Madsen's thesis, air termination receptors were installed on both sides of the blade from radius 20 m to the tip region with a spacing of 5m giving five receptors on each side.

The receptors are connected to an inner down conductor, a 50 mm² copper conductor fixed to the beam with mechanical joints. In the root end of the blade, the down conductor is connected to the flange, which acts as the electrical interface to the rest of the turbine. Fig. 34 illustrates the configuration.

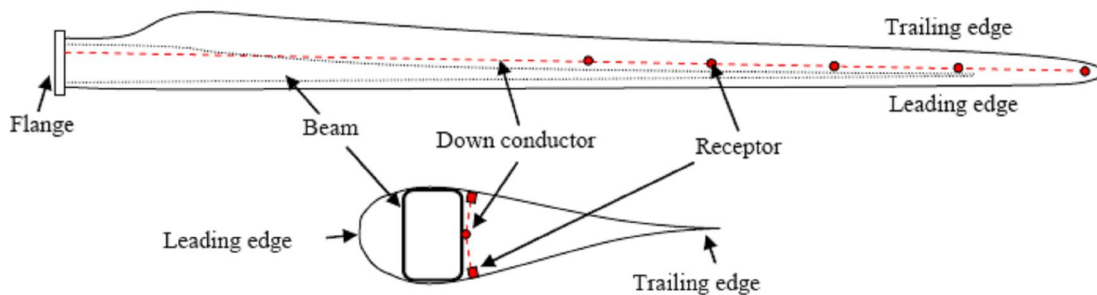


Figure 34 - Common blade design, discrete receptors connected to an internal down conductor

It was stated that when blades are subjected to a sufficiently high electric field, streamers will be emitted from all conductive components and that discharges will mainly be initiated from metallic objects connected to the down conductor. This situation is illustrated on Figure 35.

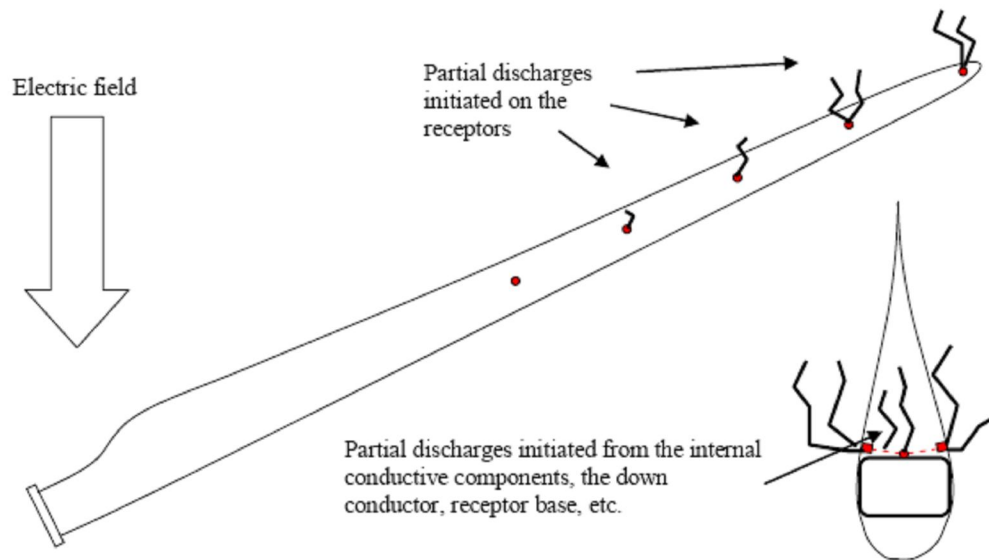


Figure 35 - Discharges on new and clean blade, mainly from metallic components.

In fact, the receptors would produce streamers very early, but since the internal down conductor is exposed to the same electric field, partial discharges would also occur inside the blade, which could be minimized by avoiding exposed metal surfaces inside the blade [49].

Furthermore, if the inductance of the down conductor system is too high, inductive voltage drops could lead to side flashes within the blade. Design of the air termination point is then very important to minimize of any types of damages.

Based on theoretical considerations, Madsen also presented the fact that attachment on insulating surfaces may occur if charge carriers are present. He implied that the outer surface of a blade would be covered by streamers of opposite polarity relative to the lightning leader.

2.3.5.2. Modeling

As mentioned above, it is important to predict where possible lightning discharges will attach on structures exposed which would allow engineers to place suitable protection measures.

There are many methods of predicting the vulnerable locations on structures as the 'protective mesh', 'protective angle', 'collection volume' and the 'rolling sphere method' which is recommended by the standards in general [50] [51].

Today, modern FEM programs import CAD data and enables advanced electric field and potential calculation, more physical oriented methods have recently been suggested [52] and [53] and were based on more physical phenomena than the simple rolling sphere method. FEM programs should give more reliable results.

Despite the relatively complex physics, it is simplified to a practical level suitable for applications on arbitrary structures.

In his thesis, Madsen applied the method on a single wind turbine following these steps of analysis:

- Construct a 3D model of the structure to be considered within an analysis volume several times larger than the largest dimension of the structure.
- Apply a background electric field and compute the potential distribution within the analysis volume.
- For the point to be considered, compute the vertical potential distribution from the point and 20m upwards.

- Perform the algorithms described by Becerra and Cooray [52] deciding whether the background field at step 2 was sufficient to fulfill the conditions for stable leader inception, at the specific point.
- By iteration; find the least background electric field, the stabilization field, sufficient for fulfilling the conditions for stable leader inception.
- For each point of interest, repeat step 3-5.

In fact, Madsen applied the formulas on a simple 3D model of a modern wind turbine:

- The turbine consisted of a conical tower with a height of 100m, equipped with a box shaped nacelle measuring 12m x 4m x 4m, and three blades each 50m long.
- The surrounding volume considered for the electrostatic calculations measure 1km by 1km and is 500m high, Figure 36.

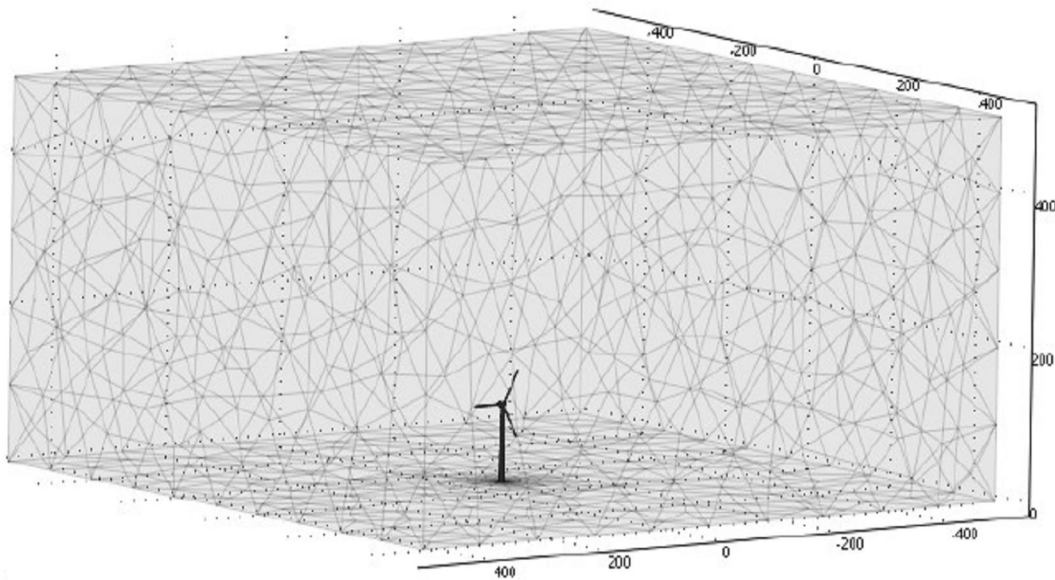


Figure 36 - FEM model of a single wind turbine to determine the normalized stabilization field at different locations.

The wind turbine and the surrounding ground area were assigned a reference potential of 0V, the sides of the analysis volume was assigned a boundary condition where the normal of the electric field was zero and the upper boundary was set to a certain potential.

The sub domain within the boundaries was air defined by its relative permittivity of 1.

By solving Laplace's equation for the sub domain, the potential distribution in the entire volume was computed, same as the stabilization field for each point considered.

The relative probability of a strike for the different points on the turbine is shown on Figure 37.

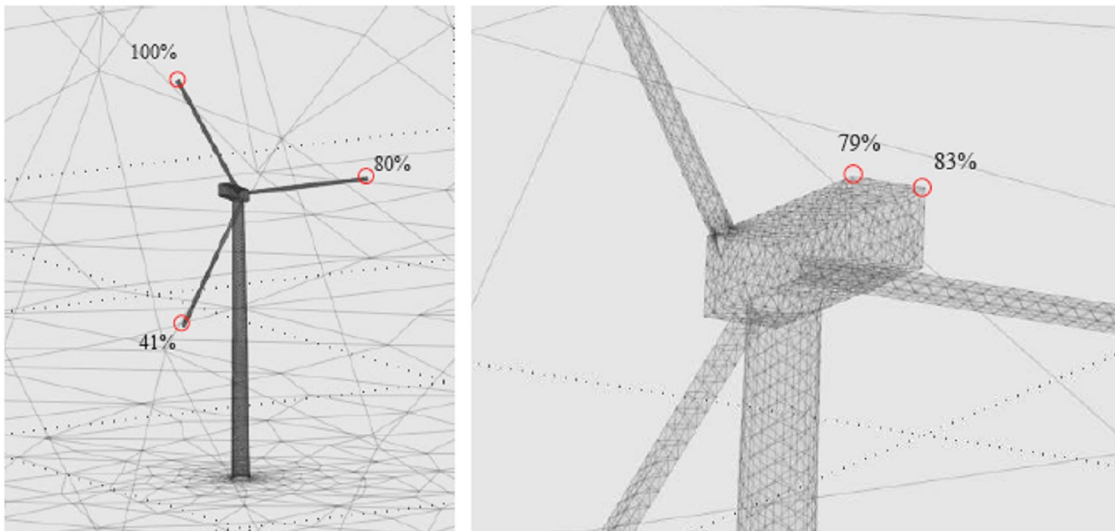


Figure 37 – Relative probability of a strike for a wind turbine with one blade in horizontal position.

As expected, it was noted that the blade pointing upwards had the highest relative probability of being struck (100%) and the lowest probability occurred at the blade tip pointing downwards (41%) [48].

The risk of having the horizontally oriented blade struck at its tip was comparable to the risk of getting a lightning strike to one of the rear corners of the nacelle.

A second simulation with one blade in an upwards vertical position revealed the following results :

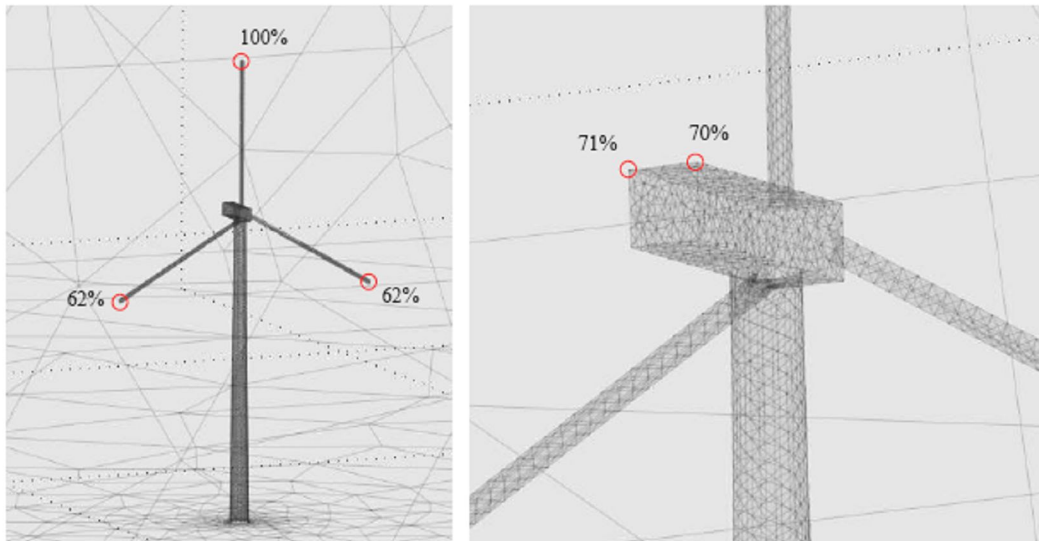


Figure 38 – Relative probability of a strike for a wind turbine with one blade in vertical position.

The highest risk of getting struck is at the tip pointing upwards (100%) where after the rear of the nacelle is most exposed (70%). The blade tips pointing downwards are not likely to be struck considering these five points (62%).

In his thesis, Madsen showed that one could locate the highest points on the structure that are more likely of getting struck with lightning by evaluating the electric field distribution around the wind turbine.

That would help justify the presence and location of receptors distributed along the length of the blade.

He recommended that once the method of estimating the stabilization electric field was extended to cover more than just corners and sharp edges, it might be applied on wind turbine blades and show why the tips were more exposed than the rest of the blades [48].

2.4. Comments

In this chapter, we reviewed worked done by previous investigators in the field of lighting exposure in order to find where might be room for improvement.

In section 2.3.1, A J Eriksson addressed the lightning attractive radius concept and procedures for estimating the number of lightning flashes to power lines. In fact, he derived expressions for the actual attractive area presented by high structures – although he focused on power lines.

His work, analysis and researches on the subject yielded a proposed formula for attractive radius ($R_a = 14 H^{0.6}$) that was compared to the traditional assumption made at that time ($R_a = 2H$).

He showed and concluded that the trend of the traditional assumption that $R_a = 2H$, displays considerable deviation from observed data, when the most rigorous source of line performance data in a high elevation range agreed well with his average attractive radius estimation.

In section 2.3.2, E.Garbagnati and L.Dellera presented a model of lightning channel progression towards the earth based on the knowledge on physics of discharge on long air gaps considering the effect of space charge.

A model with simulation of the downward, upward leaders and clouds was applied to an earthed structure with a selected horizontal distance between the downward channel and the considered structure. This allowed to define the point of impact and to evaluate the exposure of a structure to lightning (number of flashes).

They compared computed values of their model to field experimental data, and found that their model only fitted the lowest measured values of exposure.

In section 2.3.3, Farouk A.M Rizk presents an approach to assess both downward negative lightning incidences to apply to tall masts and hilly regions and upward flash from tall masts under negative cloud taking into account the effects of hilly terrain.

He expressed equations to evaluate lightning exposure and performed computations to compare his theories with field observations. At the end, we found that his results were perfectly in agreement with empirical formula based on extensive field observations

In section 2.3.4, M. Becerra and V. Cooray present a model to determine the lightning upward connecting leader inception.

In fact, they proposed a generalized leader inception model based on corona charge calculation to simulate the first meters of propagation of an upward connecting leader. The model is a simplified way to compute the space charge, the stable leader inception field, the striking distance and the leader potential gradient taking into account the effect of the sharp rods, as well as buildings corners, or edges.

They compared their results with results obtained by previous authors and observed that there was a good agreement between the stabilization fields computed with the full calculation and with the simplified geometrical procedure for corona charge calculation.

In section 2.3.5, Madsen used a modern FEM program to predict where possible lightning discharges will attach on structures exposed which would allow engineers to place suitable protection measures.

He showed that one could locate the highest points on the structure that are more likely of getting struck with lightning by evaluating the stabilization electric field distribution around the wind turbine.

With the light of these researchers results and, there is still room to improve and to add more consistencies to these data and facts applied to wind turbine.

For instance, in the next chapter the work of A J Eriksson where he compared a proposed formula for attractive radius to the traditional assumption standard made at that time can be re evaluated but this time comparing with the most recent formulas of our time regarding tall structure.

Rizk's approach of finding the lightning exposure is straight forward, and it would be interesting to apply that approach to a rotating wind turbine using his formulas and models.

The model used by Madsen is one the more recent model to evaluate field distribution. He used it for an entire wind turbine. But it would be interesting to see if his analysis can be simplified by concentrating only on the down conductor attached to the blade. The values obtained could be compared to values obtained if we used the charge simulation method like M. Becerra and V. Cooray did in their paper.

In the next chapter we will then concentrate on finding first where possible lightning discharges will attach on down conductor of a wind turbine exposed, and will then evaluate the actual lightning exposure of that specific location.

CHAPTER 3 MODELING APPROACH

In this chapter, we will use different methods in order to evaluate space potential and electric field distribution on wind turbine down conductor and we will then evaluate the actual lightning exposure of that specific location.

3.1. *Modeling Wind Turbine for Electric field distribution*

3.1.1. Finite Element Modeling (Femlab)

A first approach of modeling the field distribution outside the wind turbine is to use the software Comsol Multiphysics 3.2 (Femlab).

This software is a powerful interactive environment for modeling and solving all kinds of scientific and engineering problems based on partial differential equations.

Our modeling will be performed with a linear type of analysis and will use finite element method with an adapting meshing and error control using a numerical solver.

The idea is then to use a 2D partial differential equation solver to evaluate the electromagnetic field at the tip of a conducting down conductor within the blade of a wind turbine.

We will take two cases into consideration for further comparison:

- Case1:
 - The wind turbine tower will be represented with perfectly conducting steel conditions by a cylinder of height $H = 100$ m and $r = 1$ m.

- The conducting wire in the blades will be represented as well with perfectly conducting steel conditions by a cylinder of height $H = 60$ m and $r = 0.005$ m.
- A perfectly conducting ground will be assumed.
- Clouds and Atmosphere will be modeled by another cylinder of height $H = 2000$ m and $r = 4000$ m. The sides of the cylinder will be represented as perfectly insulated, the top of the cylinder will be represented with potential of $V = 20$ MV and the bottom will be grounded ($V = 0$ V) . Fig 39 illustrates the model.

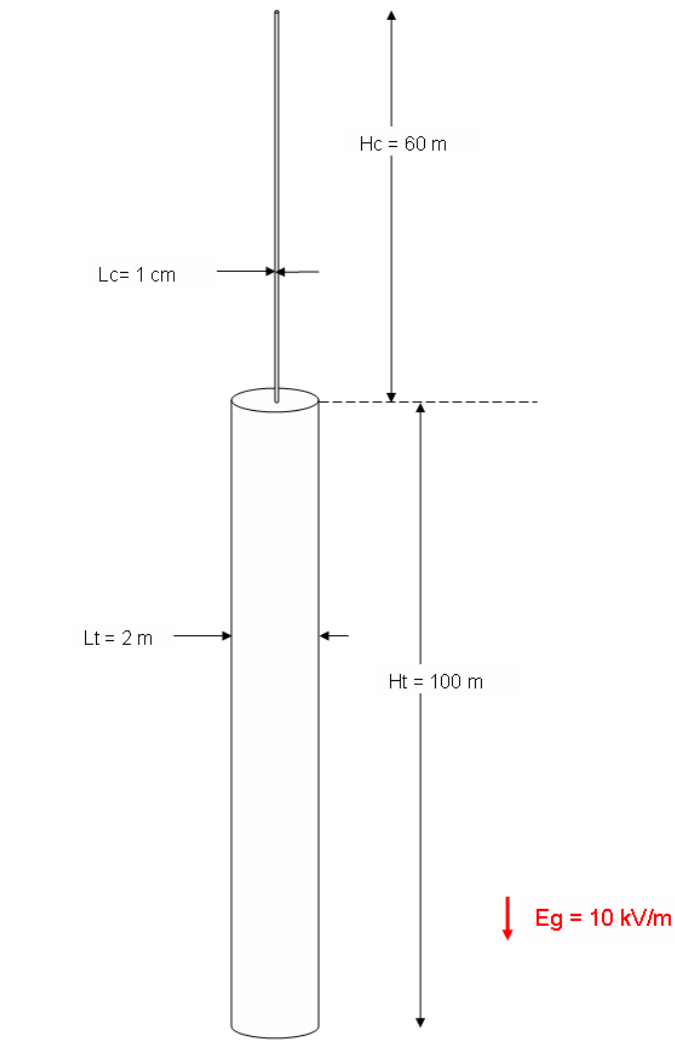


Figure 39 – Model Approach

The 2D partial differential equation we will use to solve the model is Laplace in cylindrical coordinates since the model is adapted to cylindrical symmetry.

In fact Solutions to the Laplace equation in cylindrical coordinates have wide applicability beyond electrostatics. Applying the method of separation of variables to Laplace's partial differential equation and then enumerating the various forms of solutions will lay down a foundation for solving problems in this coordinate system.

The equation is given by:

$$\nabla^2 \phi = \frac{1}{r} \frac{\partial \phi}{\partial r} + \frac{\partial^2 \phi}{\partial r^2} + \frac{1}{r^2} \frac{\partial^2 \phi}{\partial \theta^2} = 0 \quad (34)$$

In Femlab this is the generalized coefficient form equation given as a solver:

$$\nabla \cdot (-c \nabla u - \alpha u) + \beta \cdot \nabla u + a u = f \quad (35)$$

Then in order to solve Laplace equation in cylindrical coordinates, here are the values we gave to the coefficients:

$$c = -1 ; \alpha = 0 ; a = 0 , f = 0 , \beta = \frac{1}{r} \text{ and } u = \phi$$

Since we are using the equation in cylindrical coordinates, we will take advantage of the symmetry and the drawing representation will refer only to half of the original geometry.

Once the solver equation is determined, the boundary conditions have to be set in order to meet the model constrains.

For the application mode chosen to solve the problem, the software offers two basic boundary condition types:

- Generalized Neumann condition, where the boundary condition is determined by the coefficients q and g according to the following equation :

$$n \cdot (c\nabla u + \alpha u - \gamma) + qu = g \quad (36)$$

- Dirichlet conditions: u is specified at the boundary. The boundary condition equation is $hu = r$, where h is a weight that normally equals 1 and where r can be specified as needed.

Since the wind tower and the wire are conducting, there boundary will be set with a Dirichlet condition with $h = 1$ and $r = 0$.

The bottom of the cylinder representing the ground will be as well set with a Dirichlet boundary condition with $h = 1$ and $r = 0$.

The top of the cylinder representing the clouds will be also set with a Dirichlet boundary condition with $h = 1$ and $r = 20 \times 10^6$.

The two longitudinal sides of the cylinder representing respectively the edge and the symmetrical line will be will be set with a Neumann condition with $q = 0$, $g = 0$, $\alpha = 0$ and $\gamma = 0$.

Once we compute these values by initializing the meshing of the problem, fig.40 shows the representation of the finite element solution obtained:

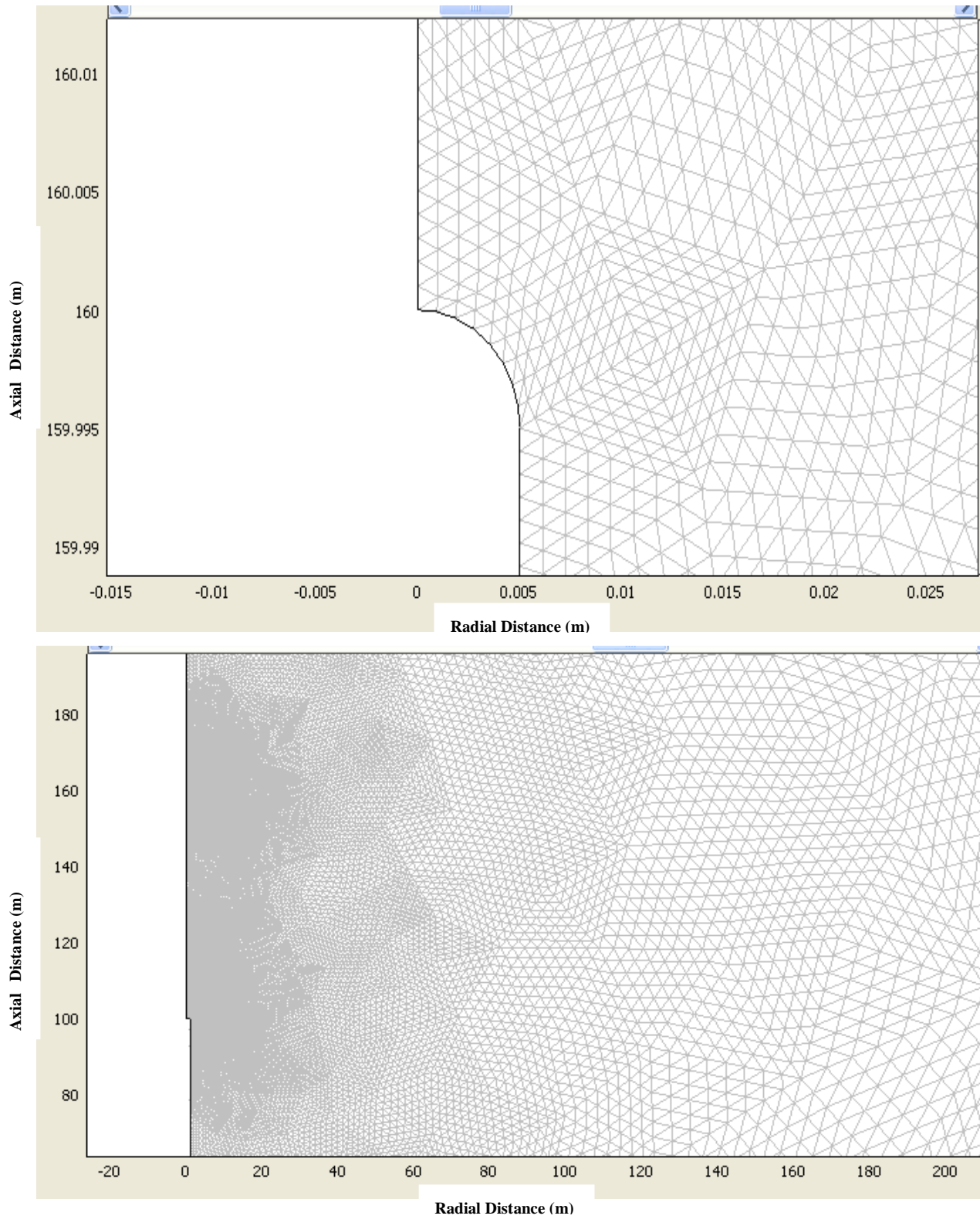


Figure 40 – Solution by finite element (a) at the tip of the down conductor (b) the full model

Looking at fig. 40(b), one can already see how the meshes are more concentrated around the structure itself, which shows that the computed solution will clearly result in a high field around the tower.

The following step is to solve the model to obtain the values of the electric field and the potential around the conductor wire. Fig.41 illustrates the electric field distribution at the tip of the down conductor.

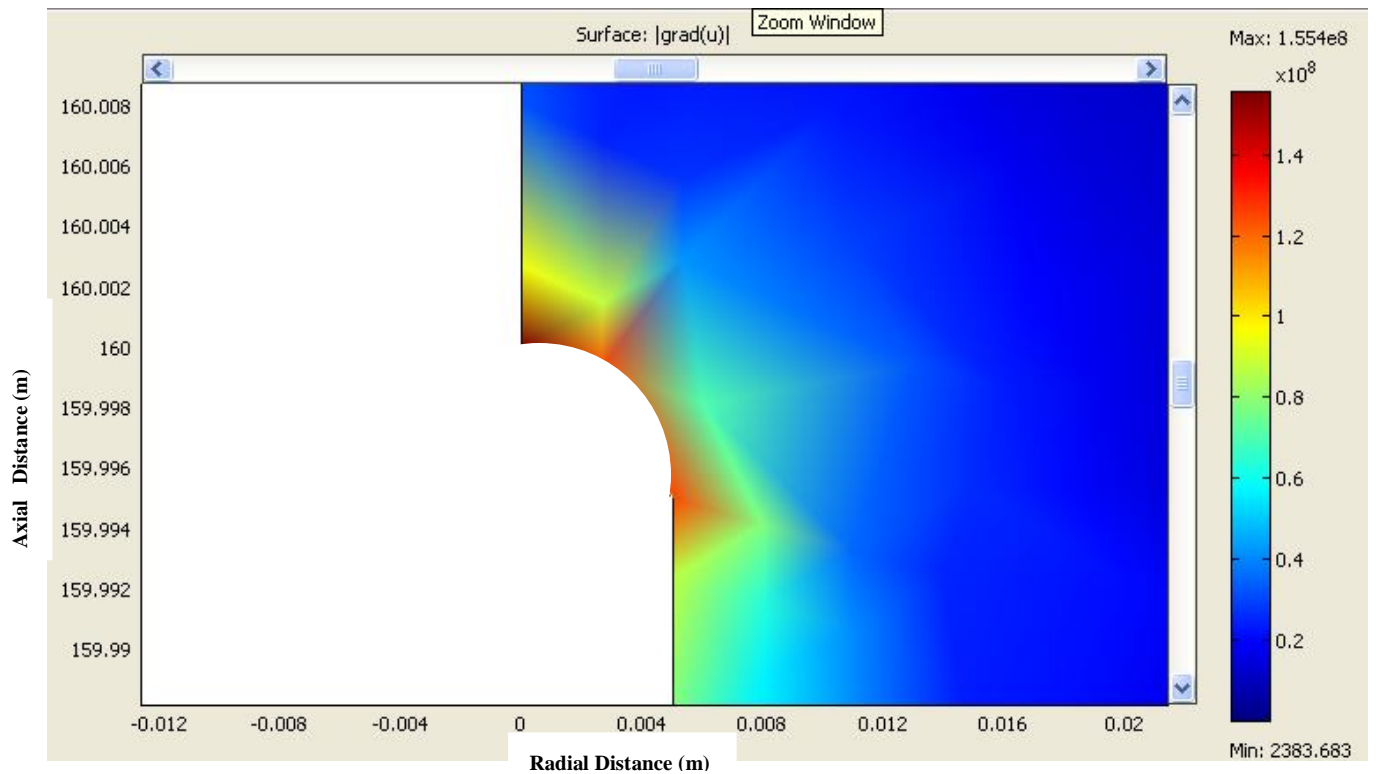


Figure 41 - Electric field distribution at the tip of the wire conductor

The numerical computed results for the fields and the potential are also respectively displayed in fig. 42 and 43.

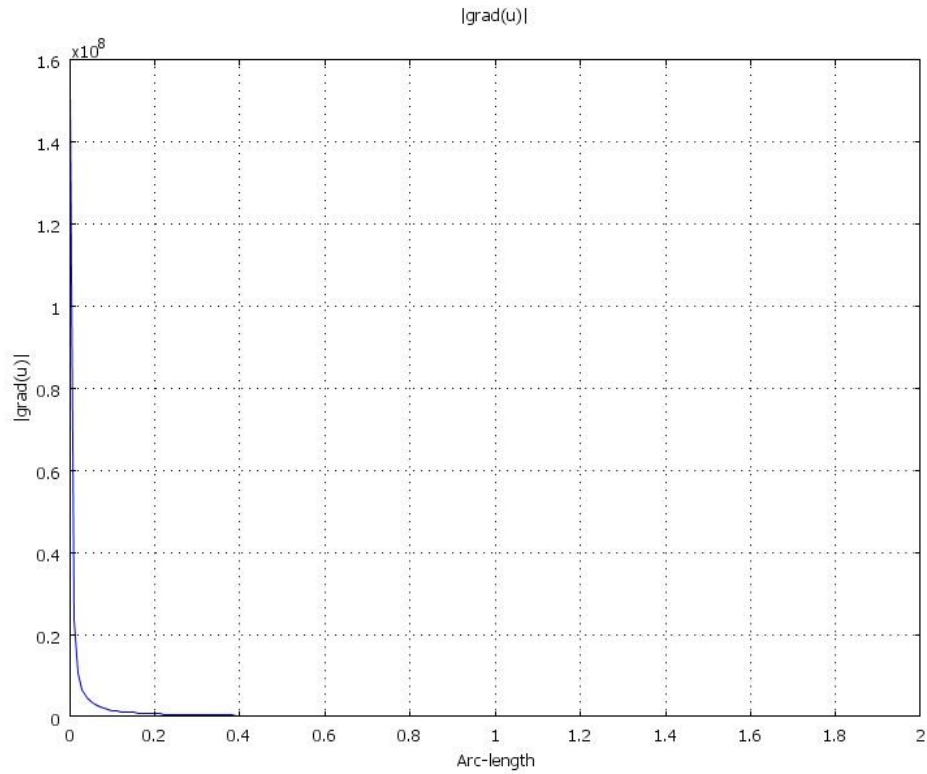


Figure 42 – Electric field distribution from 160 m to 162 m height

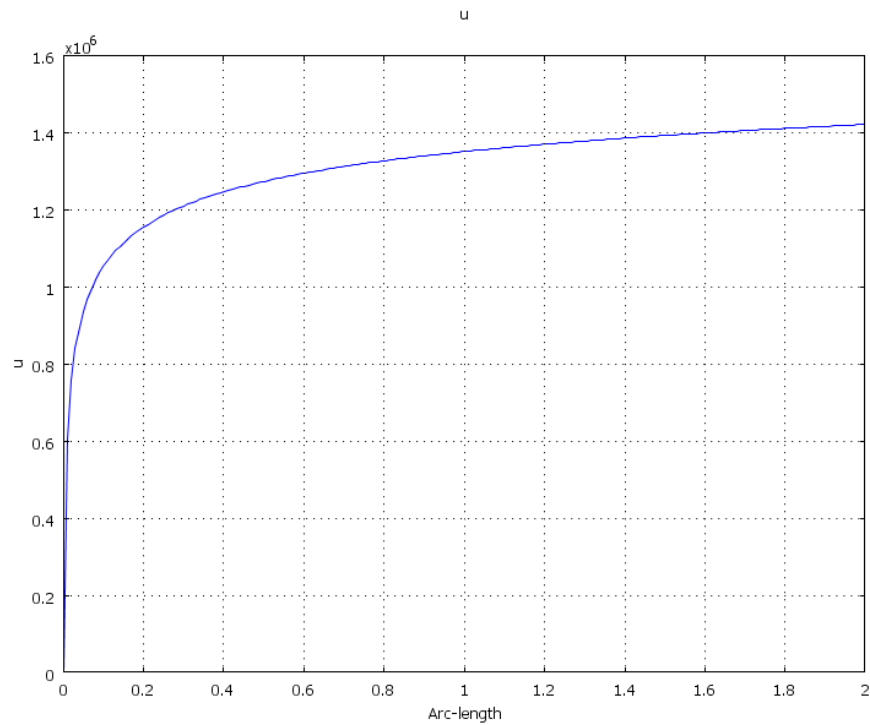


Figure 43 – Space potential distribution from 160 m to 162 m height

The results obtained are:

Height	Electric Field E (V/m)	Potential U (V)
@ tip : 160 m	1.526×10^8	~ 0
@ 162 m	49.6×10^3	1.43×10^6

Table 2 – Electric Field and Potential @ 160 m and 162 m (FEMLAB)

The Electric Field at the tip is very high as expected. The space potential of 1430 kV at 2 m from the tip confirms that streamers of several meter length will be produced.

Subsequently, we simulated another case where:

- Case2:
 - The wind tower will not be taken into consideration.
 - The conducting wire in the blade will go all the way down to ground and will still be represented with perfectly conducting conditions by a cylinder of height $H = 160$ m and $r = 0.005$ m.
 - A perfectly conducting ground will also be assumed.
 - Clouds and Atmosphere will be modeled as in case1.

The 2D partial differential equation used to solve the model is still Laplace in cylindrical coordinates.

In Femlab the generalized coefficient form equation used is still the same as in case1 as well. Here is a representation of the model:

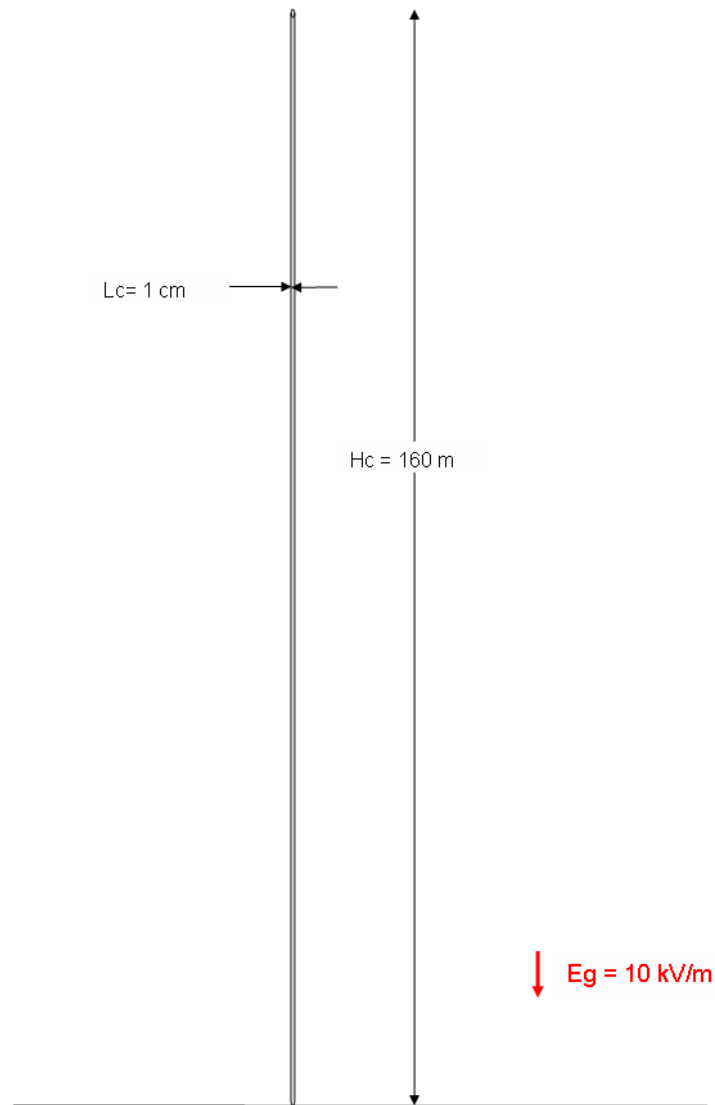


Figure 44 - Model defined in Femlab - wire conductor only

We will still solve the problem with cylindrical symmetry and the drawing representation will be only half of the original geometry. Once the solver equation is determined, the boundary conditions are set in the same way as in case1.

Once we compute these values by initializing the meshing and solving the problem, the results obtained are:

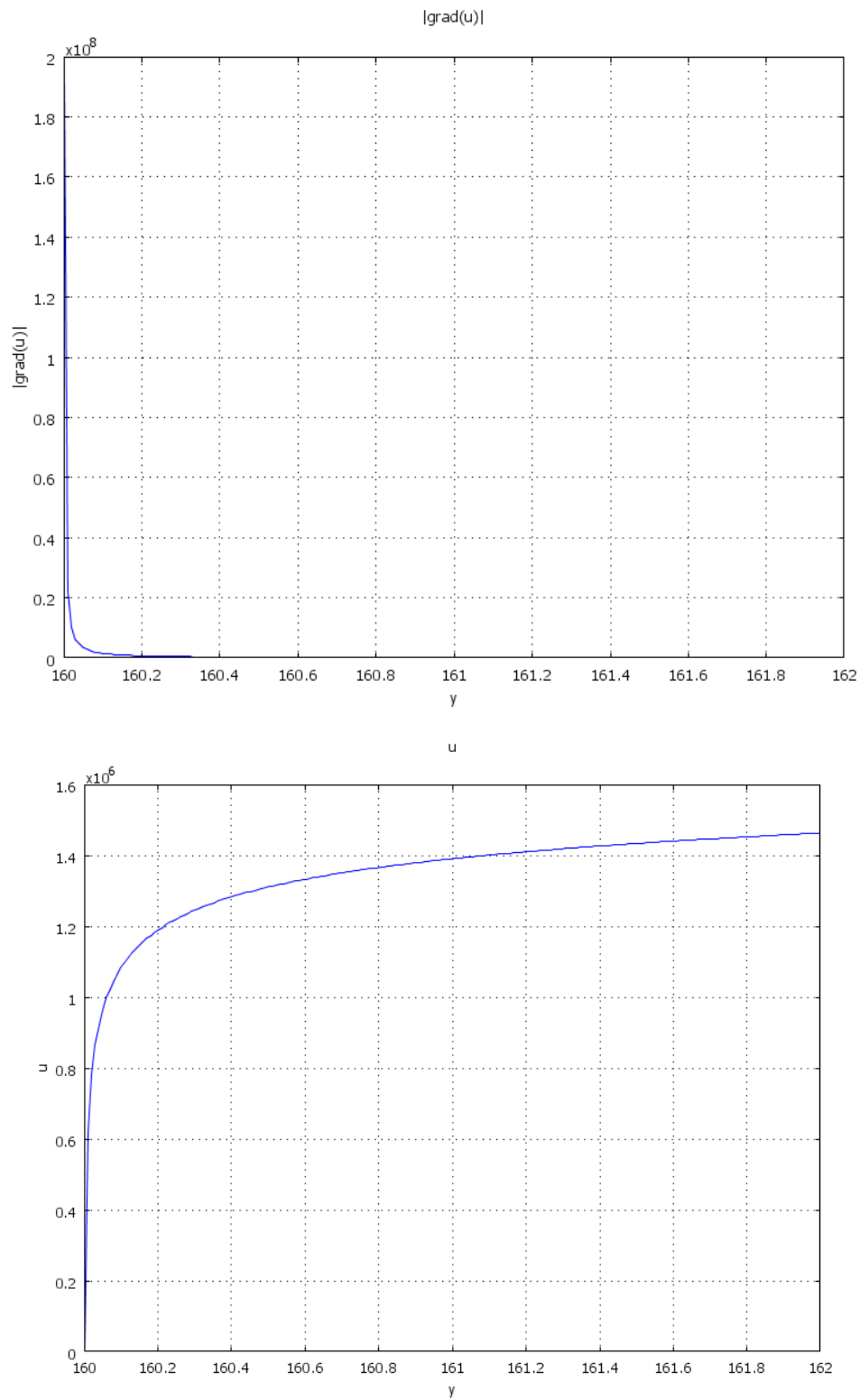


Figure 45 – (a) Electric field distribution from 160 m to 162 m height (b) Potential distribution from 160 m to 162 m height

Height	Electric Field E (V/m)	Potential U (V)
@ tip : 160 m	1.585×10^8	~ 0
@ 162 m	50.6×10^3	1.46×10^6

Table 3 – Electric Field and Potential @ 160 m and 162 m (FEMLAB)

Compared to case 1, the electric field at the tip of the down conductor is approximately 4% higher in the present case while the space potential is only 2% higher.

3.1.2. Charge Simulation Modeling

A second approach of modeling the field distribution outside the wind turbine is to use the well known charge simulation method (CSM)

In a paper Singer, Steinbigler and Weiss presented the details of CSM in 1974 [55]

The basic principle of conventional CSM is very simple. For the calculation of electric fields, the distributed charges on the surface of the electrode are replaced by N number of fictitious charges placed inside the electrode. The types and positions of these fictitious charges are predetermined but their magnitudes are unknown.

In order to determine their magnitude some contour points are selected on the surface of electrode. Then it is required that at any one of these contour points the potential resulting from superposition of effects all the fictitious charges is equal to the known electrode potential.

Let, Q_j be the j th fictitious charge and V is the known potential of the electrode. Then according to the superposition principle:

$$\sum_{j=1}^N P_{ij} Q_j = V \quad (37)$$

where P_{ij} is the potential coefficient, which can be evaluated analytically by solving Laplace's equation.

When Eqn. (37) is applied to N contour points, it leads to the following system of N linear equations for N unknown fictitious charges, then:

$$[P]_{N \times N} [Q]_N = [V]_N \quad (38)$$

where $[P]$ = potential coefficient matrix, $[Q]$ = column vector of known potential of contour points.

Eqn. (38) is then solved for the unknown fictitious charges. As soon as the required charge system is determined, the potential and the field intensity at any point, outside the electrodes can be calculated. While the potential is found by Eqn. (37), the electric stresses are calculated by super position of all the stress vector components.

Here as well, the same two cases were modeled:

- Case1:
 - The wind tower will be represented with perfectly conducting conditions by a cylinder of height $H = 100$ m and $r = 1$ m.
 - The conducting wire on the blades will be represented as well with perfectly conducting conditions by a cylinder of height $H = 60$ m and $r = 0.005$ m.
 - A perfectly conducting ground will be assumed.
 - Clouds and Atmosphere will be modeled by another cylinder of height $H = 2000$ m and $r = 4000$ m. The sides of the cylinder will be represented as perfectly insulated, the top of the cylinder will be represented with potential of $V = 20$ MV and the bottom will be grounded ($V = 0$ V)

Once we computed these values by solving the problem, the results obtained are:

Height	Electric Field E (V/m)	Potential U (V)
@ tip : 160 m	1.34×10^8	~ 0
@ 162 m	59.4×10^3	1.29×10^6

Table 4a – Electric Field and Potential @ 160 m and 162 m (Charge Simulation)

- Case2 :
 - The wind tower will not be considered.
 - Only the conducting wire on the blades going all the way to the ground will be represented with perfectly conducting conditions by a cylinder of height $H = 160$ m and $r = 0.005$ m.
 - A perfectly conducting ground will be assumed.
 - Clouds and Atmosphere will be modeled by another cylinder of height $H = 2000$ m and $r = 4000$ m. The sides of the cylinder will be represented as perfectly insulated, the top of the cylinder will be represented with potential of $V = 20$ MV and the bottom will be grounded ($V = 0$ V)

Once we computed these values by solving the problem, the results obtained are:

Height	Electric Field E (V/m)	Potential U (V)
@ tip : 160 m	1.36×10^8	~ 0
@ 162 m	59.9×10^3	1.31×10^6

Table 5b – Electric Field and Potential @ 160 m and 162 m (Charge Simulation)

Here as, well, compared to case1, both cases produce approximately the same results.

Charge simulation calculations showed that taking into account the tower results in a 1.5% reduction of the field at the tip of the down conductor. It also led to a 1.5 % reduction in the space potential 2m from the tip.

The results are close to what was obtained by Femlab.

The essential point is that we can clearly state that to make field and potential calculation for a wind turbine model, one can just consider the down conductor all the way to the ground neglecting the tower and nacelle since their presence does not significantly change the results of the field obtain at the tip of the blade or the space potential in the vicinity.

3.2. Comparison between Rizk model and IEC standard

3.2.1. Attractive Radius

According to IEC 61400-24 in 2002 [1], the annual average number of direct lightning flashes N_f to the wind turbine can be assessed by the following formula :

$$N_f = N_g \times A_d \times C_d \times 10^{-6} \quad (39)$$

where N_d is the annual average number of direct lightning strikes to the structure;

N_g is the annual average ground flash density;

C_d is the environmental factor

A_d is the average collection area for a wind turbine placed on a flat ground (assumed radius of three times the turbine height) - Figure 46.

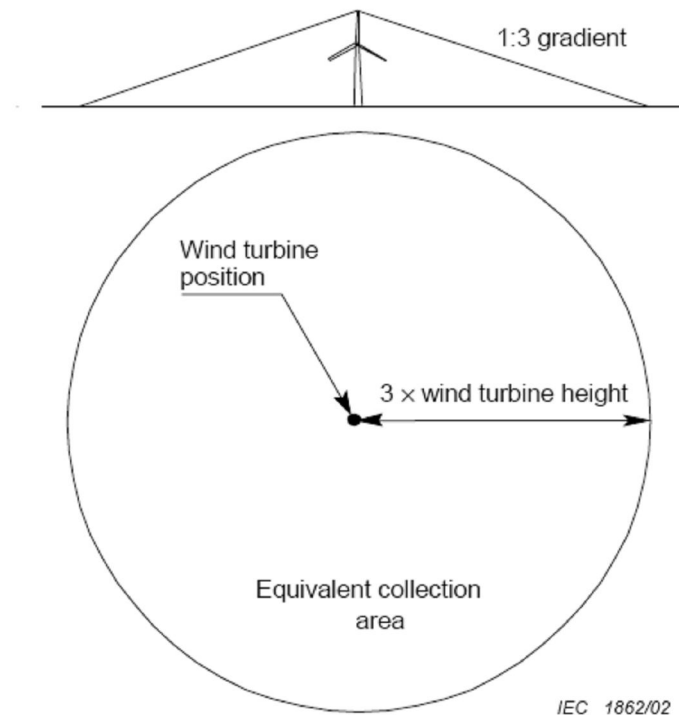


Figure 46 - Equivalent collection area of the wind turbine

In 1994, in Canada Rizk published a paper [18] where he comprised an extensive computer investigation of lightning incidence to tall masts based on a theory presented in a companion paper, for both flat and hilly regions.

He stated that the attractive radius R_a of a downward flash varies with the structure elevation h , the ambient ground field and on the ground elevation (flat, mountain....)

When assessing the lightning flash frequency to a structure, the collection of data detailing the local ground flash density (N_g) is necessary. National organizations may be able to provide this information.

If the ground flash density is not available, IEC 61024 [1] describes a way to estimate it using the following relationship:

$$N_g = 0.04 \times T_d^{1.25} \quad (4)$$

where T_d is the number of thunder storm days per year obtained from isoceraunic maps.

Then, if we follow Rizk model [18], one can assess the number of downward flashes N_{dw} to a freestanding slender tower of height $10\text{m} < h < 200\text{m}$ in a region of ground flash density N_g can be estimated as:

$$N_{dw} = \frac{N_g}{10^6} \times \pi \times (R_{ao})^2 \quad (24)$$

His model implies as well that if we consider a median return stroke current of 31kA, a regression analysis of the model yields an expression for the dependence of the overall attractive radius R_{ao} on structure of height h :

$$R_{ao} = 25.9 \times h^{0.48} \quad (19)$$

Rizk showed then clearly that the number of upward flashes per year from tall towers can also be estimated. That number N_u can be expressed as the product of the number of storms per year T_d and the cumulative probability, that once a storm did occur, the critical ground field E_{gc} is exceeded.

$$N_u = T_d \times P(E_g > E_{gc}) \quad (25)$$

Further analysis of such data suggests that the cumulative probability function $P(E_g > E_{gc})$ could be approximated by an exponential function:

$$P(E_g > E_{gc}) = e^{-(E_{gc} - E_{g0})/E_{g1}} \quad (26)$$

where E_{g0} , is a threshold field, once a storm did occur and E_{g1} is a shape parameter.

Based on information from [18], we performed computations in order to evaluate the proportion of upward and downward flashes for a tower of height h .

In the following we will use two ways for calculation the attractive radius based on Rizk's model and IEC standard.

Let us now compare the two methods, in order to see in which way they can be comparable.

Rizk's expression (19) (for downward flashes only) for the dependence of the overall attractive radius R_{ao} is:

$$Ra1 = 25.9 \times h^{0.48}$$

IEC [1] expression for the equivalent attractive radius is (including upward flashes):

$$Ra2 = 3 \times h$$

If we apply these two formulas to different heights (20 to 200 m) reasonably comparable to wind turbines, we obtain:

H (m)	20	30	40	50	60	70	80	90	100	110	120	130	140	150	160	170	180	190	200
Ra1(m)	109	133	152	169	185	199	212	225	236	247	258	268	278	287	296	305	313	321	329
Ra2(m)	60	90	120	150	180	210	240	270	300	330	360	390	420	450	480	510	540	570	600

Table 6 – Comparison Attractive Radius Rizk and IEC Model

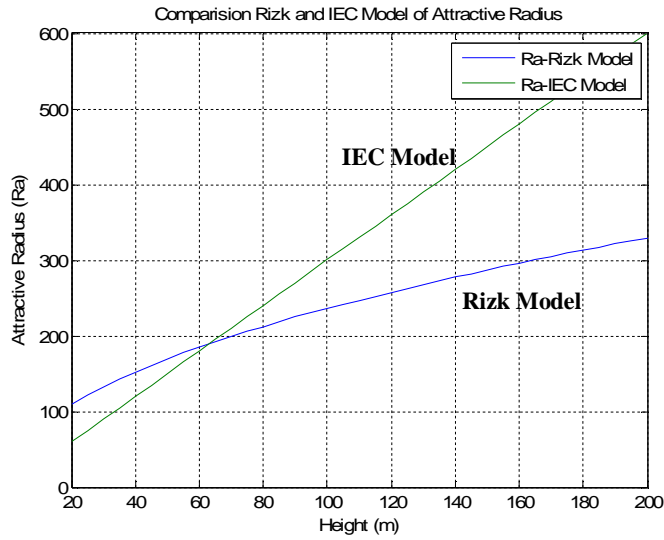


Figure 47 – Comparison Attractive Radius Rizk (for downward flash only) and IEC Model

For some heights, the difference between the two methods can be considerable, here is the ratio obtained for the height 20 to 200 m:

H (m)	20	30	40	50	60	70	80	90	100	110	120	130	140	150	160	170	180	190	200
Ra2/Ra1	0.3	0.46	0.62	0.78	0.95	1.11	1.28	1.45	1.61	1.78	1.95	2.12	2.29	2.46	2.63	2.80	2.97	3.15	3.32

Table 7 – Attractive radius Ratio between Rizk and IEC Model

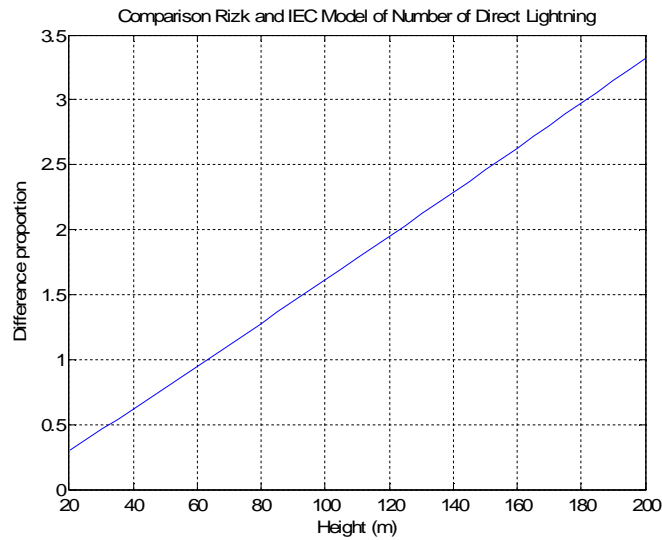


Figure 48 - Attractive radius Ratio between Rizk (for downward flash only) and IEC Model

One can see that for these values of height the attractive radius calculated with IEC model can be sometime more than 3 times the one obtained with Rizk model. Around height between 50 to 70m, both methods can be applied depending since the difference is not very significant.

3.2.2. Number of direct lightning flashes

Let us now go deeper in the investigation and calculate directly the numbers of flashes that occur on a tower first with Rizk model [18] and compare it to the value obtain with IEC standards [1].

Rizk model states that the number of downward flashes Ndw to a freestanding tower of height $10m < h < 200m$ in a region of ground flash density Ng can be estimated as: [18]

$$Ndw = \frac{Ng}{10^6} \times \pi \times (R_{ao})^2 \quad (24)$$

And that the number of upward flashes Nu can be expressed as:

$$Nu = Td \times P(Eg > Egc) \quad (25)$$

where $P(E_g > E_{gc}) = e^{-(E_{gc} - E_{g0})/E_{g1}}$ (26)

$$T_d = 25 \times N_g^{0.8} \quad (40)$$

$$E_{gc} = \frac{1600}{h} \quad (27)$$

E_{g0} , is a threshold field, once a storm did occur and E_{g1} is a shape parameter [18]

- Distribution 1: Under disturbed weather (shower) conditions, Rizk showed in his paper that $Eg0$ and $Eg1$ can be well represented by:

$$Eg0 = 2kV/m \text{ and } Eg1 = 2 \text{ kV/m.}$$

He suggested that it reasonably covers ordinary situations where it has often been reported that the ground field rarely exceeds 10 kV/m under lightning storm conditions.

- **Distribution 2:** On a plateau of high altitude, severe condition and winter lightning E_{g0} and E_{g1} can be well represented by:

$$E_{g0} = 3\text{kV/m and } E_{g1} = 6\text{ kV/m.}$$

So according to Rizk model the total number of flashes is:

$$N_f = N_u + N_d = \frac{Ng}{10^6} \times \pi \times (R_a^2) + T_d \times e^{-(E_{gc} - E_{go})/E_{g1}} \quad (41)$$

According to IEC 61400-24 [1], the annual average number of direct lightning flashes to the wind turbine can be assessed by the following formula:

$$N_f = N_g \times A_d \times C_d \times 10^{-6} \quad (39)$$

where N_f is the annual average number of direct lightning strikes to the structure;

N_g is the annual average ground flash density;

C_d is the environmental factor (Distribution1: $C_d = 1$ and Distribution 2: $C_d = 2$)

$$A_d = \pi(3h)^2$$

Lightning flash densities observed by the different LLS for different spatial resolutions vary from 1 to 47 flashes $\text{km}^{-2} \text{ year}^{-1}$, in response to processes involving different meteorological systems and their interaction with different geographical features. The highest maximum CG lightning flash density on Earth (65 flashes $\text{km}^{-2} \text{ year}^{-1}$) occurs in Java Island [56]

Case 1. Considering a Distribution 1 type in an area with low value of $N_g = 1$ flash/ km^2/year . For height from 20 to 200 m, the following presents the results obtained:

H (m)	20	30	40	50	60	70	80	90	100	110	120	130	140	150	160	170	180	190	200
Nf(Rizk)	0.04	0.06	0.07	0.09	0.11	0.13	0.14	0.16	0.19	0.22	0.25	0.30	0.36	0.43	0.52	0.62	0.73	0.85	1.00
Nf(IEC)	0.01	0.03	0.05	0.07	0.10	0.14	0.18	0.23	0.28	0.34	0.40	0.48	0.55	0.64	0.72	0.82	0.92	1.02	1.13

Table 8 – Total number of flashes for different heights for a value $N_g = 1$ flash/ km^2/year computed with Rizk and IEC methods

When we compare the results again, we note that for a value of N_g that low, the maximum difference of flashes is only 0.15 flashes. Even if the ratio goes up to 1.6 around a height of 120 m, the difference of results obtained can be accepted (numbers of flashes are around 1 fl. per year).

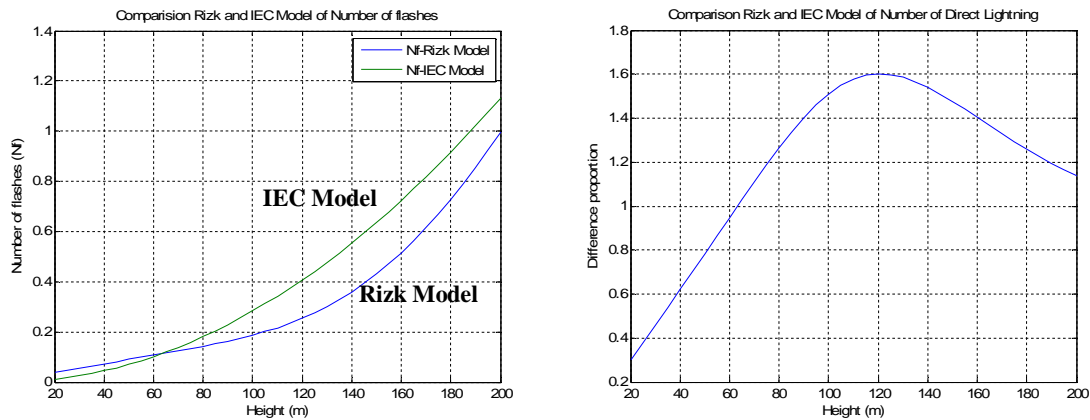


Figure 49 – Total number of flashes and ratio for different heights for a value $N_g = 1$ flash/km²/year computed with Rizk and IEC methods

Case 2. Considering a distribution 1 type in an area with low value of $N_g = 2$ flashes/km²/year (usually in cities). For height from 20 to 200 m, the following presents the results obtained:

H (m)	20	30	40	50	60	70	80	90	100	110	120	130	140	150	160	170	180	190	200
Nf(Rizk)	0.08	0.11	0.15	0.18	0.21	0.25	0.29	0.33	0.37	0.40	0.46	0.54	0.63	0.75	0.89	1.06	1.24	1.46	1.82
Nf(IEC)	0.02	0.05	0.09	1.14	0.20	0.28	0.36	0.45	0.57	0.68	0.81	0.96	1.10	1.27	1.45	1.63	1.83	2.04	2.26

Table 9 – Total number of flashes for different heights for a value $N_g = 2$ flash/km²/year computed with Rizk and IEC methods

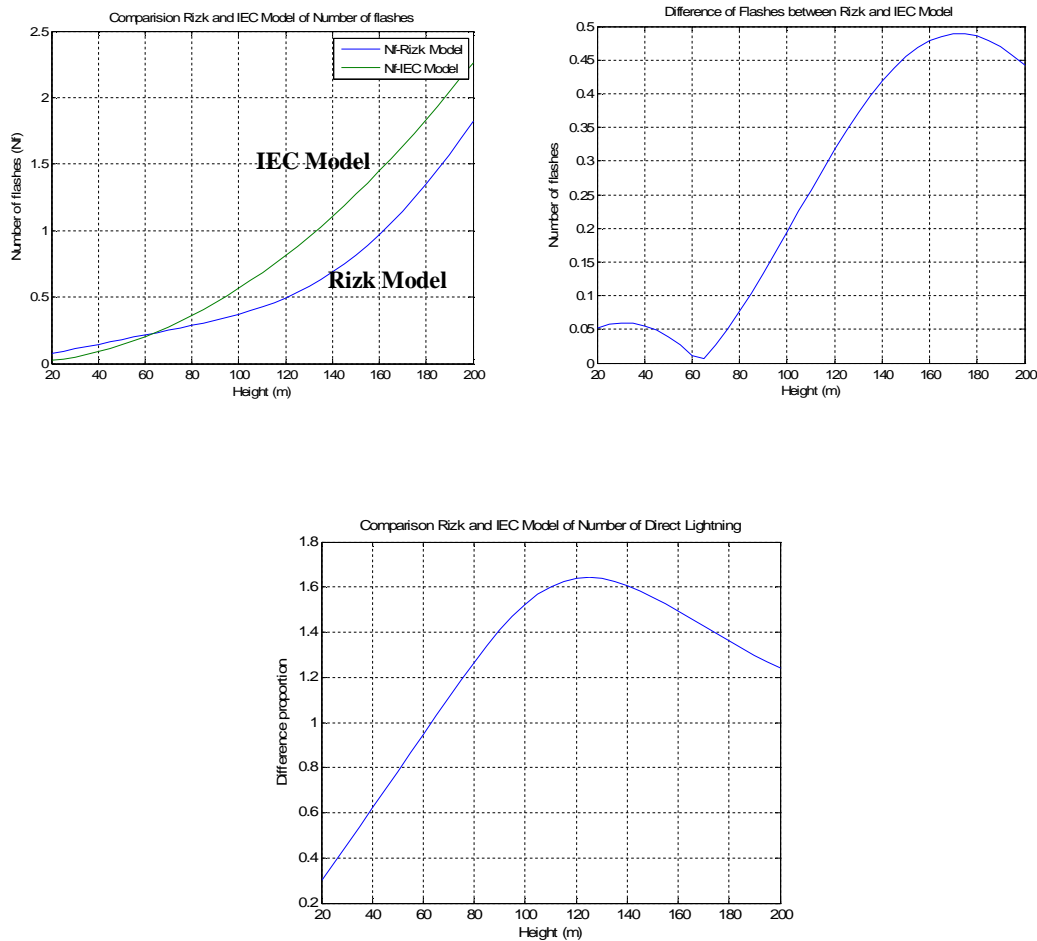


Figure 50 – Total number of flashes and ratio for different heights for a value $N_g = 2 \text{ flash/km}^2/\text{year}$ computed with Rizk and IEC methods

When we compare the results again, we find that Rizk's model gives higher values at lower structure heights and lower values at large heights. We note however that for a value of N_g that low, the maximum difference of flashes is only 0.5 flashes. Even if the ratio of the difference always goes up to 1.6 around a height of 120 m, the difference of results obtained can be neglected (numbers of flashes are around 2 fl. per year).

Case 3. Considering now an area with moderate value $N_g = 10$ flashes/ km^2 /year. For height from 20 to 200 m, the following presents results obtained:

H (m)	20	30	40	50	60	70	80	90	100	110	120	130	140	150	160	170	180	190	200
Nf(Rizk)	0.38	0.55	0.72	0.90	1.07	1.25	1.43	1.62	1.83	2.08	2.22	2.55	2.94	3.41	3.96	4.60	5.33	6.15	7.53
Nf(IEC)	0.11	0.25	0.45	0.70	1.01	1.39	1.81	2.29	2.83	3.42	4.07	4.77	5.54	6.36	7.23	8.17	9.16	10.20	11.31

Table 10 – Total number of flashes for different heights for a value $N_g = 10$ flash/ km^2 /year computed with Rizk and IEC methods

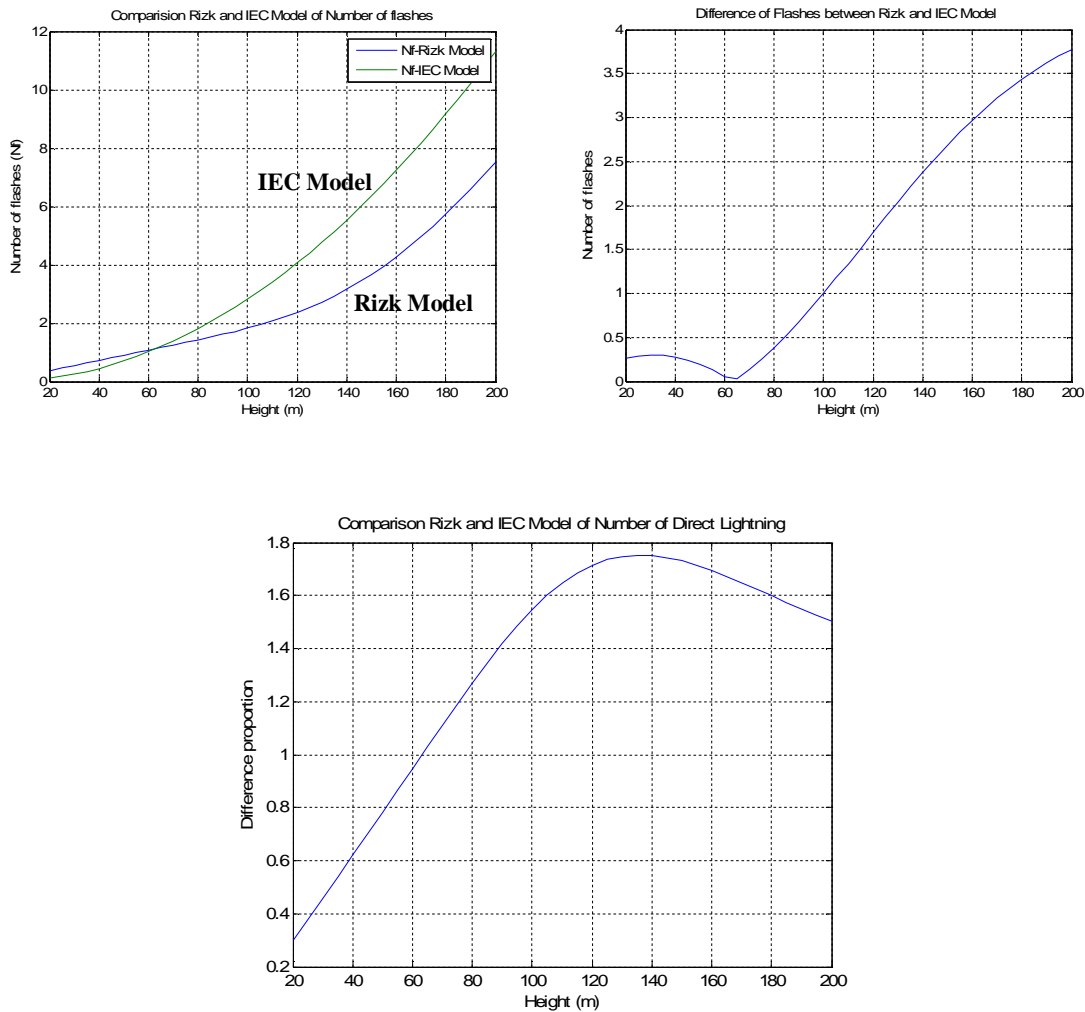


Figure 51 – Total number of flashes and ratio for different heights for a value $N_g = 10$ flash/ km^2 /year computed with Rizk and IEC methods

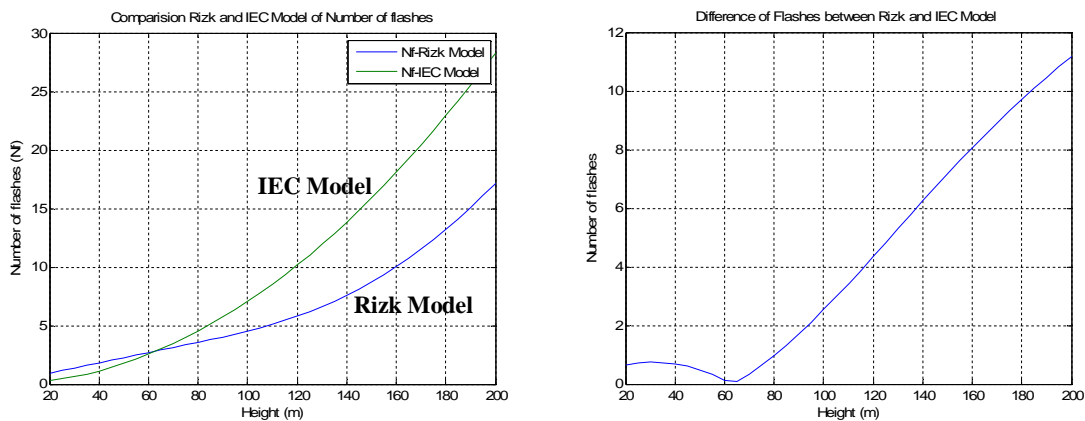
When we compare the results this time, we note for a value of N_g moderately high, the difference of results obtained can start to be considerable since maximum difference of flashes obtained by the two models is around 3 flashes around height of 200 m.

This time, the ratio of the difference goes up to almost 1.8 around a height of 140 m. This difference can still be accepted since 3 flashes in a year is not a very high number comparatively to the estimated number of flashes we should obtain.

Case 4. Considering now a distribution 1 type in an area with a high value $N_g = 25 \text{ flashes/km}^2/\text{year}$. For height from 20 to 200 m, the following presents the results obtained:

H (m)	20	30	40	50	60	70	80	90	100	110	120	130	140	150	160	170	180	190	200
Nf(Rizk)	0.93	1.38	1.82	2.25	2.68	3.12	3.56	4.02	4.54	5.13	5.82	6.64	7.60	8.73	10.04	11.5	13.2	15.1	17.1
Nf(IEC)	0.28	0.63	1.13	1.77	2.55	3.46	4.52	5.73	7.07	8.55	10.2	11.9	13.9	15.9	18.1	20.4	22.9	25.5	28.3

Table 11 – Total number of flashes for different heights for a value $N_g = 25 \text{ flash/km}^2/\text{year}$ computed with Rizk and IEC methods



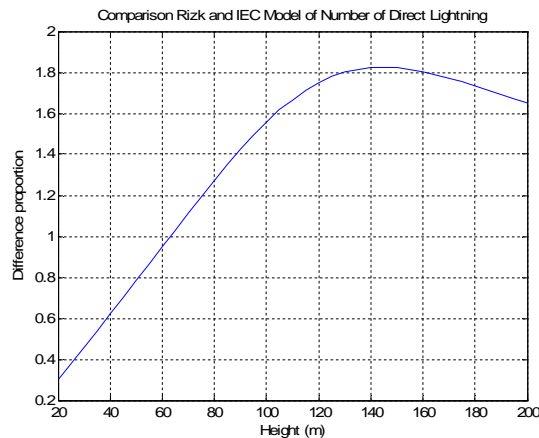


Figure 52 – Total number of flashes and ratio for different heights for a value $N_g = 25$ flash/km²/year computed with Rizk and IEC methods

Now, if one compares the results, we note for a value of N_g that high, the difference of results obtained is considerable since maximum difference of flashes obtained by the two methods is more than 10 flashes in a year. The ratio of the difference still goes up to 1.82. The two methods can not really be comparable after a height of 100m, since the difference becomes more than 4 flashes in a year comparatively to the estimated number of flashes we should obtain.

Case 5. And at last, considering now an area with a higher value $N_g = 65$ flashes/km²/year (highest on earth). For height from 20 to 200 m, the following presents the results obtained:

H (m)	20	30	40	50	60	70	80	90	100	110	120	130	140	150	160	170	180	190	200
Nf(Rizk)	2.43	3.59	4.73	5.86	6.98	8.10	9.24	10.4	11.7	13.2	14.9	16.8	19.1	21.7	24.7	28.1	31.9	36.1	40.6
Nf(IEC)	0.74	1.65	2.94	4.60	6.62	9.00	11.8	14.9	18.4	22.2	26.5	31.1	36.1	41.4	47.1	53.1	59.5	66.4	73.6

Table 12 – Total number of flashes for different heights for a value $N_g = 65$ flash/km²/year computed with Rizk and IEC methods

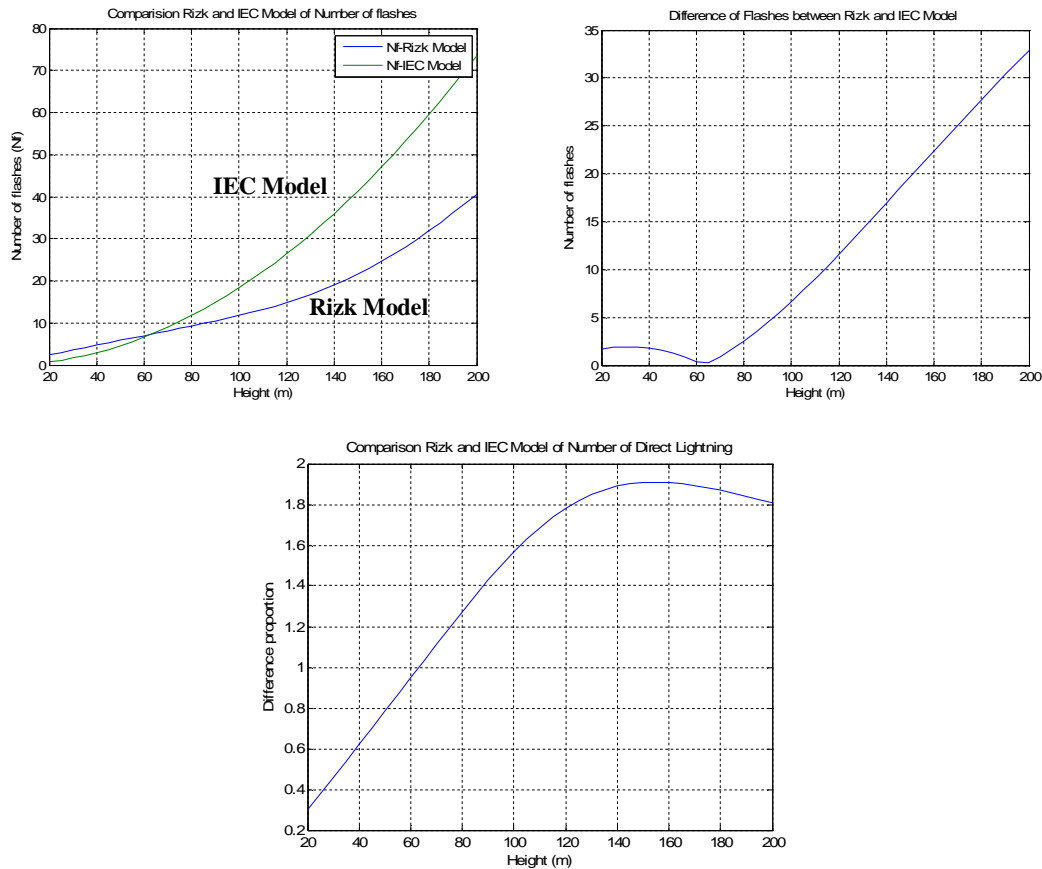


Figure 53 – Total number of flashes and ratio for different heights for a value $N_g = 25 \text{ flash/km}^2/\text{year}$ computed with Rizk and IEC methods

In this last case, one can see that for a value of N_g that very high, the difference of results obtained is very important since the maximum difference of flashes obtained by the two methods is more than 30 flashes in a year around a height of 200 m. The ratio of the difference goes up to almost 2, thus the two methods can not be comparable after a height of 80 m, since the difference becomes more than 4 flashes in a year comparatively to the estimated number of flashes we should obtain.

We can then say that the two models can be comparable when the flashes density is not very high (less than 15 fl/km²/year), and for Ng more important, they only can be comparable for lower height of structure (less than 100 to 120m).

It should be noted however that the IEC method does address the details of upward and downward flashes but only offers an approximate overall analysis.

3.3. Modeling Wind Turbine for Proportion of upward and downward flashes

3.3.1. Blade Position vs Time

The major parts of a wind turbine that are exposed to the environment are the tower, the nacelle and the rotor. The rotor, which has three blades, is the most susceptible to direct lightning strikes as it is higher off the ground than the other components.

Researches showed that Speed of upward main leader flashes is usually between 0.6×10^5 m/s and 6.7×10^5 m/s and the speed of downward stepped leader varies in the wide range of is 0.6×10^5 m/s to 2×10^6 m/s [57]

If we compare the cut out wind speed $v_{wt} = 25$ m/s of a wind turbine to an average downward leader speed $v_l = 2.5 \times 10^5$ m/s, we obtain a ratio of:

$$\frac{v_l}{v_{wt}} = \frac{2.5 \times 10^5}{25} = 10^4$$

For example, during the last 500 m of descent of the negative stepped leader assumed moving at a speed of $v_l = 2.5 \times 10^5$ m/s, we can evaluate the travel time t:

$$t = \frac{d}{v_l} = \frac{500}{2.5 \times 10^5} = 2 \text{ ms}$$

For a time $t = 2$ ms and given a cut out wind speed $v_{wt} = 25$ m/s of the wind turbine, the distance traveled by the blade will be:

$$d_b = v_{wt} \times t = 25 \times 0.002 = 5 \text{ cm}$$

Given the small distance that is traveled by the blades during this time, we can therefore conclude that the wind turbine blades are quasi-stationary compare to the lightning flash.

Now, we can start going more into details and take others variable into consideration. We know that the turbine has three blades and are rotating at a given speed.

This means, the total height of one structure can vary depending on the position of the blades which at his turn vary in function of time.

So we will take into consideration three facts:

- The blade rotates at a given speed v
- Height of the tip is function of time t
- There a three blades spaced from each other at angle : $\frac{2\pi}{3}$

Let us set the initial conditions:

- $t = 0\text{s}$, $\theta = 0$, $\alpha_i = \frac{\pi}{2}$, Hub height : 60 m

We will consider the operational data:

- *Cut-out wind speed: 25 m/s*

We know that the angular speed ω is defined by:

$$\omega = \frac{d\theta}{dt} = \frac{v_t}{R} \quad (42)$$

And the angular displacement θ measured from the vertical is given by:

$$\theta(t) = \alpha_i + \omega t \quad (43)$$

where :

ω is the angular speed, radians/s

v_t is the nominal speed, m/s

R is the radius (length of the blade), m

We know as well that at a given time t , the position of the blade when its rotating at a speed v_t can be obtain by using the trigonometric formula cosine

The vertical length associated to the blade position can be then obtained with:

$$H(t) = H_0 + R \cos(\alpha_i + \omega t) \quad (44)$$

where H_0 is the tower length and R the blade length.

Let us take a case where $t=0s$, $H_0 = 100$ m, $R = 40$ m, $\alpha_i = 0$ and $\omega t = \frac{\pi}{3}$, the blade is at a $\frac{\pi}{3}$ position.

When the blade is between 0 and π , the height of all the structure will be: the height of the tower + the vertical length associated to the blade position.

The vertical length associated to the instantaneous blade position can be obtained using (44). The total height is then:

$$H = 60 + 40 \cos\left(0 + \frac{\pi}{3}\right)$$

$$H = 60 + 40 \times 0.5$$

$$H = 80m$$

Since in reality, the wind turbine has 3 blades, we have to take them into account on the calculation of the real height of the structure (blade tip position) at any time t .

At $t = 0$ s and $\alpha_i = 0$, figure 54 (a) shows the position of the blades which is the highest configuration for the vertical length of the circle. The lowest configuration of the tower is when the blades are on a Y position like illustrated in fig. 54 (b).

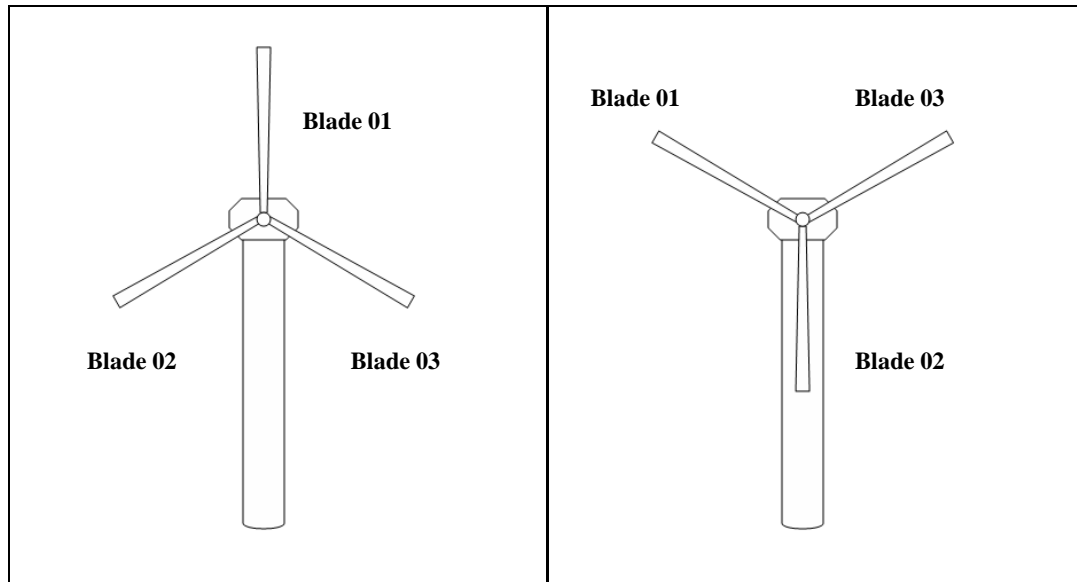


Figure 54 – (a) Highest Configuration of the wind turbine (b) Y and Lowest configuration of the wind turbine

We can then find the position of the tip of the turbine at different time.

We know that the vertical length of the blade at a position with an angle θ between 0 and π is:

$$H_b = R \cos(\alpha_i + \omega t) \quad (45)$$

Now if we take into account the speed of the rotation and the three blades, as we said earlier, there is two cycles of decrease and increase. Each happens every time the blade does a $\frac{\pi}{3}$ distance.

The speed we take into account is:

- $v_t = 25\text{m/s}$ and the blade length $R = 40$ m.

And we know that the angular displacement is obtained by using (43)

Which mean that if we want to satisfy $0 < \theta < 2\pi$, then:

$$0 < \frac{v_t}{R} \times t < 2\pi$$

$$0 < t < 2\pi \frac{R}{v_t} \text{ with } R = 40 \text{ and } v_t = 25 \text{ m/s}$$

$$0 < t < \frac{16}{5}\pi$$

So we can evaluate the position of each blade at any time t.

With the initial position of each blade:

- blade 01 at 0
- blade 02 at $\frac{2\pi}{3}$
- blade 03 at $\frac{4\pi}{3}$

Results from computing equation (45) for the three blades are illustrated in fig.55

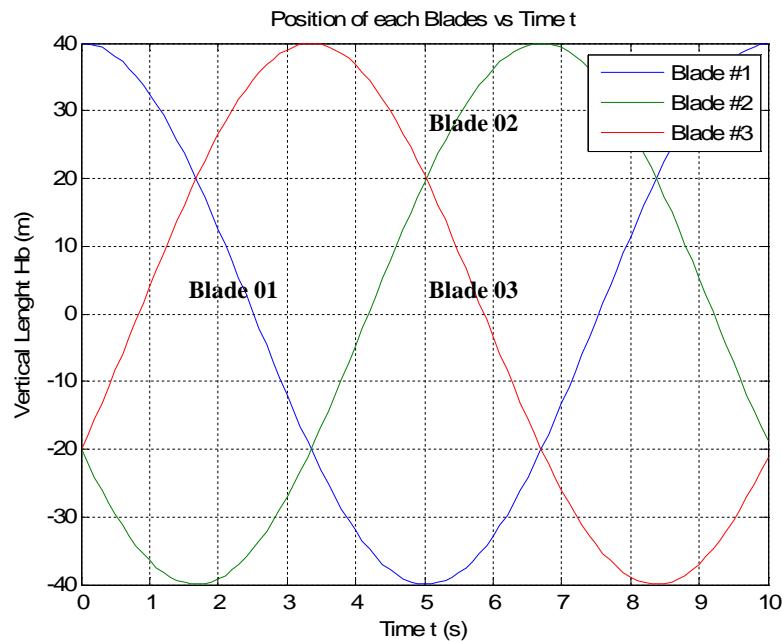


Figure 55 – Vertical length of the Wind turbine vs Time

We will of course only consider the position which is positive, i.e above the tower height (fig.56)

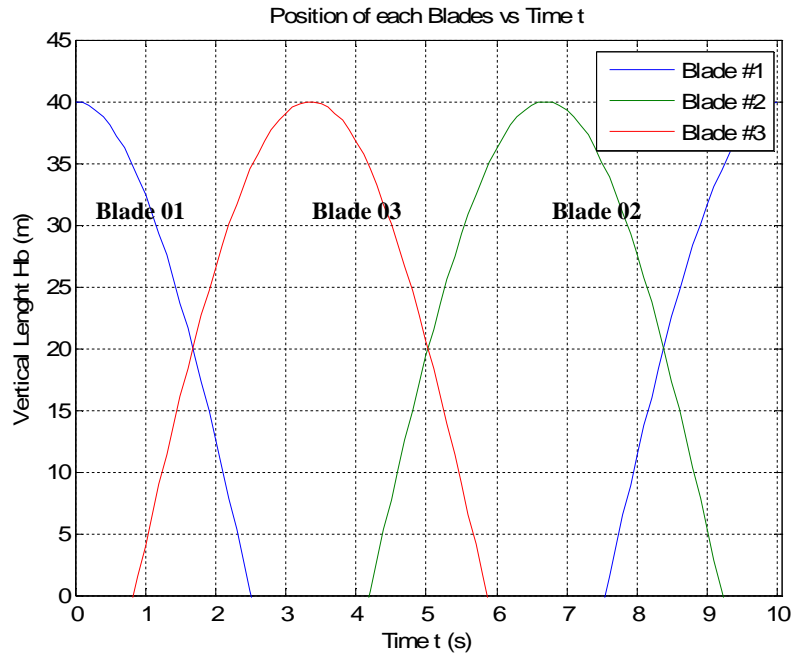


Figure 56 – Position of heights of the Wind turbine Blades vs Time

We will also only consider values of height where the three curves do not intercept each other. Those are the actual values of all possible heights of the blade system considering their lowest position configuration: the Y position.

Fig. 57 shows these values.

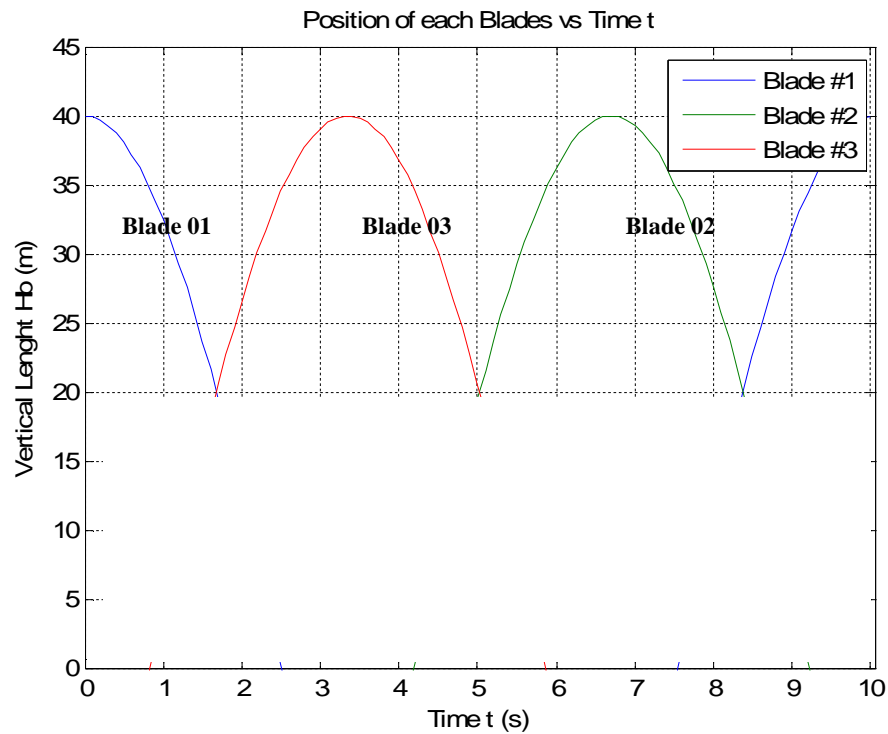


Figure 57 - Position of each blades of the wind turbine vs Time

We can see that on one revolution (2π), the total height of the blades system varies from 40 to 20 m.

So if we take into account the height H_0 of the tower and knowing the exact position of the blades system at a time t , one can now derive the total height of the structure at a given time t using (42).

Results are displayed in table 11 and fig. 58.

Time t (s)	0	0.1	0.2	0.3	0.4	0.5	0.6
Height (m)	100	99.92	99.69	99.29	98.75	98.06	97.22
Time t (s)	0.7	0.8	0.9	1	1.1	1.2	1.3
Height (m)	96.23	95.10	93.83	92.43	90.91	89.26	87.50
Time t (s)	1.4	1.5	1.6	1.675	1.8	1.9	2
Height (m)	85.63	83.67	81.61	80	81.61	83.67	85.63
Time t (s)	2.1	2.2	2.3	2.4	2.5	2.6	2.7
Height (m)	87.50	89.26	90.91	92.43	93.83	95.10	96.23
Time t (s)	2.8	2.9	3	3.1	3.2	3.3	3.351
Height (m)	97.22	98.06	98.75	99.29	99.68	99.92	100
Time t (s)	3.5	3.6	3.7	3.8	3.9	4	4.1
Height (m)	99.92	99.68	99.29	98.75	98.06	97.22	96.23
Time t (s)	4.2	4.3	4.4	4.5	4.6	4.7	4.8
Height (m)	95.10	93.83	92.43	90.91	89.26	87.50	85.63
Time t (s)	4.9	5	5.03	5.2	5.3	5.4	5.5
Height (m)	83.67	81.61	80	81.61	83.67	85.63	87.50
Time t (s)	5.6	5.7	5.8	5.9	6	6.1	6.2
Height (m)	89.26	90.91	92.43	93.83	95.10	96.23	97.22
Time t (s)	6.3	6.4	6.5	6.6	6.7	6.72	6.9
Height (m)	98.06	98.75	99.29	99.68	99.92	100	99.92
Time t (s)	7	7.1	7.2	7.3	7.4	7.5	7.6
Height (m)	99.68	99.29	98.75	98.06	97.22	96.23	95.10
Time t (s)	7.7	7.8	7.9	8	8.1	8.2	8.3
Height (m)	93.83	92.43	90.91	89.26	87.50	85.63	83.67
Time t (s)	8.38	8.41	8.6	8.7	8.8	8.9	9
Height (m)	80	81.61	83.67	85.63	87.50	89.26	90.91
Time t (s)	9.1	9.2	9.3	9.4	9.5	9.6	9.7
Height (m)	93.11	94.44	95.65	96.71	97.63	98.40	99.02
Time t (s)	9.8	9.9	10	10.05			
Height (m)	99.50	99.81	99.97	100			

Table 13 – Heights of the wind turbine rotating at different time t

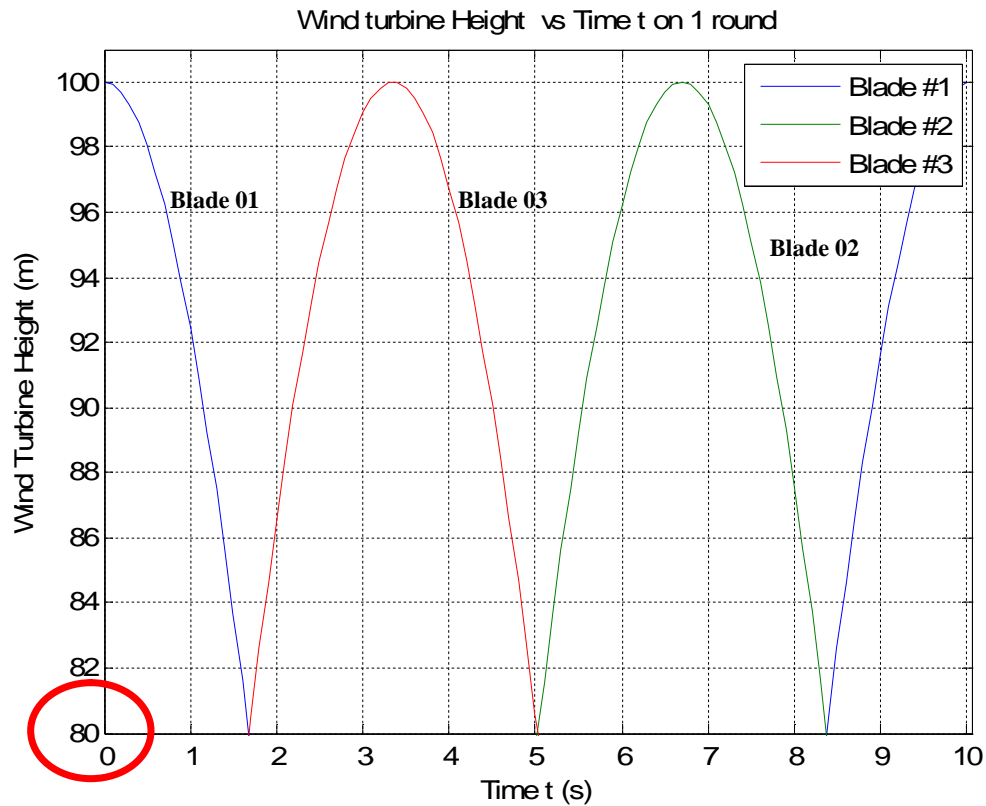


Figure 58 - Heights of the wind turbine rotating at different time t for one cycle of 2π

3.3.2. Proportion of upward and downward flashes

Since the model we are using is only considering height from 100 m to 80 m, we can use either Rizk or IEC model.

Let us use Rizk 's model [18] , the overall attractive radius R_{ao} for downward flashes will be :

$$R_{ao} = 25.9 \times h^{0.48} \quad (19)$$

Applying it to this formula to the values obtain of the different heights, these are the equivalent attractive radius we obtain as a function of height:

Time t (s)	0	0.1	0.2	0.3	0.4	0.5	0.6
Height (m)	100	99.92	99.68	99.29	98.75	98.06	97.22
Ra (m)	236.21	236.12	235.85	235.41	234.79	234.00	233.03
Time t (s)	0.7	0.8	0.9	1	1.1	1.2	1.3
Height (m)	96.23	95.10	93.83	92.43	90.91	89.26	87.50
Ra (m)	231.89	230.58	229.10	227.46	225.65	223.68	221.55
Time t (s)	1.4	1.5	1.6	1.675			
Height (m)	85.63	83.67	81.61	80			
Ra (m)	219.27	216.83	214.26	212.21			

Table 14 – Attractive radius of the wind turbine at different height at a time t

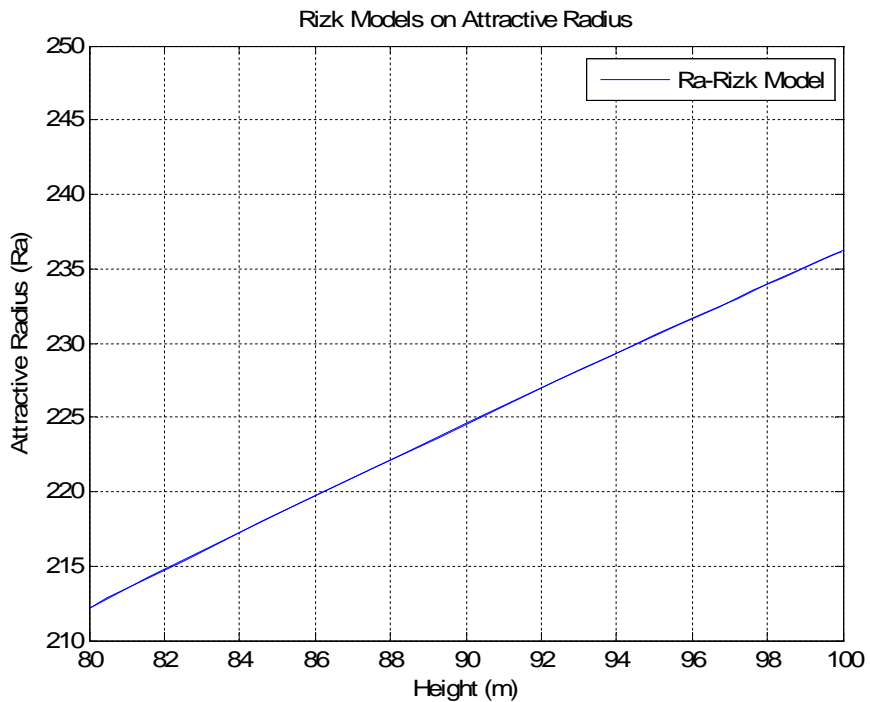


Figure 59 - Attractive radius of the wind turbine at different height at a time t

Let us now estimate the total number of flashes and the proportion of upward and downward flashes for all the equivalent heights:

So according to Rizk's model [18]:

$$N_f = N_u + N_d = \frac{Ng}{10^6} \times \pi \times (R_a^2) + T_d \times e^{-(E_{gc} - E_{g0})/E_{g1}} \quad (41)$$

$$\%up = \frac{N_u}{N_u + N_d} \quad (46) \quad \%dw = \frac{N_d}{N_u + N_d} \quad (47)$$

Computing these equations using Matlab (appendix 1), these are the results we obtain for different values of $Ng = 2, 10, 25$ and 65 flashes/km²/year and $E_{g0} = 3$ kV/m and $E_{g1} = 6$ kV/m (difficult case scenario):

Time t (s)	0				0.1				0.2			
Height (m)	100				99.9219				99.6879			
Ng	2	10	25	65	2	10	25	65	2	10	25	65
Nf	1.56	2.53	6.00	14.87	1.56	2.52	5.99	14.85	1.55	2.51	5.96	14.78
%Up	32.99	30.77	27.01	23.41	32.91	30.70	26.94	23.35	32.68	30.48	26.74	23.16
%Dwn	67.01	69.23	72.99	76.59	67.09	69.30	73.06	76.65	68.32	69.52	73.26	76.84
Time t (s)	0.3				0.4				0.5			
Height (m)	99.2989				99.7565				98.0627			
Ng	2	10	25	65	2	10	25	65	2	10	25	65
Nf	1.54	2.49	5.91	14.67	1.52	2.46	5.84	14.51	1.49	2.42	5.76	14.31
%Up	32.31	29.61	26.40	22.86	31.78	29.61	25.93	22.43	31.10	28.96	25.33	21.89
%Dwn	67.69	69.89	73.60	77.14	68.22	70.39	74.07	77.57	68.90	71.04	74.67	78.11
Time t (s)	0.6				0.7				0.8			
Height (m)	97.2203				96.2325				95.1033			
Ng	2	10	25	65	2	10	25	65	2	10	25	65
Nf	1.46	2.37	5.65	14.08	1.43	2.32	5.53	13.80	1.39	2.26	5.40	13.50
%Up	30.28	28.17	24.61	21.23	29.31	27.24	23.75	20.47	28.19	26.17	22.78	19.59
%Dwn	69.72	71.83	75.39	78.77	70.69	72.76	76.25	79.53	71.81	73.83	77.22	80.41

Time t (s)	0.9				1				1.1			
Height (m)	93.837				92.4385				90.9134			
Ng	2	10	25	65	2	10	25	65	2	10	25	65
Nf	1.35	2.19	5.26	13.17	1.31	2.12	5.11	12.81	1.26	2.05	4.95	12.44
%Up	26.93	24.97	21.70	18.62	25.55	23.66	20.50	17.56	24.04	22.23	19.22	16.42
%Dwn	73.07	75.03	78.30	81.38	74.45	76.34	79.50	82.44	75.96	77.77	80.78	83.58

Time t (s)	1.2				1.3				1.4			
Height (m)	89.2676				87.5074				85.6399			
Ng	2	10	25	65	2	10	25	65	2	10	25	65
Nf	1.21	1.98	4.78	12.05	1.16	1.90	4.61	11.65	1.11	1.82	4.43	11.24
%Up	22.43	20.70	17.85	15.22	20.72	19.09	16.42	13.96	18.94	17.42	14.93	12.66
%Dwn	77.57	79.30	82.15	84.78	79.28	80.91	83.58	86.04	81.06	82.58	85.07	87.34

Time t (s)	1.5				1.6				1.675			
Height (m)	83.6722				81.6121				80			
Ng	2	10	25	65	2	10	25	65	2	10	25	65
Nf	1.06	1.75	4.26	10.83	1.02	1.67	4.09	10.42	0.97	1.60	3.92	10.01
%Up	17.10	15.71	13.42	11.35	15.25	13.97	11.91	10.04	13.40	12.26	10.42	8.76
%Dwn	82.90	84.29	86.53	88.65	84.75	86.03	88.09	89.96	86.60	87.74	89.58	91.24

Table 15 – Number of Flashes and Proportion of upward and downward flashes for different blade tip heights at a time t and for different values of Ng

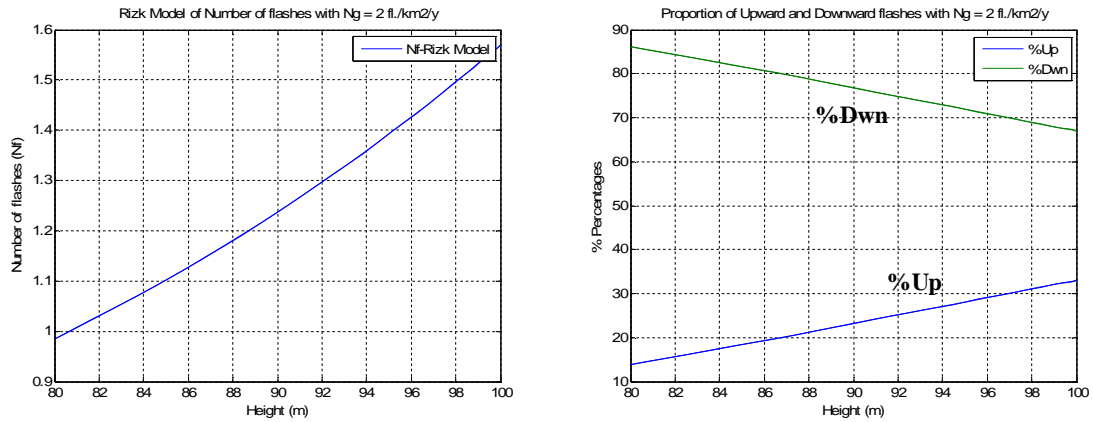


Figure 60 - Number of Flashes and Proportion of upward and downward flashes for different blade tip heights at a time t for $N_g = 2 \text{ fl./km}^2/\text{yr}$

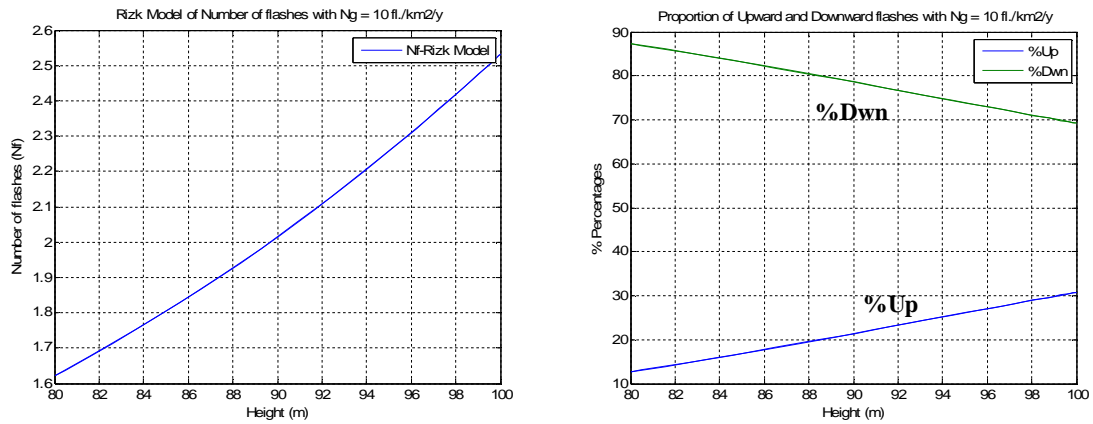


Figure 61 - Number of Flashes and Proportion of upward and downward flashes for different blade tip heights at a time t for $N_g = 10 \text{ fl./km}^2/\text{yr}$

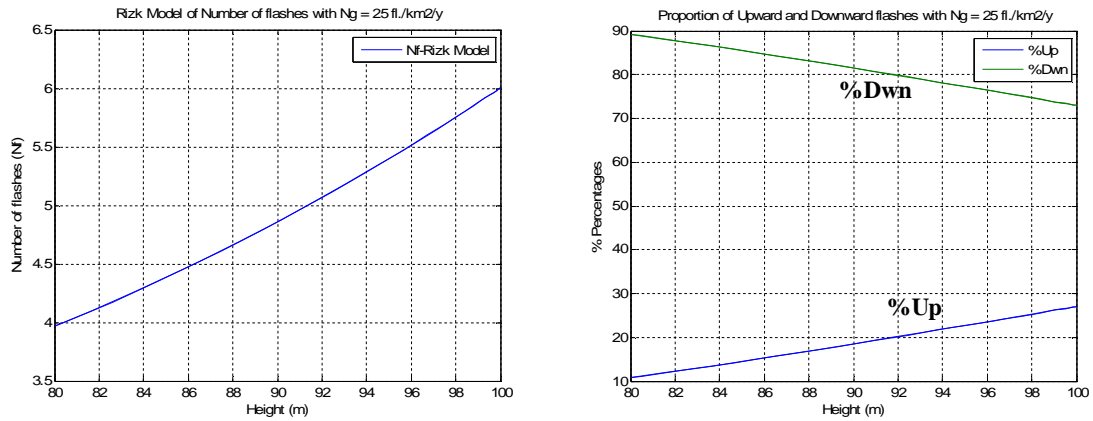


Figure 62 - Number of Flashes and Proportion of upward and downward flashes for different blade tip heights at a time t for $N_g = 25 \text{ fl./km}^2/\text{yr}$

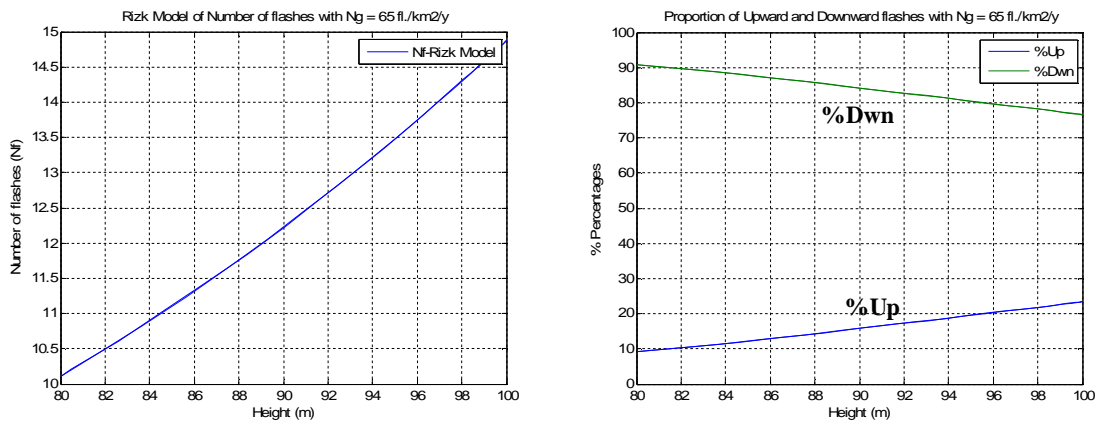


Figure 63 - Number of Flashes and Proportion of upward and downward flashes for different blade tip heights at a time t for $N_g = 65 \text{ fl./km}^2/\text{yr}$

CHAPTER 4 DISCUSSION

4.1. *Electric field and Potential Evaluation*

4.1.1. Discussion

During a thunderstorm, the ambient electric field reaches high values. Such ambient field is intensified at the tips of down conductors as well as at the structure corners and edges. These locations are characterized by steep rise of space potential and accordingly are vulnerable to inception of upward leaders.

In Chapter two, the review of the work already done showed us that two approaches are mostly use to evaluate the electric field on a protected structure are: Finite element and Charge simulation methods.

This is why we applied both of them to wind turbine.

A first approach of modeling the field distribution outside the wind turbine was to use the finite element method with an adapting meshing and error control using a numerical solver.

The second approach was to use the well known charge simulation method (CSM).

The finite element model contains information about the device geometry, material constants, excitations and boundary constraints. The elements can be small where geometric details exist and much larger elsewhere. In each finite element, a simple (often linear) variation of the field quantity is assumed.

The goal of the finite-element analysis is to determine the field quantities at the nodes. Most finite element methods are *variational* techniques which work by minimizing or maximizing an expression that is known to be stationary about the true solution.

In order to obtain a unique solution, it is necessary to constrain the values of the field at all boundary nodes.

A major weakness of the finite element method is that it is relatively difficult to model *open* configurations. The major advantage that finite element methods have over other EM modeling techniques stems from the fact that the electrical and geometric properties of each element can be defined independently. FEM can be used for three-dimensional (3-D) geometries but the large number of equations which must be solved becomes prohibitive which requires extensive computer capacity and long solution time.

This explains why in this thesis we solved finite elements in 2D.

The second approach (CSM) is very simple. For the calculation of electric fields, the distributed charges on the surface of the electrode are replaced by N number of fictitious charges placed inside the electrode.

The types and positions of these fictitious charges are predetermined but their magnitudes are unknown. In order to determine their magnitude some contour points are selected on the surface of electrode.

Then it is required that at any one of these contour points the potential resulting from superposition of effects all the fictitious charges is equal to the known electrode potential. As soon as the required charge system is determined, the potential and the field intensity at any point, outside the electrodes can be calculated.

In our thesis, the results obtained with the two approaches when evaluating the electric field and potential distribution outside a wind turbine of total height $H = 160$ m were satisfactory.

On each approach, we took into consideration two cases: the first one was to model the conductor wire only all the way to the ground and the other was taking into account the tower of the wind turbine.

First, results showed us in both cases that one can just consider the conductor wire all the way to the ground neglecting the tower and nacelle since fields and potential calculation didn't change much to the results at the tip of the blade (wire conductor).

Second, we compared the electric fields E (V/m) and potential U (V) values obtained in both cases. It was seen that there was small differences between results obtained by the two methods.

4.2. *Lightning Exposure*

4.2.1. Discussion

As defined earlier in the previous chapter, the attractive area of a structure reflects the ground area surrounding the structure that is susceptible to lightning. The attractive area is proportional to the structure's height raised to a certain exponent. This indicates that the higher the structure, the more likelihood it will trigger lightning.

Many researches were made and had led to different ways of computing that attractive radius.

In Chapter two, we showed that researches on lightning attractive radius concept were made in the past and we explained the concept and showed some expressions developed. But the cases of concern were specific to power lines [24] [19], rectangular buildings [28].

On our review, we specifically referred to two papers [1] [18] that were applied to wind turbines or any other cylindrical model.

Thus, in this thesis, we concentrated specifically on two ways of evaluating the attractive radius. The first one was based on Rizk's model for downward flashes and the second one on IEC model for all type of flashes.

The two models expressions for the overall attractive radius were defined as:

Rizk [18] (for downward flashes only):	$R_{a1} = 25.9 \times h^{0.48}$
IEC[1] (for upward and downward flashes):	$R_{a2} = 3 \times h$

We applied the two formulas to different heights (20 to 200 m) in order to reasonably compare the results obtained.

For structures less than 100 m, we know that there is a high probability that all flashes are downwards. Then the IEC equation can be assumed applicable for downward flashes and on that basis it can be fully compared to the Rizk model.

After applying these two models to different cases of high and low flash density area, we can say that the results obtained with two models were close for lower height of structure (less than 100 m).

When the height of the structure was above 100 m, the results obtained with Rizk's model for downward flashes and IEC standard started to show significant difference. That is explained by the fact the empirical IEC equation take into account upward flashes that probably would occur at those heights.

We can then surely state that the models leads to approximately the same results of attractive radius for structures of height less than 100 m.

For heights above 100 m a more appropriate comparison results of the number of direct flashes (downward and upward) given by the two methods is determined. In fact, we compared the two equations:

Rizk's model:

$$N_f = N_u + N_d = \frac{Ng}{10^6} \times \pi \times (R_{ao})^2 + T_d \times e^{-(E_{gc} - E_{go})/E_{g1}} \quad (41)$$

IEC model:

$$N_f = Ng \times Ad \times Cd \times 10^{-6} \quad (39)$$

where N_d is the annual average number of direct lightning strikes to the structure;

Ng is the annual average ground flash density;

R_{ao} is the Rizk model overall attractive radius

E_{g0} is a threshold field and E_{g1} is a shape parameter of the ground field statistical distribution

Cd is the environmental factor (Distribution1: $Cd = 1$ and Distribution 2: $Cd = 2$)

$$Ad = \pi(3h)^2$$

We also applied the two formulas to different heights (20 to 200 m) in order to comprehensibly compare the results obtained.

We could see that the results of the two models are rather close when the ground flash density is less than 15 fl/km²/year. For higher values of Ng , the results are close only for lower height of structure (less than 100 to 120m).

Excluding areas of extreme ground flash density, we can conclude that the two models lead to practically the same results for the number of direct flashes on structure of height between 20 to 200m.

A factor that has to be considered in wind turbine lightning exposure is the fact that the blades rotate at a certain speed which would continuously modify the height of the structure.

We have clearly shown that a proper model for attractive radius and number of flashes evaluation for wind turbine that can be used is Rizk's model. We analyzed a case of a wind turbine of height 100m considering the rotation of the blades at a certain practical speed.

We evaluated the number of flashes and the proportion of upward and downward flashes in function of time and height of the wind turbine for different values of flashes density area.

The results obtained showed us that in fact, the number of flashes and the proportion of upward and downward flashes do change in function of time per cycles.

A cycle was defined as the portion of time when the height of the blade tip varies before going back to the same height.

In a specific case considered in the previous chapter, the height of the structure, because of the rotation of the blades, varied by 20 m during one revolution. That 20 m variation took place every 1.675s.

Every $t = 1.675s$, the nominal number of flashes and the proportion of upward and downward flashes then vary as well.

Results obtained showed us that the numbers of flashes expected are almost doubled from one extreme position to the other during that time frame.

The proportion of upward and downward flashes can also vary by approximately 20% during that same time frame.

4.2.2. Recommendations

The variation tendency of the values obtained above are cyclic and follow a certain stability and redundancy, and taking into account that $t = 1.675s$ is a small amount of time; these values could be averaged in order to get a final value of number of flashes and proportion of upward and downward flashes for any time t .

For example, for the case in section 3.2.2 where $N_g = 2\text{fl./km}^2/\text{yr}$, the number of flashes varied from $N_{f1} = 0.97 \text{ fl}$ ($H_t = 80\text{m}$) to $N_{f2} = 1.6 \text{ fl}$ ($H_t = 100\text{m}$).

A final value of number of flashes for a wind turbine of height 100 m, rotating could be suggested as an average:

$$N_{ff} = \frac{N_{f2} + N_{f1}}{2} \quad (48)$$

$$N_{ff} = \frac{1.57 + 0.97}{2}$$

$$N_{ff} = 1.27 \text{ Flashes}$$

The proportion of downward flashes varied from $\%_{\text{down}1} = 87\%$ ($H_t = 80 \text{ m}$) to $\%_{\text{down}2} = 67\%$ ($H_t = 100 \text{ m}$).

The proportion of upward flashes varied from $\%_{\text{up}1} = 13\%$ ($H_t = 80 \text{ m}$) to $\%_{\text{up}2} = 33\%$ ($H_t = 100 \text{ m}$).

Final values for proportion of upward and downward flashes for a wind turbine of height 100 m, rotating could be averaged at:

$$\%dwnf = \frac{\%dwn_1 + \%dwn_2}{2} \quad (49)$$

$$\%upf = \frac{\%up_1 + \%up_2}{2} \quad (50)$$

$$\%dwnf = \frac{87 + 67}{2}$$

$$\%upf = \frac{33 + 13}{2}$$

$$\%dwnf = 77\%$$

$$\%upf = 23\%$$

With our model of approach and these equations, one can now evaluate a final value of number of flashes and proportion of upward and downward flashes for a any wind turbine of any height taking into consideration the rotation of the blades and for any time t.

Finally, since the IEC model is more generalized, versus Rizk's model which is more precise and which take much more constraints into consideration, we would then recommend the use of the latter for further work.

CHAPTER 5 : CONCLUSION

Based on the analysis presented in the previous chapters, the following conclusions have been reached:

1. Calculation of electric field and space potential in the vicinity of the downward conductor tip by finite elements and charge simulation techniques confirmed minor influence of the wind turbine tower (and nacelle).
2. For lightning exposure studies, the above result justifies representation of the wind turbine as a slender grounded structure.
3. Comparison of the stepped leader and the wind turbine blade speeds showed that for lightning exposure studies, the wind turbine blade can be considered as quasi-stationary.
4. A schematic study of wind turbine blade lightning exposure by Rizk's model [18] for tall slender structures and an empirical formula adopted in an IEC standard [1] was undertaken.
5. In general Rizk's model results in higher values for the attractive radius at lower down conductor tip heights (e.g below 70 m) while giving lower attractive radii at larger heights.
6. The above conclusion is practically independent of the ground flash density.
7. The discrepancy between the results obtained by Rizk's model and from

the IEC empirical formula appears to be caused by the inability of the IEC formula to account separately for downward and upward flashes, which are height dependant.

8. The dependence of the number of flashes to a wind turbine blade on its position during rotation has been systematically studied.
9. It has been shown that for a practical wind turbine dimensions the proportion of upward to downward flashes is sensitive to the blade position during rotation.

- **Suggestions for future work**

The present work used a simple exposure model which can be improved in future investigations by considering:

1. Comparison between dry and wet surface conditions of the wind turbine blade.
2. Effect of the space charge formation near the lightning receptors.
3. The application of this model to actual wind parks and the analysis of proximity effects.
4. The vulnerability of wind turbine designs to various lightning protection systems.
5. Induced lightning issues when the wind turbine is stroke.

CHAPTER 6 : REFERENCES

1. IEC TR61400-24 First Edition 2002-07 – Wind Turbine Generation System Part 24 : Lightning Protection
2. Protecting wind turbine electronics from lightning – K.V. Varadarajan – Nov. 2006
3. Lightning protection for wind turbine blades and bearing - Cotton, Nick Jenkins and Krishnan Pandiaraj UMIST, Manchester, UK – 2001
4. Begley DL, Dodd CW, McCalla Jr TM, Smith JG. Lightning: hazard to wind turbines. *NASA Report N83-73594 – 1983*
5. Danish wind power association - www.windpower.org
6. J. C. Willett, J. C. Bailey, V. P. Idone, R. E. Orville, A. Eybert-Berard and L. Barret, “Submicrosecond intercomparison of radiation fields and currents in triggered lightning return strokes based on the transmission -line model,” - 1989
7. V.A .Rakov, R. Thottapillil, and M. A. Uman, “On the empirical formula of Willett relating lightning return-stroke peak current and peak electric field,” - 1992
8. F. Rachidi and R. Thottapillil, “Determination of lightning currents from far electromagnetic fields,” – 1993
9. Current and electromagnetic field associated with lightning-return strokes to tall towers - Farhad Rachidi, Wasyl Janischewskyj, Ali M. Hussein, Carlo Alberto Nucci Silvia Guerrieri, Behzad Kordi, and Jen-Shih Chang, *Senior Member, IEEE- 2001*
10. C. A. Nucci, “Lightning-induced voltages on overhead power lines. Part II: Coupling models for the evaluation of the induced voltages” *Electra*, no. 162, pp. 121–145, 1995
11. Vestas – wind power solution – www.vestas.com
12. GHCC – Earth Science Office NASA - <http://www.ghcc.msfc.nasa.gov/GOES/>
13. Rakov & Uman, *Lightning Physics and Effects* (2003), pp. 373-393; Uman, *The Lightning Discharge* (1987), pp. 281-312; and Hill in *Golde’s Lightning* (1977) pp.385-406
14. Janiscgowskyj W., Hussein AM., Shostak V., Rusan I., Li JX., and Chang JS - Statistics on Lightning strikes to the Toronto CN tower, 1975 to 1995
15. K.Yamamoto, T.Noda, S.Yokoyama, A.Ametani - Experimental and Analytical Studies of Lightning Overvoltages in Wind Turbine Generation Systems - 2007
16. Storms: www.kcstorm.org
17. Behzad Kordi, Rouzbeh Moini, Wasyl Janischewskyj, Ali M. Hussein, Volodymyr O. Shostak, and Vladimir A. Rakov - Application of the Antenna Theory Model to a Tall Tower Struck by Lightning – 2003

18. Farouk A.M. Rizk, Fellow IEEE Institut de recherche d'Hydro-QuCbec (IREQ) - Modeling of Lightning Incidence to Tall Structures part I and II – 1994
19. IEEE Working Group on Lightning Performance of Transmission lines. "A simplified method for estimating lightning performance of transmission lines" IEEE Trans. PAS-104, pp 919-932, April 1985.
20. Eriksson, A J. "Lightning and tall structures "TRANS SAIEE, Vol. 69, Pt 8, August 1978.
21. Prentice, S A. "Frequency of lightning discharge". LIGHTNING Vol 1, Chapter 14 (Academic Press, London, 1977) edited by R H Golde.
22. Anderson, R B, Niekerk, H R, Kroninger, H and Meal, D V, development and field evaluation of lightning earth flash a counter", Proc. IEE, Vol. 118-124, March
23. McCann, G D, "The measurement of lightning currents in direct strokes", AIEE Trans., Vol. 63, pp 1157-1164, 1944.
24. A J Eriksson – The incidence of lightning strikes to power lines – IEEE Transactions on Power Delivery, Vol. PWRD-2, No. 3, July 1987
25. Golde, R.H, "The frequency of occurrence and the distribution of lightning flashes to transmission lines", AIEE Trans., Vol. 64, pp 902-910, 1945.
26. Golde, R H, "The lightning conductor", LIGHTNING Vol 2, Chapter 17, (Academic Press, London, 1977) edited by R H Golde.
27. Eriksson, A J, "The lightning ground flash – an engineering study", Ph.D. Thesis, University of Natal, 1979 (CSIR Special Report ELEK 189, Pretoria, December 1979).
28. M. Bacerra and V. Cooray, Member IEEE – A Simplified Physical Model to Determine the Lightning Upward Connecting Leader Inception – IEEE Transactions on Power Delivery, Vol.21, No.2, April 2006
29. N. Goelian, P. Lalande, A. Bondiou-Clergerie, G. L. Bacchiega, A. Gazzani, and I. Gallimberti, "A simplified model for the simulation of positive- spark development in long air gaps," *J. Phys. D: Appl. Phys.*, vol. 30, pp. 2441–2452, 1997
30. *Les Renardieres Group: Positive Discharges in Long Air Gaps*, 1977.
31. I.Gallimberti, "The mechanism of long spark formation," *J. Physique Coll.*, vol. 40, no. C7, pp. 193–250, 1972. Suppl. 7.
32. H. Singer, H. Steinbigler, and P. Weiss, "A charge simulation method for the calculation of high voltage fields," *IEEE Trans. Power App. Syst.*, vol. PAS-93, pp. 1660–1668, Jan. 1974.
33. F. A.M. Rizk, "A model for switching impulse leader inception and breakdown of long air-gaps," *IEEE Trans. Power Del.*, vol. 4, no. 1, pp. 596–603, Jan. 1989.
34. M. Abdel-Salam and E. Z. Abdel-Aziz, "On the calculation of electric field and potential at singularity points in ionized field problems," in *Proc. IEEE Industry Applications Soc. Annu. Meeting Conf. Rec.*, vol. 2, Oct. 4–9, 1992, pp. 1627–1631.

35. P. Laroche, P. Lalande, and A. Bondiou-Clergerie, Modeles de connexion d'un éclair au sol., TP 2001-134. ONERA Document.
36. W. H. Press, B. P. Flannery, S. A. Teukolsky, and W. T. Vetterling, *Numerical Recipes: The Art of Scientific Computing*. Cambridge, U.K.: Cambridge Univ. Press, 1986.
37. N. I. Petrov and R. T. Waters, "Determination of the striking distance of lightning to earthed structures," *Proc., R. Soc., A*, vol. 450, pp. 589–601, 1995.
38. P. Lalande, "Study of the Lightning Stroke Conditions on a Grounded Structure," Doctoral Thesis, Office National d'Etudes et de Recherches A'erospatiales (ONERA), 1996.
39. L. Deller, E. Garbagnati, CESI and ENEL – Lightning Stroke Simulation by Means of the leader Progression Model – Submitted January 1989, printed April 1989
40. Les Renardières Group "Research on long air gap discharges at Les Renardières", *Electra* n. 29, July 1972, pages 53-157. - 1973 Results1, *Electra* n. 35, July 1974, pages 49-156 - 1975 Results and conclusions1, *Electra* n. 53, July 1977, pages 31-153 - *Electra* n. 74, January 1981, pages 67-216.
41. G.D. McCann "The measurements of lightning currents in direct strokes11, *AIEE Transactions*, 1944, Vol. 63, pages 1157-1164.
42. R.B. Anderson, R.D. Jenner "A summary of eight years of lightning investigation in Southern Rhodesia1@, *Trans. of South Africa IEE*, July/Sept. 1954, pages 215-294.
43. F. Popolansky "Preliminary report on lightning observations on high objects in Czechoslovakia11 Paper CIGRE 33-76 (WG 01) 24 IWD presented at the meeting of CIGRE 33 WG 01 at Coulommiers, France, Aug. 1976.
44. D. Muller-Hillebrand "On the frequency of lightning flashes to high objects. A study of the gulf of Bothnia11 *Tellus*, Volume 12, n. 4, Nov. 1960, pages 444-449.
45. S. Szpor; K. Miladowska; J. Wieckowski "Lightning current records on industrial chimneys in Poland" *Proceedings of CIGRE*, August 1974, paper N. 33-10.
46. Beck as summarised in N. Ciano; E.T. Pierce "A ground lightning environment for engineering usage" *Stanford Research Institute. Techn. Rept. 1*, August 1972.
47. MAZEN ABDEL-SALAM - *IEEE TRANSACTIONS ON INDUSTRY APPLICATIONS*, VOL. 25, NO. 6, NOVEMBER/DECEMBER 1989 - Combined Method Based on Finite Differences and Charge Simulation for Calculating Electric Fields
48. Soren Find Madsen - Interaction between electrical discharges and materials for wind turbine blades particularly related to lightning protection - PhD thesis, 2006 – Orsted DTU, Electric Power Engineering - The Technical University of Denmark
49. "IEC 62305 -1 Ed. 1.0: Protection against lightning – Part 1: General principles", IEC, first edition, January 2006

-
50. "IEC 1024-1-1 Protection of structures against lightning – Part 1-1: General principles– Section 1: Guide A – Selection of protection levels for lightning protection systems", IEC, first edition, August 1993
 51. Larsen, F.M and T. Sorensen, "New lightning qualification test procedure for large wind turbine blades", Proceedings of International Conference on Lightning and Static Electricity, Blackpool, UK, 2003
 52. Becerra, M. and V. Cooray, "A simplified model to represent the inception of upward leaders from grounded structures under the influence of lightning stepped leaders", Proceedings of the International Conference on Lightning and Static Electricity, Seattle Washington, USA, September 2005
 53. Becerra, M., V. Cooray and H.Z. Abidin, "Location of the vulnerable points to be struck by lightning in complex structures", Proceedings of the International Conference on Lightning and Static Electricity, Seattle Washington, USA, September 2005
 54. F.A.M. Rizk, "Modeling of Transmission Line Exposure to Direct Lightning Strokes", IEEE Trans on Power Delivery, Vol. PWRD-S, No. 5. October 1990, pp 1983-1997.
 55. H. Singer, H. Steinbigler and P. Weiss, "A charge simulation method for the calculation of high voltage fields", Trans IEEE, Vol. PAS-93, pp. 1660-67, 1974.
 56. O. Pinto, Jr., I.R.C.A. Pinto and K.P. Naccarato - Maximum cloud-to-ground lightning flash densities observed by lightning location systems in the tropical region - Atmospheric Electricity Group — ELAT, Brazilian Institute of Space Research (INPE), Brazil – July 2006.
 57. Wada, A.; Miki, M.; Asakawa, A. – Upward Lightning Flashes Observed at the 200-m Fukui Chimney in winter – 2004

APPENDIX

- Function to evaluate the Attractive Radius for different values of Height H with Rizk and IEC models.

```

function [] = attractive(k)           % This function is to evaluate the Attractive radius
k=1;
for n=20:5:200

    ra(k)= 25.9*(n^(0.48));          % Attractive radius
    r(k) = ra(k)^2;
    Ad(k)= 3*n;
    A(k) = Ad(k)^2;
    x(k) = n;
    c(k) = A(k)/r(k)                % Ratio between Rizk and IEC model
    k=k+1;
end

figure(1)                            % Figure 1 - Attractive Radius
plot(x,ra,x,Ad);
grid on;
legend('Ra-Rizk Model','Ra-IEC Model');
xlabel('Height (m)');
ylabel('Attractive Radius (Ra)');
title('Comparision Rizk and IEC Model of Attractive Radius');

figure(2)                            % Figure 2 - Ratio between Rizk and IEC model
plot(x,c);
grid on;
xlabel('Height (m)');
ylabel('Difference proportion');
title('Comparison Rizk and IEC Model of Number of Direct Lightning');

```

- Function to evaluate the Number of flashes and proportion of upward and downward flashes for different values of ground flash density Ng with Rizk models.

```

function [] = flashes(x)                                % This function is to evaluate the number of flashes and
                                                       the proportion of upward and downward flashes
k=1;
Eg0 = 2;
Eg1 = 3;
Ng1 = 2;                                               % Ground flash density
Ng2 = 10;
Ng3 = 25;
Ng4 = 65;
for n=0:0.100:x
    p1(k)=60+40*sin(pi/2+0.625*n);
    ra(k)= 25.9*(p1(k)^(0.48));

    Nd1(k) = Ng1*10^(-6)*pi*(ra(k))^2;                % Number of downward flashes
    Nd2(k) = Ng2*10^(-6)*pi*(ra(k))^2;
    Nd3(k) = Ng3*10^(-6)*pi*(ra(k))^2;
    Nd4(k) = Ng4*10^(-6)*pi*(ra(k))^2;

    egc(k)= 1600/p1(k);

    Td1(k) = (25*Ng1)^(0.8);                           % Number of storm per year
    Td2(k) = (25*Ng2)^(0.8);
    Td3(k) = (25*Ng3)^(0.8);
    Td4(k) = (25*Ng4)^(0.8);

    Nu1(k)= Td1(k)*exp(-(egc(k)-Eg0)/Eg1);             % Number of upward flashes
    Nu2(k)= Td2(k)*exp(-(egc(k)-Eg0)/Eg1);
    Nu3(k)= Td3(k)*exp(-(egc(k)-Eg0)/Eg1);
    Nu4(k)= Td4(k)*exp(-(egc(k)-Eg0)/Eg1);

    Nfr1(k) = Nu1(k)+Nd1(k);                           % Number of total flashes
    Pu1(k)= (Nu1(k)/Nfr1(k))*100;                       % Proportion of upward flashes
    Pd1(k)= (Nd1(k)/Nfr1(k))*100;                       % Proportion of downward flashes

    Nfr2(k) = Nu2(k)+Nd2(k);
    Pu2(k)= (Nu2(k)/Nfr2(k))*100;
    Pd2(k)= (Nd2(k)/Nfr2(k))*100;

    Nfr3(k) = Nu3(k)+Nd3(k);
    Pu3(k)= (Nu3(k)/Nfr3(k))*100;
    Pd3(k)= (Nd3(k)/Nfr3(k))*100;

    Nfr4(k) = Nu4(k)+Nd4(k);
    Pu4(k)= (Nu4(k)/Nfr4(k))*100;
    Pd4(k)= (Nd4(k)/Nfr4(k))*100;

```

```
k=k+1;
end

figure(1)
plot(p1,Nfr1);
xlim ([80 100]);
grid on;
legend('Nf-Rizk Model','Nf-IEC Model');
xlabel('Height (m)');
ylabel('Number of flashes (Nf)');
title(' Rizk Model of Number of flashes with Ng = 2 fl./km2/y');

figure(2)
plot(p1,Pu1,p1,Pd1);
xlim ([80 100]);
grid on;
legend('%Up','%Dwn');
xlabel('Height (m)');
ylabel('% Percentages');
title(' Proportion of Upward and Downward flashes with Ng = 2 fl./km2/y');

figure(3)
plot(p1,Nfr2);
xlim ([80 100]);
grid on;
legend('Nf-Rizk Model','Nf-IEC Model');
xlabel('Height (m)');
ylabel('Number of flashes (Nf)');
title(' Rizk Model of Number of flashes with Ng = 10 fl./km2/y');

figure(4)
plot(p1,Pu2,p1,Pd2);
xlim ([80 100]);
grid on;
legend('%Up','%Dwn');
xlabel('Height (m)');
ylabel('% Percentages');
title(' Proportion of Upward and Downward flashes with Ng = 10 fl./km2/y');

figure(5)
plot(p1,Nfr3);
xlim ([80 100]);
grid on;
legend('Nf-Rizk Model','Nf-IEC Model');
xlabel('Height (m)');
ylabel('Number of flashes (Nf)');
title(' Rizk Model of Number of flashes with Ng = 25 fl./km2/y');

figure(6)
plot(p1,Pu3,p1,Pd3);
xlim ([80 100]);
grid on;
legend('%Up','%Dwn');
```

```
xlabel('Height (m)');  
ylabel('% Percentages');  
title(' Proportion of Upward and Downward flashes with Ng = 25 fl./km2/y');  
  
figure(7)  
plot(p1,Nfr4);  
grid on;  
xlim ([80 100]);  
legend('Nf-Rizk Model','Nf-IEC Model');  
xlabel('Height (m)');  
ylabel('Number of flashes (Nf)');  
title(' Rizk Model of Number of flashes with Ng = 65 fl./km2/y');  
  
figure(8)  
plot(p1,Pu4,p1,Pd4);  
xlim ([80 100]);  
grid on;  
legend('%Up','%Dwn');  
xlabel('Height (m)');  
ylabel('% Percentages');  
title(' Proportion of Upward and Downward flashes with Ng = 65 fl./km2/y');
```

- Function to evaluate the position of the tip of the blade versus time.

```

function [p1,p2,p3] = position(x)                % this function is to evaluate the position of the
                                                blade vs time
k=1;
for n=0:0.1:x
    p1(k)=60+40*sin(pi/2+0.625*n);              % Position of blade1
    p2(k)=60+40*sin(pi/2 + 0.625*n + (2*pi/3)); % Position of blade2
    p3(k)=60+40*sin(pi/2 + 0.625*n + (4*pi/3)); % Position of Blade3
    k=k+1;
end
n=0:0.1:x
plot(n,p1,n,p2,n,p3)
axis([0 x 80 101]);
grid on;
legend('Blade #1','Blade #2','Blade #3');
xlabel('Time t (s)');
ylabel('Vertical Lenght Hb (m)');
title('Position of each Blades vs Time t');
title('Wind turbine Height vs Time t on 1 round');
ylabel('Wind Turbine Height (m)');

```